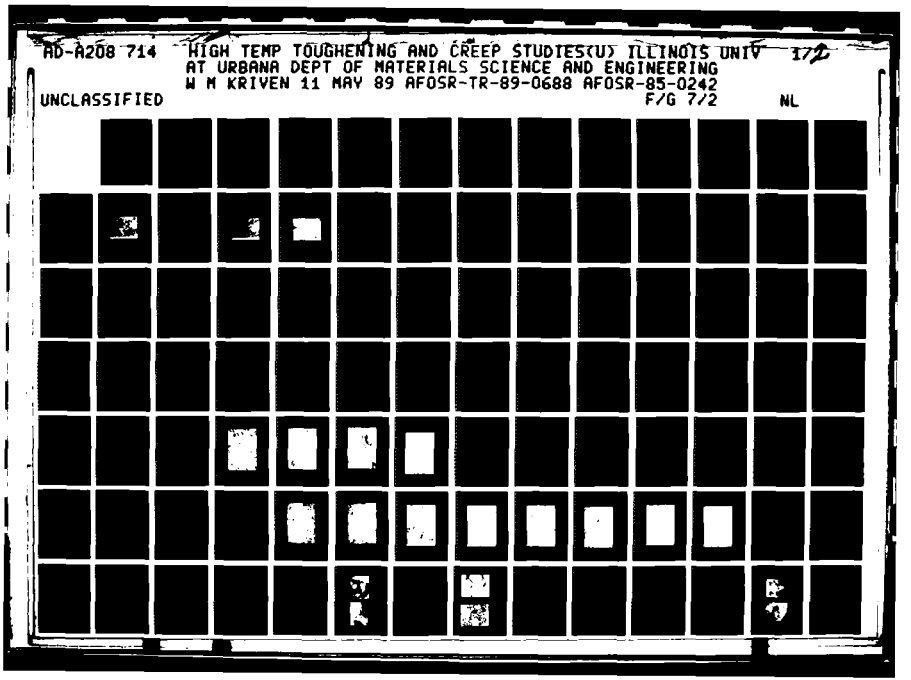
AD-A208 714 HIGH TEMP TOUGHENING AND CREEP STUDIES(U) ILLINOIS UNIV 1/2
AT URBANA DEPT OF MATERIALS SCIENCE AND ENGINEERING
W M KRIVEN 11 MAY 89 AFOSR-TR-89-0688 AFOSR-85-0242
UNCLASSIFIED F/G 7/2 NL

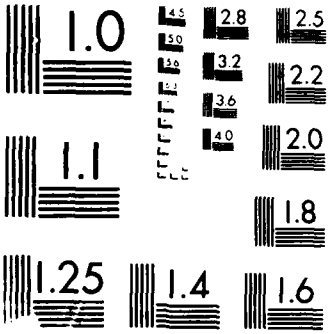
1.0
1.1
1.25
1.4
1.6
1.8
2.0
2.2
2.5
2.8
3.2
3.6
4.0
4.5
5.0
5.6

SECURITY CLASSIFICATION OF THIS PAGE

AD-A208 714

REPORT DOCUMENTATION PAGE

DTIC ELECTE JUN 07 1989 S D B CS

1a. REPORT SECURITY CLASSIFICATION Unclassified	1b. RESTRICTIVE MARKINGS NA
2a. SECURITY CLASSIFICATION AUTHORITY NA	3. DISTRIBUTION/AVAILABILITY OF REPORT Approved for public release; distribution unlimited.
2b. DECLASSIFICATION/DOWNGRADING SCHEDULE NA	
4. PERFORMING ORGANIZATION REPORT NUMBER(S) CONTRACT # AFOSR-85-0242	5. MONITORING ORGANIZATION REPORT NUMBER(S) AFOSR-TR- 89-0688 NA
6a. NAME OF PERFORMING ORGANIZATION UNIVERSITY OF ILLINOIS / 6b. OFFICE SYMBOL (If applicable) NA	7a. NAME OF MONITORING ORGANIZATION AFOSR/NE
6c. ADDRESS (City, State and ZIP Code) 105 South Goodwin Avenue Urbana, IL 61801	7b. ADDRESS (City, State and ZIP Code) BLDG 410 Bolling AFB DC 20332-6600
8a. NAME OF FUNDING/SPONSORING ORGANIZATION AFOSR / 8b. OFFICE SYMBOL (If applicable) NE	9. PROCUREMENT INSTRUMENT IDENTIFICATION NUMBER CONTRACT # AFOSR 85-0242
8c. ADDRESS (City, State and ZIP Code) AFOSR/NE BLDG 410 Bolling AFB, DC BLDG 410 20332-6600	10. SOURCE OF FUNDING NOS. PROGRAM ELEMENT NO.: 61102F; PROJECT NO.: 2306; TASK NO.: A2; WORK UNIT NO.:
11. TITLE (Include Security Classification) High Temp Toughening and Creep Studies in Composite Ceramics	
12. PERSONAL AUTHOR(S) Professor Waltraud M. Kriven	
13a. TYPE OF REPORT Final Report / 13b. TIME COVERED FROM 6-1-85 TO 2-28-89	14. DATE OF REPORT (Yr., Mo., Day) 1989-5-11 / 15. PAGE COUNT 93 + reprints
16. SUPPLEMENTARY NOTATION NA	
17. COSATI CODES FIELD / GROUP / SUB. GR.	18. SUBJECT TERMS (Continue on reverse if necessary and identify by block number) High Temperature Transformation toughening with the lanthanide sesquioxides, alternative tougheners, SiC, Ca_2SiO_4

19. ABSTRACT (Continue on reverse if necessary and identify by block number)

The aim of this work was to develop the lanthanide sesquioxides (Ln_2O_3) as high temperature transformation tougheners in ceramic-matrix composites. The matrix chosen was silicon carbide. The advantage of the sesquioxides e.g., dysprosia (Dy_2O_3) is that they have a volume increase (8-10%) and transformation temperature (≤ 2200 °C) approximately double that of zirconia which is known to be a room temperature toughener. Theoretical crystallographic and experimental kinetic studies have been made of the relevant monoclinic (B) to cubic (C) transformation mechanism in Dy_2O_3. Processing techniques by tantalum encapsulation and hipping have identified that a rapid quench rate and complete removal of silica film is required for retention of B-DyO_3 in SiC. Several new transformation tougheners alternative to zirconia have been identified. Among these, dicalcium silicate (Ca_2SiO_4) having a volume change of 12% on transformation, has been studied as a room temperature analogue to Dy_2O_3. It was dispersed in matrices of calcium zirconate (CZ) and magnesia. Preliminary mechanical data confirm that Ca_2SiO_4 is indeed a transformation toughener, giving a 5-fold increase in toughness. It is anticipated that with more sophisticated processing a 10-to-15-fold increase in toughness can be achieved, and that a variety of other matrices can be toughened, (e.g. glass and cements).

20. DISTRIBUTION/AVAILABILITY OF ABSTRACT UNCLASSIFIED/UNLIMITED ☒ SAME AS RPT. ☐ DTIC USERS ☐	21. ABSTRACT SECURITY CLASSIFICATION UNCLASSIFIED
22a. NAME OF RESPONSIBLE INDIVIDUAL ~~Waltraud M. Kriven~~ Spiezi...	22b. TELEPHONE NUMBER (Include Area Code) / 22c. OFFICE SYMBOL NC

DD FORM 1473, 83 APR EDITION OF 1 JAN 73 IS OBSOLETE.

SECURITY CLASSIFICATION OF THIS PAGE

CERAMICS DIVISION

MATERIALS SCIENCE AND ENGINEERING

University of Illinois

Urbana, Illinois

"HIGH TEMPERATURE TOUGHENING AND CREEP STUDIES IN COMPOSITE CERAMICS"

Principal Investigator: Professor W. M. Kriven
Project Title: AFOSR 85-0242
Project Period: June 1st 1985 to Feb. 28th 1989

May 11, 1989
FINAL REPORT

Prepared for:
AIR FORCE OFFICE OF SCIENTIFIC RESEARCH
Bolling AFB, DC 20332-6600
Building 410

University of Illinois at Urbana-Champaign

Contents

Section 1 Summary 1

2. Publications and Theses 15

3. Conference Presentations 16

4. Determination of the Critical Particle Size of Dicalcium Silicate in the Transformation Toughening of Magnesia. (E. S. Mast) 19

5. Processing and Microstructure of Dysprosia in Silicon Carbide Matrix Composites. (Shin Kim) 80

6. Reprints

SECTION 1 - SUMMARY

Early in 1985, the lanthanide sesquioxides (Ln_2O_3) were identified as potential high temperature transformation tougheners alternative to zirconia (ZrO_2). Their 8-10% volume increase accompanying the monoclinic (B) to cubic (C) transformation suggested that they should be more powerful than ZrO_2. In addition, the Ms temperature was raised up to 2200°C indicating that, based on thermodynamics alone, transformation toughening up to this temperature should be possible. Hence a proposal was written to the AFOSR with the aim of transformation toughening silicon carbide (SiC) with dispersions of monoclinic dysprosia particles giving a microstructure analogous to zirconia-toughened-alumina (ZTA).

The processing of SiC-Dy_2O_3 composites proved to be a difficult task, essentially because of the existence of a thin silica (SiO_2) film around the SiC particles. This caused the formation of a Dy_2O_3 + Si-containing liquid which surrounded all the SiC grains as an extensive interphase. As described more fully in Section 5, the processing work was slow and a range of densification techniques were used, including

(i) hot pressing at 2000°C in a graphite die.
(ii) hot pressing followed by ejection from the hot zone to achieve faster cooling kinetics.
(iii) sintering in an inert atmosphere at 2100°C followed by furnace quenching.
(iv) hipping at 2000°C in Ta encapsulation.

Oxygen getting additives of boron and carbon have been used with some reduction of silica containing phase and improved retention of high temperature B phase.

Prolonged annealing in air at 1500°C for 50 hr resulted in extensive formation of unidentified phases particularly in specimens which were hot pressed in the graphite die. However, in the Ta encapsulated hipped specimens, the microstructure was stable and unchanged after annealing in air. The ~5 wt% Si present in the Dy_2O_3 wetting phase after hipping was still unchanged after annealing, and no new phases were detected by XRD. Prior

washing of SiC powders with HF did have a tendency to reduce the Si content in the Dy_2O_3 phase. In completing this work it is proposed to investigate ways to remove the SiO_2 film and to determine its effect in retarding the B to C transformation, if any.

Thus, the work to date gives a glimmer of hope that Dy_2O_3 may still be a transformation toughener of SiC matrices up to elevated temperatures (~1850°C). Important factors in processing have been identified viz., very fast quench rate and total removal of SiO_2 is required.

Meanwhile, theoretical crystallography and experimental kinetic studies were made of pure dysprosia whose M_s temperature on cooling is 1850 °C and on heating is 1950 °C. An M.S. thesis by Mr. O. Sudre aided by Dr. K. Venkatachari describes the theoretical mechanism of the crystallography of the A (hexagonal) to B(monoclinic) to C (cubic) transformation. The structure changes are complex since the X-ray unit cells contain large numbers of formula units per cell, i.e. hexagonal (Z = 3) to monoclinic (Z =6) to cubic (Z = 16). The structural correspondences proposed are presented in Figs. 1a, b. A crystallographic model for the B $\leftrightarrow$ C shear mechanism has been postulated. From lattice parameter measurements extrapolated to the transformation temperature (1950°C), calculations indicate that the volume change $\frac{\Delta V}{V_{mono}}$ on cooling:

(i) at room temperature is (+) 8.54%

(ii) at 1950°C is (+) 5.07%.

This corresponds to a volume change of 2.5 to 3 times larger than in ZrO_2, with a strain energy 4 times larger than for ZrO_2 at room temperature. In ZrO_2, the volume increase on transformation is 3% at 950° and 4.9% at room temperature. This may be a reason for the observation that the transformation could not be nucleated at room temperature. At elevated temperatures the strain energy is 0.294 which is still comparatively large.

Experimental studies of dysprosia have shown that, unlike in ZrO_2, cooling kinetics play a crucial role in retention of the high temperature B phase of Dy_2O_3 down to room temperature. Quench rates of 10^6°C/sec have been achieved by melting sintered bars of Dy_2O_3 with a CO_2 laser and roller quenching between two titanium rollers. In the TEM the microstructure was seen to be fine-grained and highly defected. Annealing at 400°-500°C removed many defects. Further annealing at 600°C and above caused sudden

transformation to C phase, accompanied by shattering or self disintegration of flakes. This effect was recorded by hot stage high voltage transmission electron microscopy (HVEM at the Argonne National Lab. Tandem Facility). Annealing of the B phase flakes was carried out for different times at different temperatures and the amount of C phase formed was determined by quantitative x-ray diffraction. The results were analyzed using the Avrami equation:

$$f(t) = e^{-kt^n}$$

where $f(t)$ = fraction of monoclinic phase left untransformed.
t = time
n = kinetic law constant (order of the transformation)
k = kinetic constant

The constant k can be related to the activation energy E_a by

$$k = k_o\, e^{-E_a/RT}$$

As seen in Fig. 2a, b, the E_a was measured as 396 KJ/mole below 600°C and it decreased to 31 KJ/mole at higher temperatures. This suggests that a reconstructive mechanism operates below 600°C and a displacive mechanism above it.

On another level, during the course of this work, several new transformation tougheners alternative to zirconia were identified and a review paper by Kriven was published[1].

As seen in Fig. 3, there are some close analogies between the polymorphic transformations in zirconia the lanthanide sesquioxides and in Ca_2SiO_4. In both cases the monoclinic phase appears as an intermediate phase between two higher symmetry phases, and transformation from the monoclinic on cooling involves large, positive volume changes. The volume change in Ca_2SiO_4, (abbreviated as C_2S) is 12%, even larger than in Dy_2O_3. Although it does not offer the possibility of high temperature transformation, dicalcium silicate expands the number of matrices such as other silicates and glasses which may benefit from transformation toughening. The polymorphic transformations in dicalcium silicate are illustrated in Fig. 4

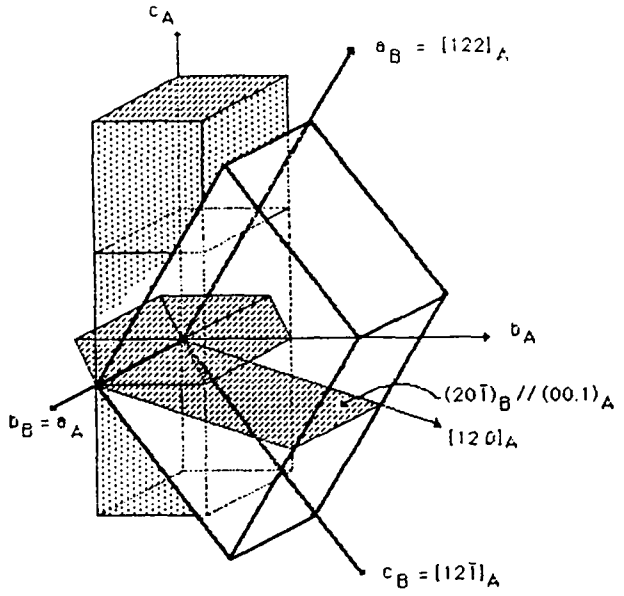

Fig. 1a The structural relationship between three, stacked, primitive subcells of tbe hexagonal A phase and the monoclinic (Z=6) x-ray cell of the B phase lanthanide sesquioxides.

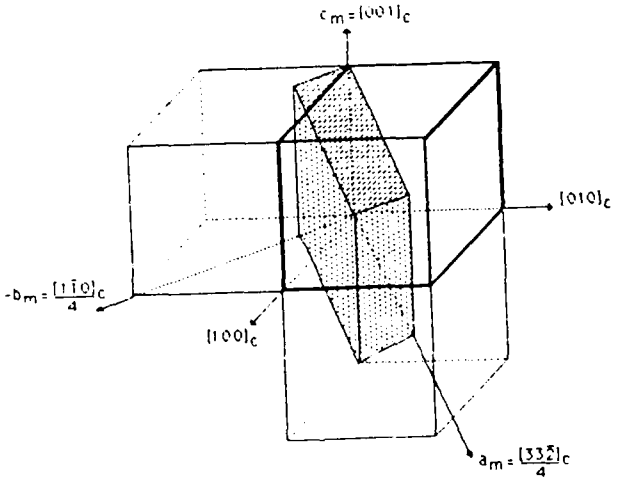

Fig. 1b The structural relationship between the monoclinic, (Z=6), (hatched) and cubic (Z=16) x-ray unit cells of the lanthanide sesquioxides.

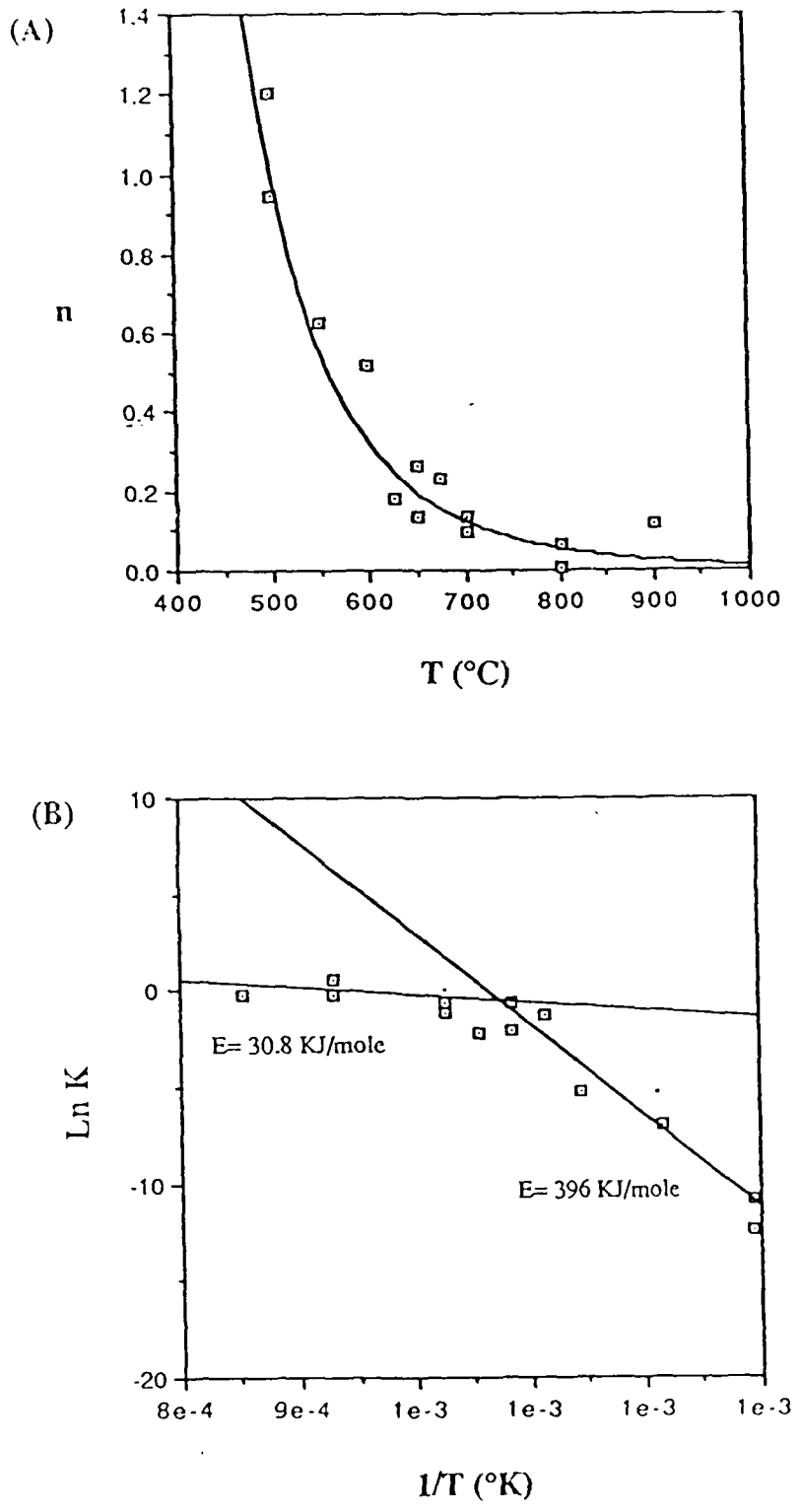

Fig. 2. Kinetic study (a) of the order parameter n as a function of temperature. (b) LnK as a function of (K).

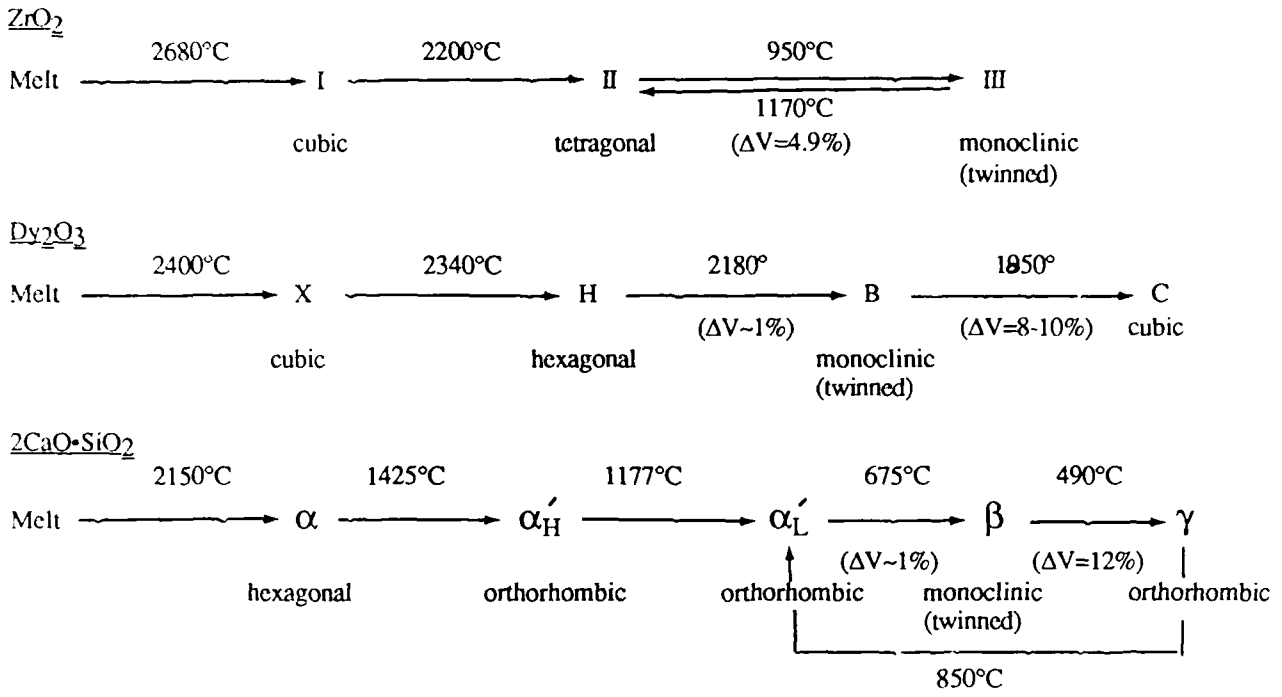

Fig. 3. Comparison of polymorphic transformations in ZrO_2, Dy_2O_3 and Ca_2SiO_4

Ca_2SiO_4 Polymorphic Transformations

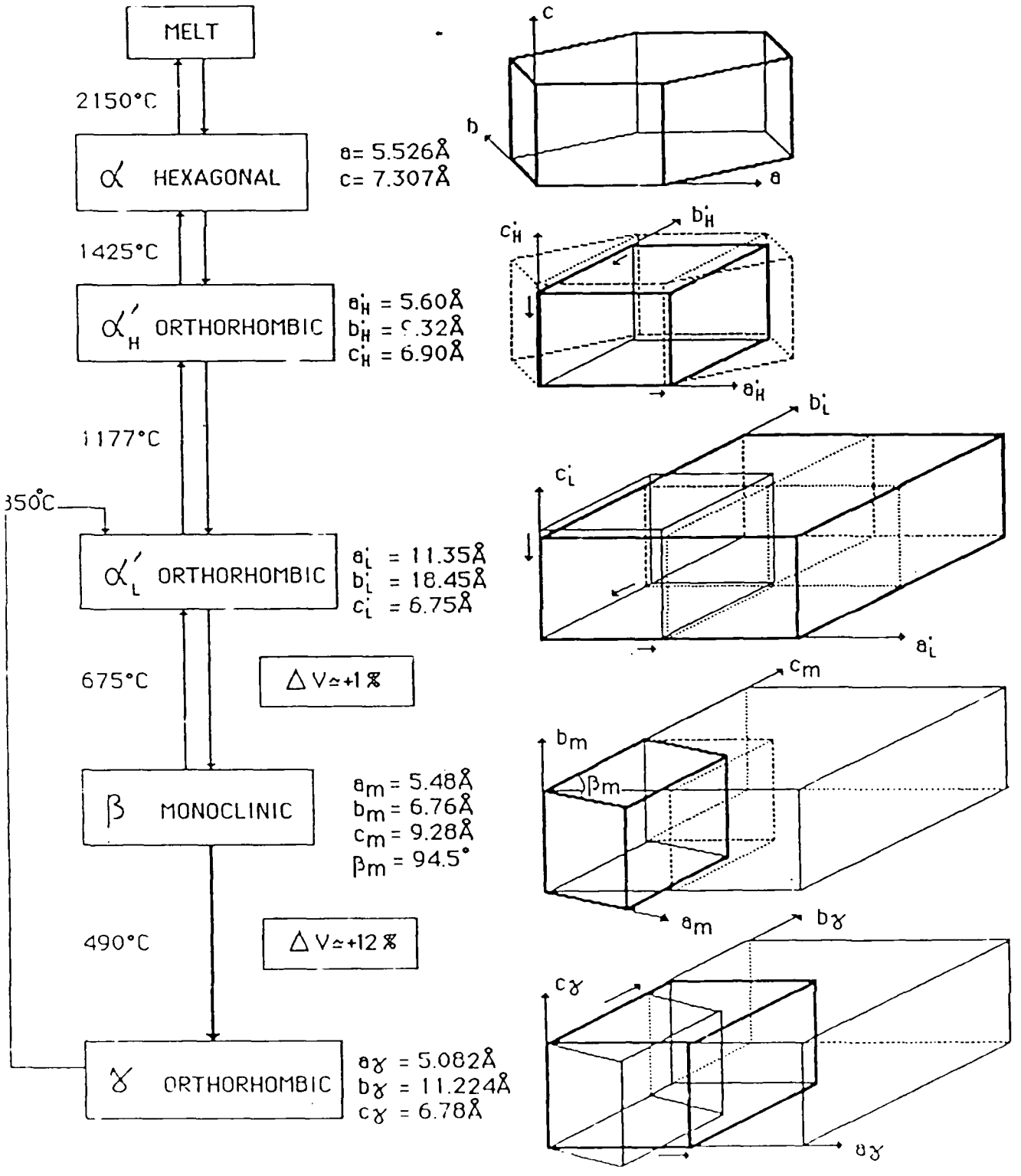

Fig. 4

During the past four years, collaboration in the form of a shared Ph.D. student has taken place between Professor W. Kriven and J. F. Young who is an established authority in cement chemistry. This fruitful interdisciplinary interaction has yielded insight and background knowledge into the behavior of dicalcium silicate from the perspective of work done in cement chemistry which is relevant to potential transformation toughening applications. The findings were distilled into a publication by Kriven, Chan and Barinek.[2] In particular, it was recognized that a particle size effect operates in β-C_2S as it does in ZrO_2. This is the key parameter controlling crack-tip stress-induced transformations. Particles of C_2S can be metastably retained in the β phase by dispersion into a constraining matrix. Two theses on this topic by C. J. Chan (Ph.D.) and E. A. Barinek (M.S.) have recently been submitted.

Composites of 0 to 30 vol% β-C_2S in calcium zirconate (CZ) matrices were fabricated by sintering and hot pressing techniques.[2] The microstructure consisted of irregularly shaped, twinned β-C_2S particles intergranularly dispersed in a CZ matrix. The material was analogous to zirconia toughened alumina (ZTA).

Processing techniques have been developed so that several parameters were optimized simultaneously. These included:

(i) density
(ii) complete reaction between components
(iii) optimum vol% C_2S addition
(iv) cooling rate
(v) critical particle size for stress-induced transformation

When the β-C_2S particle size was too large, spontaneous transformation would occur on cooling, causing cracking and disintegration of the pellet. When the particle size was too small, even the roughest surface grinding could not induce the $\beta \leftrightarrow \gamma$ transformation.

Definition of the critical particle size is discussed in the paper by Kriven, Chan and Barinek[2]. While in ZrO_2 the "critical particle size" refers to a single crystal tetragonal particle which transforms to a twinned monoclinic particle, the situation is reversed in the case of C_2S. Here, the

$\alpha_L' \rightarrow \beta$ transformation produces twins (by a martensitic mechanism) so that the β phase is twinned before transformation to γ. In addition, rapid quenching through the $\alpha \rightarrow \alpha_H'$ transformation at 1425°C causes cracking across twins which reduces even further, the critical volume for transformation to within one twin. Thus an ambiguity exists in the definition of the critical particle size for transformation in the C_2S system. While SEM and TEM analyses revealed a correlation between grain size and twin width, results suggested that the critical particle size may be determined by:

(i) overall C_2S grain size
(ii) β twin thickness
(iii) both twin thickness and twin length

Observations of polished surfaces of 30 vol% C_2S-CZ composite indicated that the stress-induced transformation of β-C_2S particles could be induced by surface grinding. Parallel lamellar features in C_2S particles appeared in SEM micrographs (Fig. 5a). Corresponding X-ray diffractometry of ground surfaces indicated that the transformation to γ had occurred (Fig. 5b). A transformation zone of such particles at the wake of a crack emanating from a Vickers indent could be identified by SEM (Fig. 6a, b). Preliminary mechanical data by the Vickers indentation technique (Fig. 7) indicated a five-fold increase in toughness in 10 vol% C_2S compositions. Considerable improvements to this are expected by optimization of composition and particle size distribution. A patent disclosure to the University of Illinois of these preliminary results has been made.

REFERENCES

1. "Possible Alternative Transformation Tougheners to Zirconia: Crystallographic Aspects," W M. Kriven. J. Am. Ceram. Soc., (1988), in press.

2. "The Particle Size Effect of Dicalcium Silicate in a Calcium Zirconate Matrix," W. M. Kriven, C. J. Chan and E. A. Barinek. Proc. Third Int. Conf. on Science and Technology of Zirconia, Tokyo (1980). Advances in Ceramics, Vol. 24, part A (1988) 145-155.

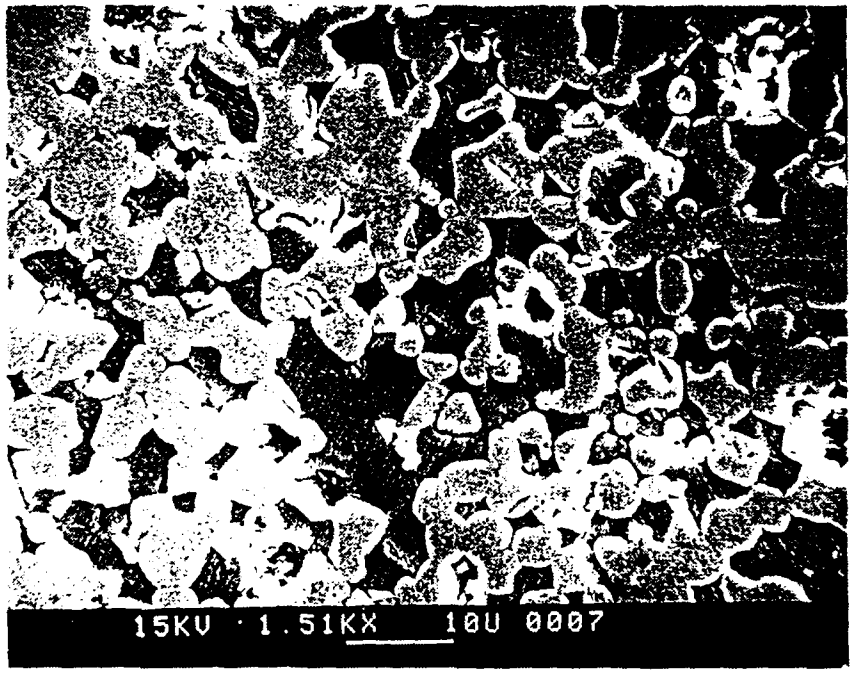

Fig. **5a** SEM micrograph of a calcium zirconate (CZ)-30 vol% C_2S composite. The C_2S has a slightly darker colour. The specimen was gently sawed with a diamond tipped blade, causing the β-C_2S to transform to γ. The γ-C_2S grains are visible by the parallel striated features, which give rise to γ peaks in X-ray diffractometry patterns.

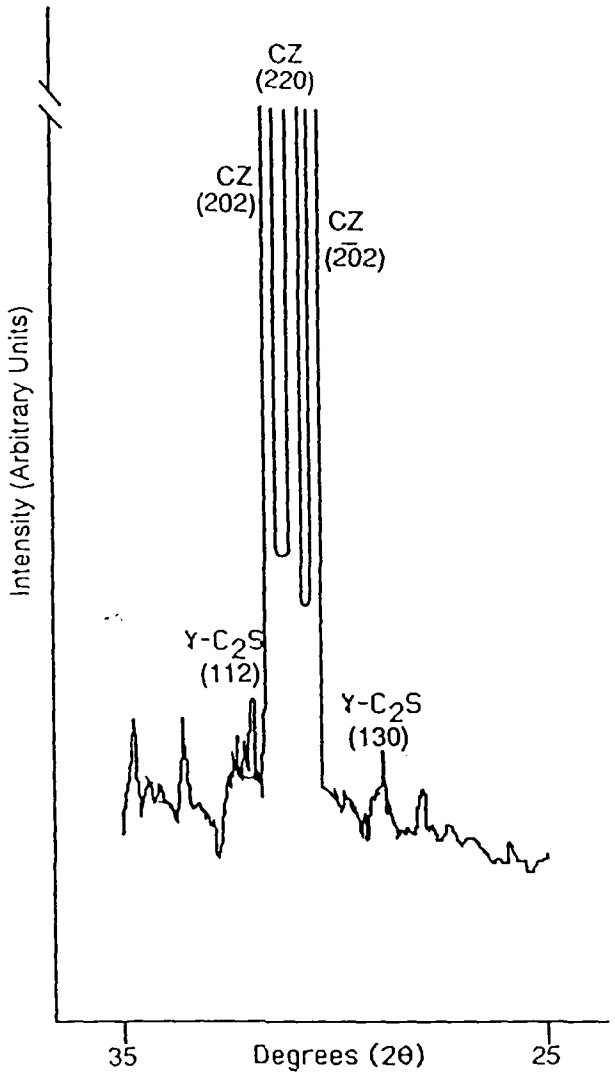

Fig. **5 b** X-ray spectrum of the ground and polished surface showing the presence of gamma dicalcium silicate and calcium zirconate.

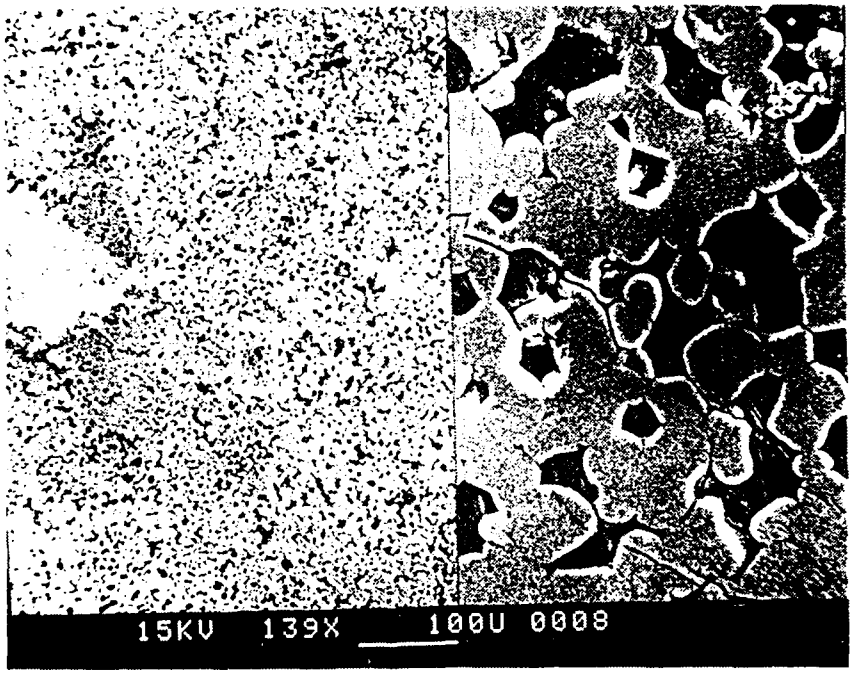

Fig. 6a SEM micrograph (corresponding to Fig. 5) of a region adjacent to the crack. The magnified insert on the right shows that the C_2S grains contain striation features and so transformed to γ.

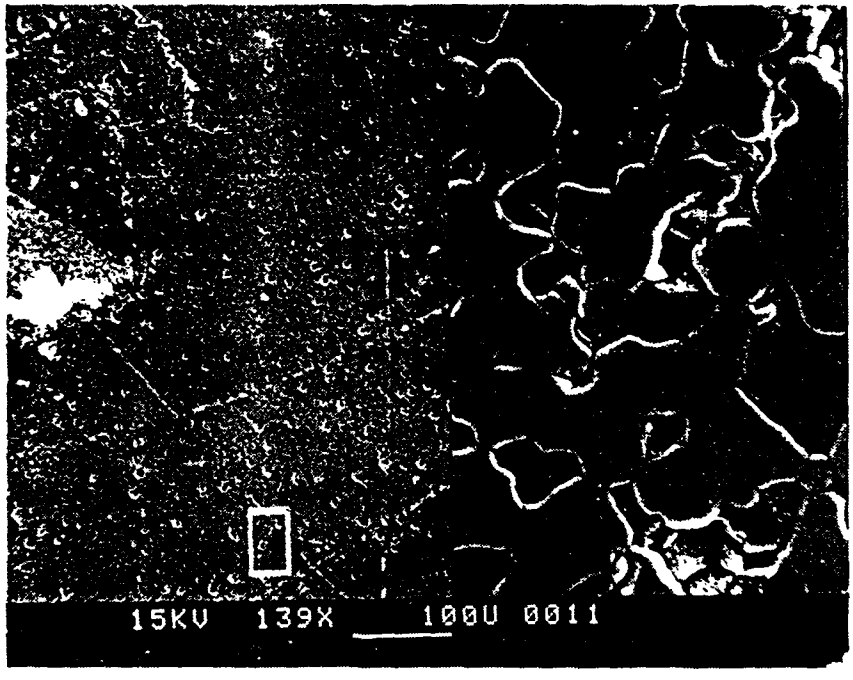

Fig. **6b** SEM micrograph of a polished CZ-30 vol% C_2S composite in the region of a Vickers indent. Away from an demanding crack, no striated features were observed in the C_2S grains, as seen in the magnified insert to the right of the figure.

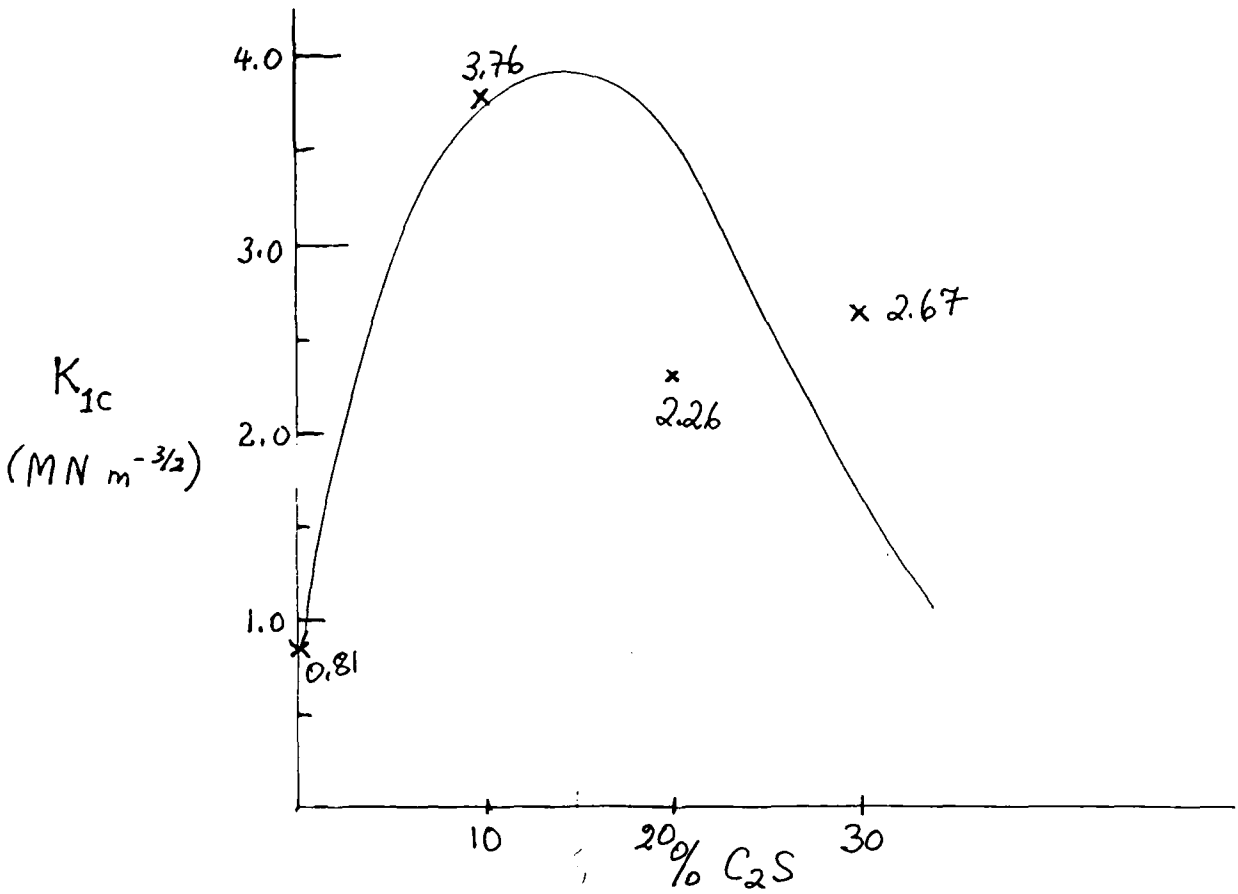

Fig. 7 Preliminary toughness data from Vickers indentation measurements for various compositions of β-C_2S dispersed in calcium zirconate

SECTION 2 - PUBLICATIONS

"Particle Size Effect of Dicalcium Silicate in a Calcium Zirconate Matrix", W. M. Kriven, C. J. Chan and E. A. Barinek, Science and Technology of Zirconia III, edited by S. Somiya, N. Yamamoto and H. Yangida. American Ceramic Soc., Advances in Ceramics 24, (1988) part A, 145-155.

"Possible Alternative Transformation Tougheners to Zirconia: Crystallographic Aspects," W. M. Kriven, J. Am. Ceram. Soc. (1988) 71 [12] 1021-1030.

"Microstructural Characterization of Laser-Melted Roller-Quenched Dicalcium Silicate," C. J. Chan, K. R. Venkatachari, W. M. Kriven and J. F. Young. Proc. 46th Annual Meeting of the Electron Microscopy Society of America (EMSA). Edit. G. W. Bailey, San Fransisco Press. Milwaukee, WI, Aug. (1988), 582-583.

"Analytical Electron Microscopic Studies of Doped Dicalcium Silicates," C. J. Chan, W. M. Kriven and J. F. Young, J. Am. Ceram. Soc., 71 [9] (1988) 713-719.
Paper won Brunauer Award of the American Ceramic Society (1988).

THESES

"Investigation of the Monoclinic (B) to (C) Transformation of Dysprosium Sesquioxide (Dy_2O_3)." M.S. thesis by O. Sudre. Submitted Dec. 1987.

"The Development of Dicalcium Silicate as a Transformation Toughener." M.S. thesis by E. A. Barinek. Submitted Dec. 1987.

"Effect of Phase Transformations, Chemical Doping and Matrix Constraint on the Microstructural Development of Dicalcium Silicate." Ph.D. thesis by C. J. Chan. Supported jointly by NSF and AFOSR through Professors J. F. Young and W. M. Kriven. Submitted Feb. 1989.

"Determination of the Critical Particle Size of Dicalcium Silicate in the Transformation Toughening of Magnesia." M.S. thesis by E. S. Mast, anticipated submission date Oct. 1989.

"Processing, Microstructure and Phase Transformation of Dysprosia in Silicon Carbide Matrix Composites." Ph. D. thesis by Shin Kim, anticipated submission date Jan. 1990.

PUBLICATIONS IN PREPARATION

"Transformation Toughening of Calcium Zirconate by Dicalcium Silicate." E. A. Barinek and W. M. Kriven.

"Crystallography and Kinetics of the Monoclinic (B) the Cubic (C) Transformation in Dysprosia." O. Sudre, K. R. Venkatachari and W. M. Kriven.

At least two further papers from theses are in progress.

SECTION 3 - CONFERENCE PRESENTATIONS

"Possible transformation tougheners alternative to zirconia-crystallographic aspects," W. M. Kriven*. Presented at the Annual Meeting of the American Ceramic Society, April (1986), Chicago.

"Microstructure characterization of non-stoichiometric dicalcium silicates doped with aluminum oxide," C. J. Chan*, W. M. Kriven and J. F. Young. Presented at the American Society for Electron Microscopy (EMSA) 44th Annual Meeting, Albuquerque USA, Aug. 10-15 (1986).

"Possible transformation tougheners alternative to zirconia-crystallographic aspects," W. M. Kriven* presented at the Advanced Ceramics II Lecture Meeting, held at Tokyo Institute of Technology, Japan Sept. 4-5th (1986).

"Dicalcium silicate in the CaO-ZrO-$Si0_2$ system," W. M. Kriven* and C. J. Chan, presented at the Third Int. Conf. on Science and Technology of Zirconia, held at Tokyo, Japan, Sept. 9-11th (1986).

"Transformation mechanisms in confined zirconia particles and in other potential new tougheners of ceramics", W. M. Kriven* (invited paper) presented at Fall Meeting of the Metallurgical Society (TMS) of the AIME, on Physical Metallurgy and Materials, Orlando, Florida, October (1986).

"Possible transformation tougheners alternative to $Zr0_2$-crystallographic aspects" W. M. Kriven.* Abstract (#54-BP-87), presented at the Annual Meeting of the American Ceramic Society, April (1987), Pittsburgh, USA.

"Effect of kinetics on Ca_2SiO_4 microstructure development,"C. J. Chan* and W. M. Kriven. Abstract (#112-B-87), presented at the Annual Meeting of the American Ceramic Society, April (1987), Pittsburgh, USA.

"Development of dicalcium silicate as a transformation toughener," E. A. Barinek* and W. M. Kriven. Abstract (#272-B-87), presented at the Annual Meeting of the American Ceramic Society, April (1987) Pittsburgh, USA.

"Possible transformation tougheners alternative to ZrO_2: crystallographic aspects," W. M. Kriven.* Presented at 12th Conf. on Composites Materials and Structures, Jan. 20-22nd (1988) Cocoa Beach, Florida, USA.

"The stabilizing role of glassy phases on the β to γ transformation in dicalcium silicate," C. J. Chan*, W. M. Kriven and J. F. Young. Abstract (#46-BP-88). Presented at the 90th Annual Meeting of the American Ceramic Society, Cincinnati, May 1-5th, 1988.

"Monoclinic to cubic transformation in dysprosium sesquioxide," O. Sudre, K. R. Venkatachari and W. M. Kriven. Abstract (#47-BP-88). Presented at the American Ceramic Society, Cincinnati, May 1-5th, 1988.

"Microstructural characterization of laser-melted, roller-quenched dicalcium silicate," C. J. Chan,* K. R. Venkatachari, W. M. Kriven and J. F. Young. Presented at the 46th Annual Meeting of the Electron Microscopy Society of America (EMSA), Milwaukee, Aug. 7-12th, 1988.

"Transformation tougheners alternative to zirconia - crystallographic aspects" W. M. Kriven* (invited keynote address). Austceram 88, Int. Ceram. Conf. and Exhibition, held in Sydney, Australia, Aug. 21-26th 1988.

"The monoclinic to cubic transformation of dysprosia," W. M. Kriven* and O. Sudre, Austceram 88, Int. Ceram. Conf. and Exhibition, held in Sydney, Australia, Aug. 21-26th 1988.

"Martensitic toughening in ceramics: possible alternative tougheners to ZrO_2," W. M. Kriven.* Invited paper at DOE-sponsored Int'l Workshop on First-Order Displacive Phase Transformations, held in Berkeley, California, Oct. 23-28th, 1988.

"The monoclinic (B) to cubic (C) transformation mechanism in dysprosia," O. Sudre, K. R. Venkatachari and W. M. Kriven.* Abstract (#100-B-89). Presented at the 91st Annual Meeting of the American Ceramic Society, Indianapolis, April 23-27, 1989.

"Processing and phase transformation of dysprosia in silicon carbide matrix," S. Kim* and W. M. Kriven. Abstract (#18-SI-89). Presented at the 91st Annual Meeting of the American Ceramic Society, Indianapolis, April 23-27, 1989.

"Sintering and microstructural development of dicalcium silicate in magnesia," E. S. Mast* and W. M. Kriven. Abstract (#7-SI-89). Presented at the 91st Annual Meeting of the American Ceramic Society, Indianapolis, April 23-27, 1989.

"Eutectic sintering for formation of dicalcium silicate in magnesia," E. S. Mast*, R. Pilapil and W. M. Kriven. Abstract (#43-BP-89) Presented at the 91st Annual Meeting of the American Ceramic Society, Indianapolis, April 23-27, 1989.

"Martensitic transformations in ceramics," W. M. Kriven* To be presented at the International Conference on Martensitic Transformations (ICOMAT-89), Sydney, Australia, July 3-7, (1989).

"Investigation of the monoclinic (B) to cubic (C) transformation in the lanthanide sesquioxides", W. M. Kriven*, P. D. Jero, O. Sudre and K. R. Venkatachari. To be presented at the International Conference on Martensitic Transformations (ICOMAT-89), Sydney, Australia, July 3-7, (1989).

"Martensitic nucleation and transformation in $\beta \rightarrow \gamma$ dicalcium silicate", W. M. Kriven*, C. J. Chan and E. A. Barinek. To be presented at the International Conference on Martensitic Transformations (ICOMAT-89), Sydney, Australia, July 3-7, (1989).

Determination of the Critical Particle Size of Dicalcium Silicate in the Transformation Toughening of Magnesia

by

E.S. Mast and W.M. Kriven

U.S. Air Force Final Report

Spring 1989

Urbana, Illinois

OUTLINE

1. INTRODUCTION
    1.1 Background
    1.2 Project Objectives
2. REVIEW
    2.1 Previous Work
    2.2 Current Research
3. EXPERIMENTAL
    3.1 Material Processing
    3.2 Characterization
    3.3 Dicalcium Silicate Synthesis
        3.3.1 Dicalcium Silicate Powder Characterization
        3.3.2 Polymer Additions
        3.3.3 Sonic Sieve
            3.3.3.1 Sedigraph
            3.3.3.2 XRD
            3.3.3.3 SEM
        3.3.4 Annealing Effects
        3.3.5 Air Classifier
            3.3.5.1 Sedigraph
            3.3.5.2 XRD
    3.4 Composite Pellet Formation
        3.4.1 Effect of Polymer/Acid/Base Additions
4. RESULTS & DISCUSSION
    4.1 Sieving vs Air Classifying
    4.2 Dusting Properties
    4.3 Densities
    4.4 Microstructures
        4.4.1 SEM
    4.5 Initial Acoustic Emission
        4.5.1 Energy vs. Frequency Histogram
        4.5.2 Particle Size vs. Transformation Energy
        4.5.3 Effect of Thermal History
        4.5.4 Effect of Twin's Presence
        4.5.5 Microcracking
5. CONCLUSIONS AND FUTURE WORK
6. REFERENCES

1. INTRODUCTION

The importance of dicalcium silicate (Ca_2SiO_4 or C_2S) has been studied for some time in various fields. A diagram of its five polymorphic phases is shown in Figure 1.

The β form commonly occurs in Portland Cement but it must be stabilized from undergoing transformation to the more thermodynamically stable γ phase. In the field of cement, hydraulicity is of major concern. The study of β-dicalcium silicate (an impure form known as belite) is important since less calcium hydroxide is formed on hydration, it has a low heat of hydration and helps to form a strong matrix.

It also occurs naturally as minerals known as bredigite (α'-Ca_2SiO_4) larnite (β-Ca_2SiO_4) and an unnamed form (γ-Ca_2SiO_4). In addition dicalcium silicate is of interest in the refractory industry, as in cement the phase transformation from β to γ is considered deleterious. In basic magnesia refractories calcium is usually present as an impurity, which in the presence of silica forms dicalcium silicate. This reaction can occur in refractory bricks when in service or during production. Its formation may even be promoted since C_2S is one of the higher melting silicates.

The β to γ phase transformation is quite powerful since it is accompanied by a 12% volume expansion. Until now there was no attempt to use the energy of this transformation constructively. In addition this large volume expansion makes it a prime candidate for its study as a possible transformation toughener, since the transformation seems to be martensitic in nature. It has shown positive results in preliminary studies(1).

1.1 Background

There are several ways of controlling a martensitic polymorphic transformation:

1) Chemical stabilization,

2) Particle size,

3) Matrix constraint,

Chemical impurities added to the system are thought to act as substitutional cations on the Ca^{2+} sites. The distortion of the surrounding lattice by this substitution affects the rate and/or ability to transform from the monoclinic to the orthorhombic phase.

The ability of a particle to transform is directly dependent on its size. Below a critical cutoff size the particle will not transform to the γ phase. A "single crystal" particle requires a certain amount of energy to overcome the transformation barrier. The difficulty of nucleatiig a transformation increases as the particle size decreases. This was shown specifically for C_2S by Chan(2). X-ray diffraction showed that for a decrease in particle size the magnitude of the γ phase peak subsided while the β phase peak appeared and then increased in magnitude.

Matrix constraint is the primary mechanism used in transformation toughening. This is an appropriate mechanism since the hydrostatic constraining force exerted on the β C_2S particle by the matrix will act in such a way as to alter the energy at the particle surface interface. A disruption of this stress field by the associated stress-strain field of an approaching crack will lower the interfacial energy and thereby allow the formation of the equilibrium γ phase. The exact mechanisms and crystallographic details of this process have yet to be worked out. The process becomes crystallographically complicated very quickly. During the $\alpha'_L \leftrightarrow \beta$ transformation crystallographic twins form(3). The size and orientation of these twins controls the morphology of the β phase. This subsequently plays a role in the kinetics of the $\beta \rightarrow \gamma$ structure change. During the transformation the twinned β converts to an untwinned γ phase. The

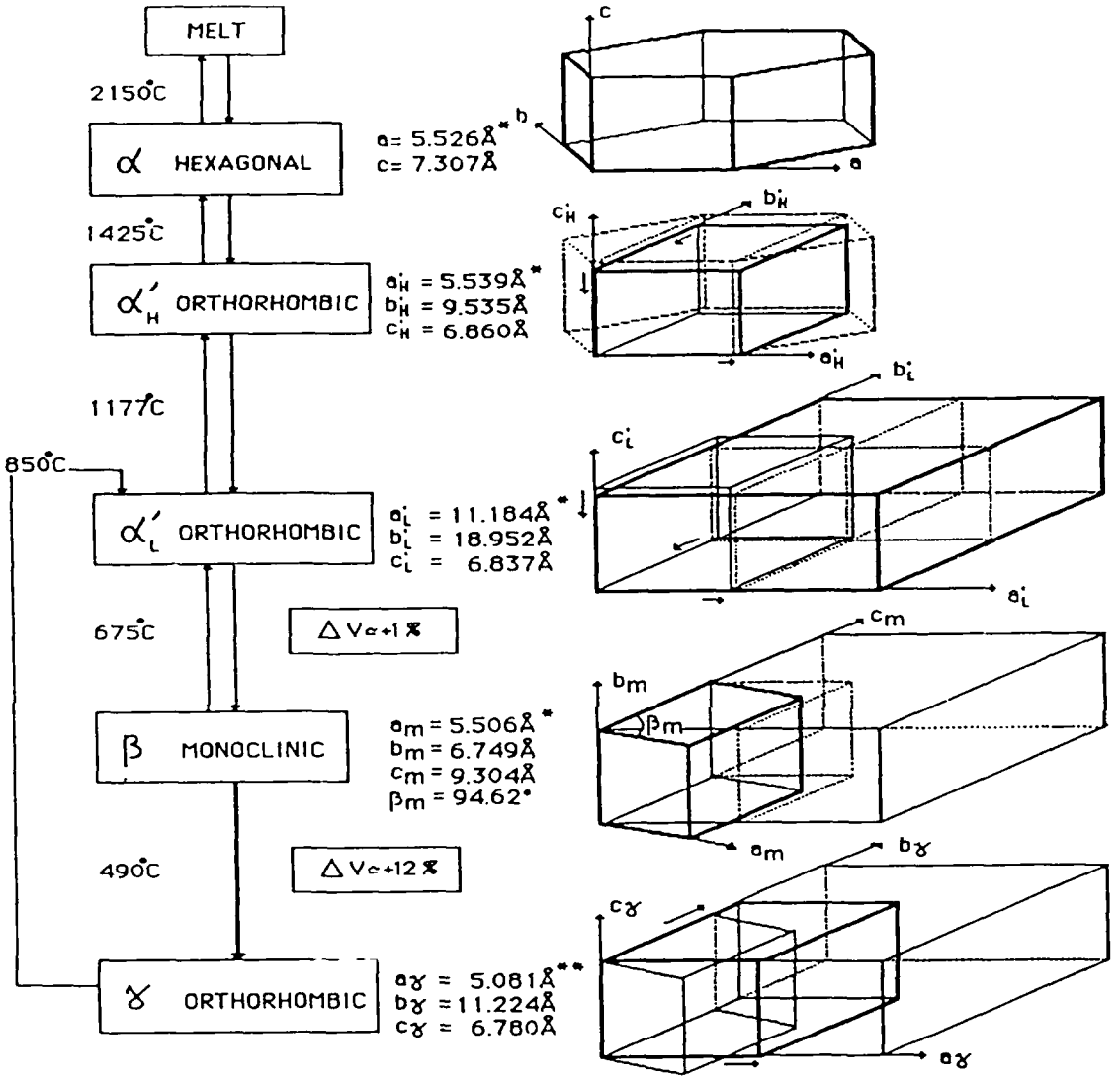

FIGURE 1 Polymorphic transformations of dicalcium-silicate, β to γ is basis of transformatin toughening studies.

* Powder X-ray data from Regourd et al. [12]

For α'_L phase, the single crystal studies on doped Ca_2SiO_4 by Saalfeld [13] and Udagawa and Urabe [14] found that the superlattice is actually along the c-axis and 3 times that of the basic cell.

** Powder x-ray data from Udagawa and Urabe [14]

twins could actually play a key role in the macroscopic $\beta \rightarrow \gamma$ transformation.

1.2 Project Objectives

The goal of this research is to produce a composite of C_2S in magnesia which displays the toughening ability of C_2S for a relatively soft, low elastic modulus material. As shown by the phase diagram, Figure 1.2, there are no intermediate compounds on the MgO-C_2S tie line. Their solid solubilities in one another are low, and the eutectic is at 1800°C.

To produce the maximum toughening effect the composite must be fully dense. Most importantly the critical particle size of C_2S must be determined. Then for optimization of the system the critical volume percent of toughener must be determined. These last two effects may prove to be interdependent due to interlocking stress fields. Optimal firing, cooling and annealing schedules need to be determined concurrently with the composite investigations.

2. REVIEW

This portion of the project was started by E. Mast nineteen months ago. Much old literature, from the late sixties and early seventies, was found on the study and control of C_2S in the basic refractory industry. Some useful literature was also obtained from the cement industry, although the emphasis in both of these fields was directed towards suppressing or eliminating the $\beta \rightarrow \gamma$ transformation. When the transformation occurred it became known as "dusting." Dusting is the phenomenon where refractory bricks containing C_2S were reduced to a pile of "dust" upon exiting the furnace. The uncontrolled $\beta \rightarrow \gamma$ transformation of the C_2S could cause the destruction of a monolithic brick into small ruble. If harnessed, this powerful mechanism could be used for transformation toughening, that is if the mechanism is martensitic.

Martensitic transformations were first discovered in metals. Quenching of steels can create the martensite structure. In fact this

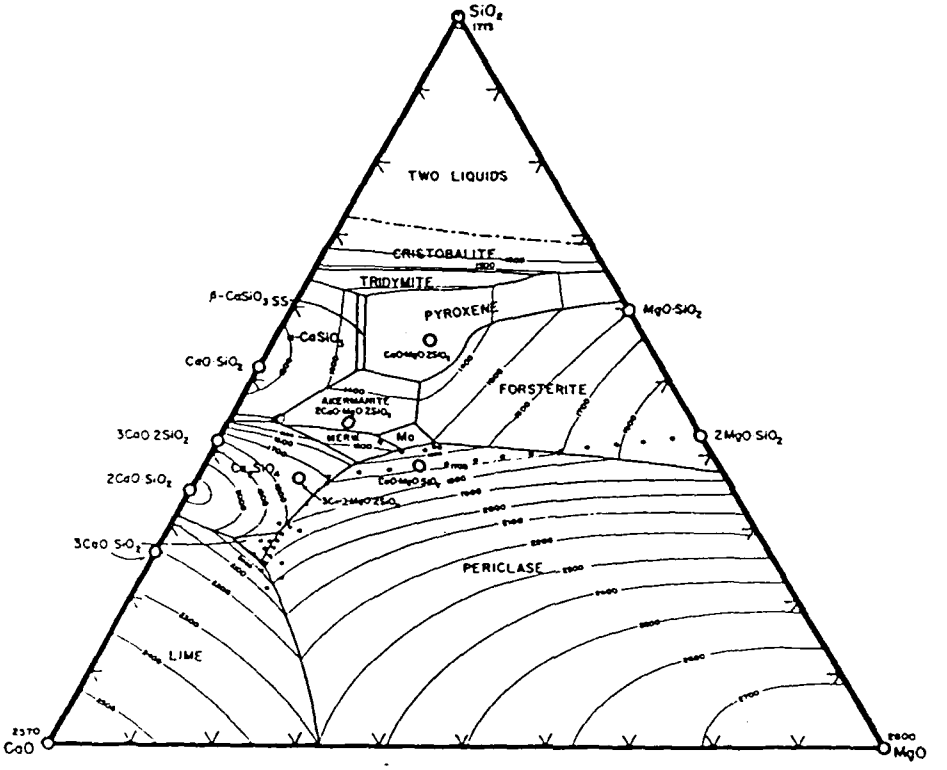

FIGURE 1.2 Magnesia-calcia-silica phase diagram showing magnesia dicalcium-silicate compositional tie line used in current research.

thermodynamically unstable compound is one of the keys to making steel what it is. Internal stresses locked in from quenching are responsible for creating an energy barrier to the kinetics of the transformation. In toughening the external energy applied to overcome the free energy of the transformation energy barrier is acquired from a strain field. This specific type of transformation is termed a shear strain-induced martensitic transformation. As classified by Cohen(4) the necessary and sufficient requirements for martensitic phase transformations are:

a) displaciveness of the lattice distortive type involving a shear-dominant shape change,

b) the transformation does not require diffusion

c) kinetics and morphology during the transformation are dominated by a sufficiently high shear-strain energy in the process.

For C_2S to have a martensitic mechanism it must fulfill these three criteria.

For quite a long time it was thought that this mechanism could not exist in ceramics due to the increased crystaliographic complexity. This idea was suggested to be false in 1968 by King and Yavorsky(5) and proven false by others later. Zirconia was chosen for the material of interest with good reason. It is relatively simple to understand crystallographically and can be controlled by chemical stabilization. It was a good model system shown by its current commercialization applications in such materials as partially stabilized zirconia (PSZ), zirconia toughened alumina (ZTA), and others.

The next logical step in the development of transformation toughening of ceramics is the location of materials alternative to zirconia. This will do at least two things:

a) give a better understanding of the atomistic mechanisms involved in toughening materials

b) gain a further insight into the possible uses of martensitic mechanisms in ceramic systems.

2.1 Previous Work

Some success was seen in the first year of research. Specifically it was initially shown that the system was chemically compatible, and areas for further concentration were defined. Magnesia is not a stabilizer for C_2S. It has minimal solubility in C_2S and likewise for C_2S in MgO.

The first task was to find a satisfactory method for the production of dicalcium silicate for the addition to the magnesia matrix. The method settled upon used calcium carbonate and silicic acid. Both had good reactivities.

The prepared C_2S was attritor milled for various times and then added to a matrix of magnesia. This method was tried first since it was the one currently used by Barinek[1]. It was soon realized that this method was not suitable for my work. Although promising results were obtained, the attritor mill produced a wide distribution of C_2S particle sizes. These distributions were characterized by sedigraph techniques. It was shown that any individual distribution could be shifted systematically by controlling the time of attritor milling. These results were reproducible but only within certain limits.

At the optimal point of attritor milling, thirteen to fourteen minutes, the pellets formed with this C_2S transformed uncontrollably. This was attributed to the presence of a distribution of C_2S particle sizes in the matrix. It is thought that the presence of a

few "large" β C_2S grains which were unstable, induced a self transformation. This is due to the size effect as mentioned previously. If these grains were much larger than the critical particle size for the matrix they would transform to the γ phase without outside stresses to constrain the transformation. The strain induced into the matrix by these transformed grains could in turn induce the same transformation in C_2S grains which would have normally been stable. As this wave spread through the body a progression of β→γ phase changes would ensue and in time the once monolithic piece would be reduced to a pile of powder.

A second problem discovered in the processing was a decrease in the density of the composite pellet as the particle size of the C_2S decreased. At the point of optimal attritor mill time the density of the aggregate pellet was below ninety percent. For best results a fully dense body is desired. This is obvious since a porous body could not exert a hydrostatic pressure on the critical particle size β-C_2S grains. A β-C_2S grain next to a pore would not be in equilibrium and the associated nonuniform stress field would permit the β→γ transformation.

The jobs ahead were to then:

a) narrow the C_2S particle size distribution range

b) alter powder processing to increase the composite density

The former included just trying to define a particle size for these lenticular particles with lath morphology. And to make particle size cuts as clean as possible, thereby narrowing the particle size distribution range. It was clear that another method besides attritor milling needed to be employed in obtaining the desired distribution.

The later involved altering the surface chemistry of the magnesia used as the matrix material. The raw magnesia is a submicron powder with an associated high surface charge. This electrostatic type charge makes the powder difficult to work with. There are unlimited methods of approaching this problem.

2.2 Current Research

The current state of affairs is to take what has been learned from research on the above two problems and use it to make a dense coherent pellet containing C_2S grains of critical particle size and test their toughness. The optimal volume percent loading and related grain size of the C_2S will be determined next. The toughness increase will be maximized in this ideal system.

3. EXPERIMENTAL

3.1 Material Processing

Processing is one of those things that could go on indefinitely. It is a rare situation when one can no longer make improvements in a process. Unfortunately this case is not special. The method of processing has been changing and improving as the project progresses.

3.2 Characterization

Several methods were used to analyze the powders and the resulting composite pellets. One of the most powerful and useful was scanning electron microscopy (SEM). The morphology of the C_2S powder was continually checked and studied using the SEM. X-ray diffractometry (XRD) also allowed a continual analysis of the phases present during the steps of processing. Other methods included the sedigraph for a spherical Stoke's equivalent particle size analysis. A sonic sieve and an air classifier to determine particle size distributions and extract desired particle size cuts.

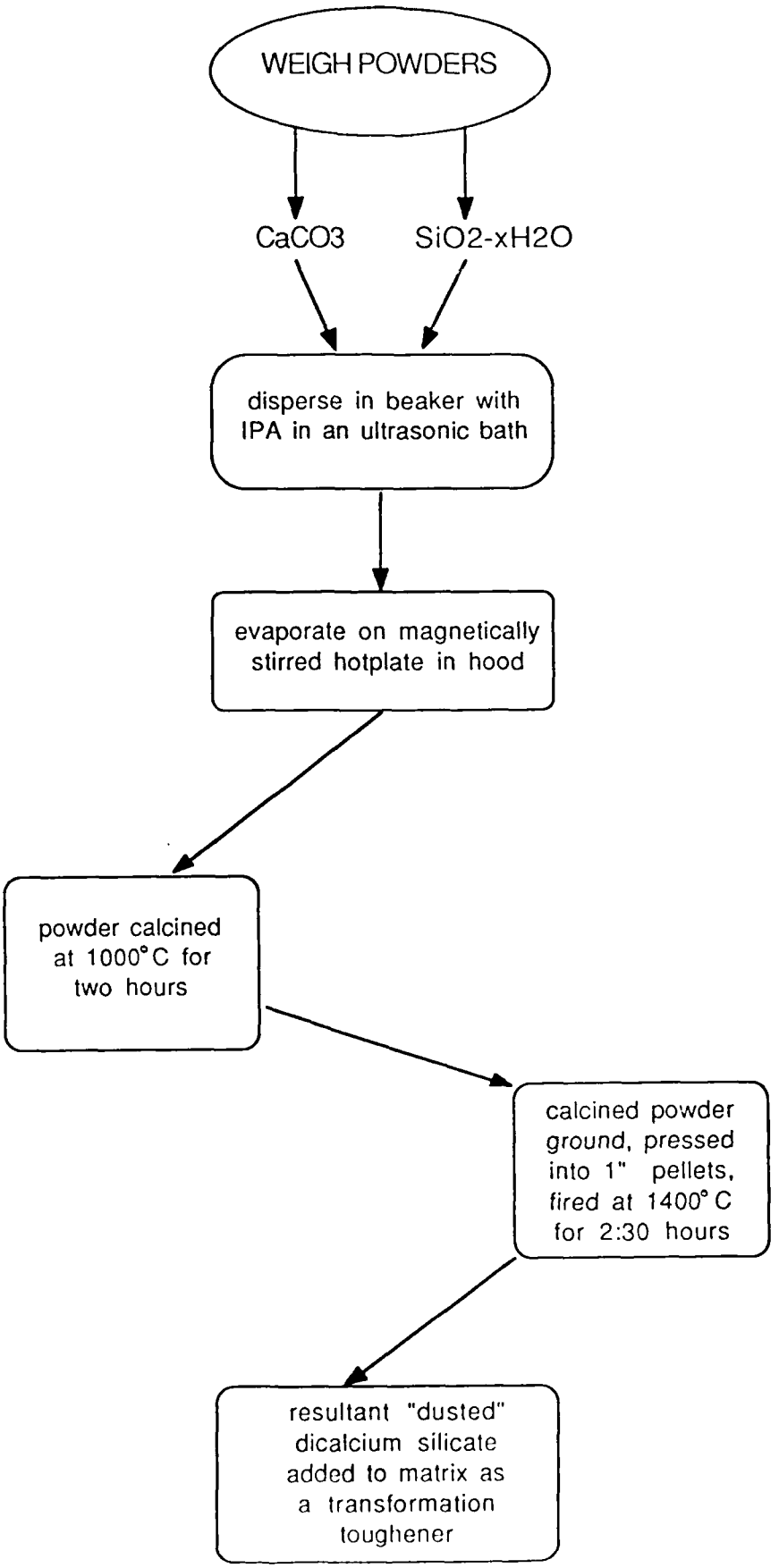

FIGURE 3.3 Flow chart showing processing used in formation of dicalcium-silicate.

3.3 Dicalcium Silicate Synthesis

Specifics on the raw materials used are included in Appendix 1. Figure 3.3 gives the flow chart for C_2S production. The new C_2S forming method is as follows:

i) mix calcite and silicic acid ultrasonically in isopropanol (IPA)
ii) evaporate off alcohol on a hot plate with stirring in a hood
iii) initial calcination at 1000°C for 3 hours in a Teresco furnace
iv) mix/grind with mortar and pestle, sieve with 100 micron sieve
v) press 1" pellets, B60A as binder, 2500 lbs. uniaxial pressure
vi) react at 1450°C for 2 hours
vi a) anneal at 900°C for 2 hours (only used with air classifying)
vii) transformed powder ultrasonicated in IPA with B60A to decrease fragility
viii) stirred/dried on a hotplate in a hood
ix) particle size separation of dried powder

3.3.1 Dicalcium Silicate Powder Characterization

Variables in processing of the C_2S were altered or steps were added as more was learned about its nature. It is a very fragile material just after forming composed of loosely joined bundles of laths easily disrupted by further handling. When this happens individual laths can be knocked off which decreases the effective particle size. For this reason steps; vi a to viii, were added after observations of how the powder was acting during processing. Discussion of this is below. Steps; iv and v, were added when some

unreacted powders remained after processing. In this alternating way of processing and characterization the current method of processing resulted.

3.3.2 Polymer Additions

A rough determination of the amount of B60A required to coat the surface of a gram of C_2S was determined by a test tube series. To a rack of test tubes, each containing two grams of C_2S in IPA, different amounts of B60A acrylic resin was added. The C_2S was as prepared before size fraction separation. Ultrasonicating was used to mix the solutions. After allowing the solutions to come to equilibrium overnight it was determined that 0.3 mls of a $2.5X10^{-5}$g/ml solution per gram was best. The solution with lowest bulk volume was termed the best. This is because a monolayer coverage of the polymer, without agglomeration, will give the best packing of the powder. The surface charge will be just saturated with no additional agglomeration from additional polymer. It is hoped, but not proven directly, that this polymer, when dried onto the surface and in the cracks of the C_2S, will give added strength to the particles during further processing. The fragility of the larger particles was of a major concern if they had happened to have the critical particle size.

3.3.3 Sonic Sieve

A complete particle size analysis series was done for several different batches of C_2S to check the integrity of the formation process. The results showed relative consistency but gave a spread on the small particle size end of the distribution. The tabulated results of this series is contained in Figure 3.3. From the C_2S powder collected, both polymer treated and untreated, composite pellets were formed containing 15 volume percent loading. Pellets were fired just as the pure magnesia matrix pellets were fired. The pellets were not annealed.

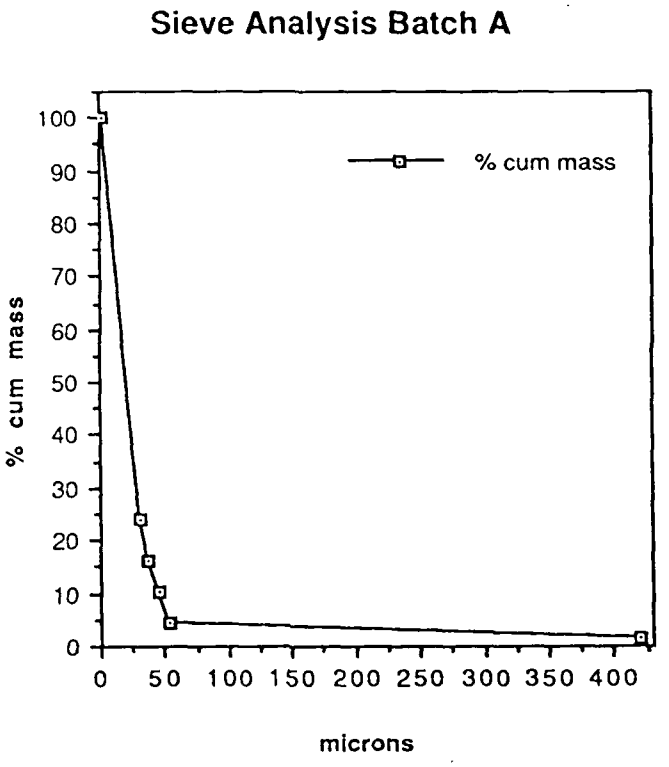

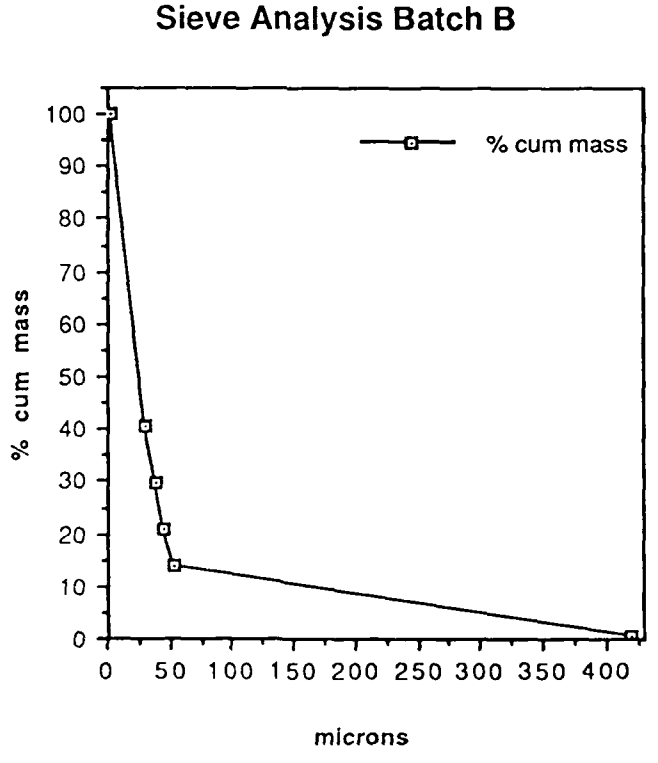

FIGURE 3.3.3 Particle size analysis by sieving of dicalcium silicate as formed.

There seemed to be a difference in the polymer treated C_2S composite pellets in that they tended to complete their transformations faster and more completely than the untreated ones. This was based on empirical observations. Nothing quantitative could be attained.

The pellets of -20 +10 micron size C_2S transformed only at the surface. Magnesia has a relatively low vapor pressure. So one possible explanation is MgO at the surface volatilized and left a C_2S enriched layer which initiated its own transformation. This surface transformation occurred within a day after the pellet was removed from the furnace and kept in a dessicator. Densities of the green and fired pellets were measured. Transformation had begun before densities were taken. These pellets continued transforming over the period of a month. Annealing should have caused equilibrium to occur, allowing full transformation even before complete cooling. Therefore the critical particle size cannot be attained using sonic sifting since this (-20 +10 micron) is the smallest size attainable by this method. Attention will now be diverted to air classification to see if it can offer a smaller narrower distribution for addition to the composite.

3.3.3.1 Sedigraph

The sedigraph uses X-rays to determine particle size and will give a Stoke's equivalent particle size distribution. This method uses a spherical particle approximation. It will also give a relative size distribution of a powder. As mentioned previously it was used to determine the particle size distribution after attritor milling. This will be a useful method for determining and given distribution between two cuts from the air classifier.

3.3.3.2 XRD

A series of standards were prepared from the sonic sieve fractions of both annealed and not annealed treated γ C_2S, and not treated unannealed C_2S. A comparison between the annealed and both of the unannealed, one with B60A and one without B60A, fractions yielded an interesting result. The 2Θ values of 2.59 and 2.80 with respective (h k l)'s (041) and (040) gave a relative intensity difference. The peaks also showed slight shifts. This has not been studied further. A higher resolution machine with higher precision needs to be used in order to quantify these effects.

The X-raying of pellet surfaces gives a semiquantitative analysis of the relative amounts of β and γ phases. A controlled induced transformation, such as by grinding, can be followed with this method.

3.3.3.3 SEM

The scanning electron micrographs give the best results to date. They show the progression in particle size distributions of both the sonically sifted and air classified C_2S. The micrographs are included in Appendix 2.

The morphology of the larger particles appears more spherical while the smaller fractions appear more lath like.

Cracks generated from the powerful 12% volume expansion of the β-γ transformation in C_2S separate bundles of laths. The cracks extend along the c-axis direction parallel to the lath length. At the same time these cracks occur between laths separating them into bundles. The different methods of comminution increased the cracking and proliferated individual lath separation. These fragile pre-cracked bundles are easily disrupted and split-up into smaller bundles or single laths. This was first noticed when sonically sifted C_2S of a larger particle size was ultrasonicated in a solution of alcohol.

3.3.4 Annealing Effects

For the full effect of the transformation the pellets need to be annealed. A temperature of 900°C was chosen as the annealing temperature, this is the temperature Chan used. Annealing of the final composite pellets assured a more reactive equilibrium structure for the β-C_2S. A control of the $\alpha'_L \leftrightarrow \beta$ transformation at ~675°C is necessary to control the twin characteristics of the β-C_2S. It is thought that the atomic kinetics are fast enough at 900°C to attain the equilibrium structure. This will guarantee the fastest $\beta-\gamma$ transformation possible with no mechanistic hindrance from diffusion.

3.3.5 Air Classifier

The sonic sieves did not give satisfactory results for the particle size required. The air classifier offers a possible alternative which can provide the extremely narrow distributions required.

With the air classifier the classifying wheel speed and air volume are controlled to give a distinct cut point for a material. One feed jar and two collection jars are employed, one collection jar for the coarse fraction and one collection jar for the fine fraction. To obtain one distribution two cut points are selected. This means that the selected material needs to be run through a minimum of twice. Particle size reduction is severe and the resulting powder shows some contamination from the process. The contamination has not been quantified but there is a distinctive color change from the white powder which goes in and the gray powder which is collected in the jars. The contamination is most severe on the first run but appears to get only slightly worse with continued cutting of the powder.

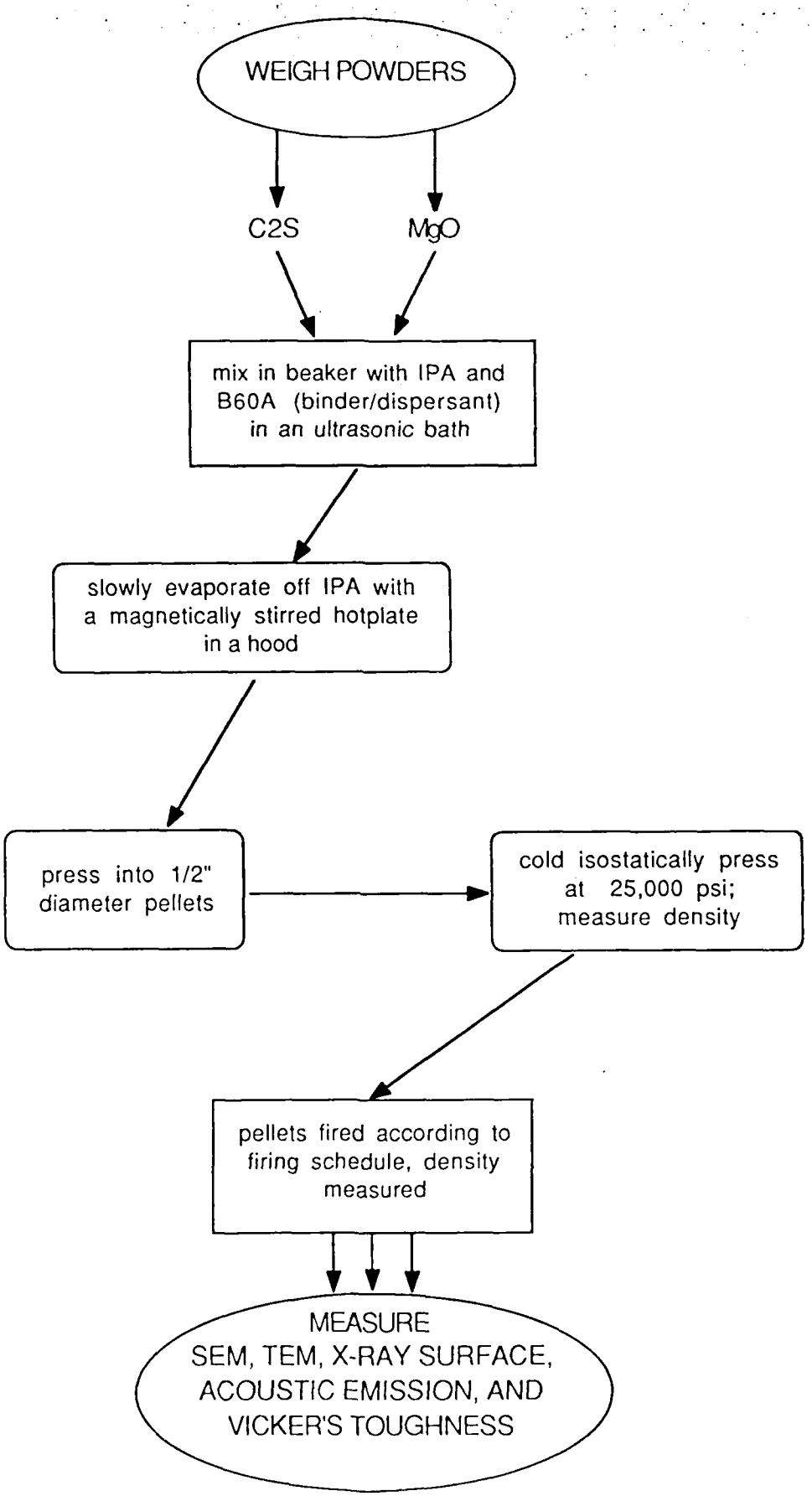

FIGURE 3.4 Flow chart showing processing used in formatin of composire pellets.

3.3.5.1 Sedigraph

A complete analysis of the particle size fractions obtained from the air classifier at different speeds is included in Appendix 3. The distributions are much narrower than those from the attritor mill, they are comparable to those of the sonic sifter but at a smaller particle size. This is exactly the type of distribution desired, the only other way to obtain these type of cut sizes may be from a wet chemical technique.

A graph showing the three cuts of C_2S used in the formation of 15 volume percent loaded composites is shown in Appendix 3.

3.3.5.2 XRD

The air classified C_2S powder was not X-rayed for phase determination due to the small amounts of powder obtained by this method.

3.4 Composite Pellet Formation

A flow chart giving the processing steps for the formation of the composite pellets is shown in Figure 3.4. In obtaining a dense composite a dense matrix was a prerequisite. Four surface modifiers were tried with the pure matrix material and processed analogously to the composite.

3.4.1 Effect of Polymer/Acid/Base Additions

A series of experiments was conducted in which two different polymers, an acid, and a base were individually added to the magnesia matrix material and densities measured. Dicalcium silicate was not used in this series. The amount of additive per gram of powder varied. Accompanying density changes were tabulated and graphed in Appendix 4. The order of additions was randomized to exclude any systematic error. The amount of uniaxial pressure

required to obtain coherent pellets dropped drastically with all additions.

The sub-micron magnesia starting material was most likely prepared in a wet chemical method by precipitation. Therefore it is difficult to know whether it has a positive, negative, or neutral surface charge which would depend on the pH of the solution from which it was formed. The surface charge must be suppressed to allow for the best particle packing in the pressing step and therefore the highest green density.

The base, acid and two polymers used were respectively ammonium hydroxide, nitric acid, B60A an acrylic resin, and B-76 a polyvinyl butyral. The amounts of each added is included in Appendix 4. Stock solutions of nitric acid and ammonium hydroxide were prepared and had calculated pH's of 0.07 and 11.50 respectively. The processing of the magnesia pellets was as follows:

i) add acid/base to approximately 250ml of IPA ultrasonicate

ii) add 5.000g of MgO powder to ultrasonicating solution, ultrasonicate at least five minutes for mixing

iii) evaporate off alcohol on a hot plate with stirring in a hood

iv) dry powder forced through 100 micron sieve

v) press $^1/_2$" pellets ~750 lbs. uniaxial pressure

vi) fire at 1550°C in Teresco furnace for 3 hours

Tables were formed using Excel on the Macintosh, the results were then plotted using Cricketgraph.

A trend was seen just as in the case of the polymers. For the nitric acid there was an initial increase up to 0.30ml in the density followed by a decrease, then another gradual increase was seen for further increases in concentration up to about 3.00ml. For the ammonium nitrate the trend was almost exactly opposite, there was a sharp decrease in density at 0.30ml. This was followed by an increase in density up to about 1.5 ml of base, then again exactly

paralleling the trends in the acid there was a gradual decrease in density up to about 3.00ml NH_4OH. The trends in the final densities of the acid and base were opposite in nature. An explanation for this behavior is just the same as that for the polymer system. Repeating from before, the initial peak in the density data arises from fulfillment of the surface charge on the powder surface. After this point the second peak is due to the formation of agglomerations or flocs, partial flocculation is known to increase the density of a body when the flocs reach a certain concentration. Initially agglomerations decrease the density which is what was observed. But the further increase in acid or base brought about an increase in the floc concentration and thus density. This second peak is explained by the fact that packing of a range of particle sizes is more efficient than the packing of mono-size spheres. For the processing of the powders I will stick to the area of the first peak where there are no agglomerates to complicate things. By adding the C_2S after the initial preparation of MgO the formation of flocs of pure C_2S could probably be avoided.

4. RESULTS & DISCUSSION

4.1 Sieving vs Air Classifying

The smallest size fraction obtainable with a lower limit (-20 +10 microns) was still too large for a fifteen volume percent loading of C_2S. The -10 micron C_2S particle size distribution was too wide and did not allow for control.

4.2 Dusting Properties

In the pellets where a self induced transformation occurred X-ray analysis showed no detectable β-C_2S remaining. This correlates well with the theory. By containing a particle size larger than the critical particle size the matrix could not supply the restraint necessary to inhibit transformation resulting in a complete β–γ transformation of all the C_2S.

The thermal stress relief anneal at 725°C was added in order to allow for a decrease in the C_2S stress field. There is an accumulative -6.5% thermal contraction from the above transformations. After this step was included the pellets containing C_2S of the critical particle size dusted completely. The stress relief caused the apparent critical particle size to increase slightly. This anneal also allowed for an immediate and complete transformation of the pellets containing the C_2S slightly greater than the critical size. Previously the pellets transformed from the surface out over a given time interval depending on the C_2S particle size.

4.3 Densities

Densities were measured using the Archimedes technique. Hexachloro-1,3-butadiene (98%) was used as the fluid due to its good surface wetting. Densities were all above 95% in the composites formed from the three air classifier cuts mentioned earlier.

4.4 Microstructures

The primary method of microstructure characterization at this time is by SEM. After bodies containing the critical particle size of C_2S have been formed then work will commence on the TEM. With TEM the effect of twin size and lattice correspondence effects can be better studied.

4.4.1 SEM

Initial success can be seen from the SEM micrographs in Appendix 2. The morphology of the larger particles appears more spherical while the smaller fractions appear more lath like. Particles are well distributed within the matrix . The shape of the classified C_2S is maintained after densification of the matrix around the particle. Any porosity present appears to be near the C_2S grains.

Surfaces were prepared by:

a) Polishing to six microns with diamond paste

b) Thermal etching immediately after polishing according to the schedule in Appendix 5.

4.5 Initial Acoustic Emission

Acoustic emission is a method which uses a transducer to "listen" to events occurring in a body, such as the phase transformation of a particle or the propagation of a crack. The theory is nearly identical to sonar listening for submarines. Just as the reader, when he was young, probably listened to trains by placing his ear on the railroad track, the transformation of a particle can be heard by a transducer coupled to the pellet. If the train derailed while someone was listening he would be able to tell that something different from the normal had just happened. Likewise when different events occur in the sample there would be a difference in what is "heard." Three separate events that were recorded while a pellet was undergoing self induced transformations are shown in Appendix 6.

4.5.1 Energy vs. Frequency Histogram

By collecting multiple events arising from a particular type of phenomena, an energy-frequency histogram can be produced. Statistically there will be variation in the magnitude of a particular type of event due to the mechanics and electronics of the detection system, therefore a histogram is used to give a representative energy distribution for an event type.

4.5.2 Particle Size vs. Transformation Energy

Since the energy released from the transformation of the particle is directly related to the energy received by the transducer, the transformation of a larger particle will relate to a higher energy signal being received by the transducer.

Several ideas, or questions related to this area of study now arise.

a) Is it possible to obtain a particle size distribution determined by the energy of the transformations?

b) Which particles actively contribute to the toughening effect? Which ones transform first?

c) Does the transformation of the larger particles induce a transformation in the smaller surrounding particles?

d) What is the size of the transformation zone? How many particles does it affect?

By employing a double transducer technique the location of a specific event can be determined.

4.5.3 Effect of Thermal History

It has been seen that the rate of cooling through some of the upper transformations will have a definite effect upon the β–γ transformation. In pellets that contain a C_2S particle size just larger that the critical particle size, for that particular volume percent loading, self induced transformation occurs. The 6.5% thermal shrinkage of the C_2S, if not relieved, will have an effect on the transformation. Acoustic emission can be used to monitor the effects of this stress on the transformation. A prime opportunity is offered here to study the interrelated effects of a known hydrostatic stress,

known particle size distribution and reducibility of the transformation.

The rate of decay of the body can also be analyzed as the transformation zone progresses through it. The matrix constraint stress relief due to either the disruption of the surrounding uniform stress field by the transformation of neighboring particles or directly by exposure to the unconstrained free surface might initiate this self induced transformation.

4.5.4 Effect of Twin's Presence

Twins are formed when the C_2S undergoes the $\alpha'_L-\beta$ transformation. The propagation of the transformation through the twin structure is not well understood. The use of acoustic emission may be able to help understand how twins accommodate this transformation and how the lattice correspondence relation between the b and c axes occurs. Do all the twins "pop" into position simultaneously or is it actually a multiple event with the twins falling rapidly like dominoes?

The monoclinic-orthorhombic ($\beta-\gamma$) transformation in dicalcium silicate is unique from the analogous tetragonal-monoclinic transformation in zirconia since it enters the transformation already twinned. Whereas the zirconia forms twins during this transformation. It may be possible to detect the effects of the twins on the transformation by analyzing differences in the characteristic energy, frequency or other parameter. Twin width, length and/or volume may alter the characteristics of the transformations as received by the electronic instrumentation.

4.5.5 Microcracking

Since microcracking in addition to transformation toughening is a contributor to toughness increase of a ceramic it would be beneficial to find how the two are interrelated. Acoustic emission can be used to determine the link of how a portion of the energy of a transformation can be transferred to the initiation of a microcrack.

These two events should be easily distinguishable by their characteristic energy and frequency.

The stress of the matrix material surrounding a transforming particle must be relieved in some manner. This relief can be in the form of microcracking or the rapid expansion of microcracks already present in the particle's associated stress field. The elastic modulus can help determine the propensity of microcrack formation.

It should also be possible to observe a transformation which formed microcracks to initiate further transformations. The multiple event may occur at the speed of sound, but it should still be possible to resolve the contributions of the individual events from the superimposed signal which is received.

5. CONCLUSIONS AND FUTURE WORK

A composite of matrix stabilized β-C_2S in magnesia has been obtained in which the particle size has been controlled.

Firstly the toughness needs to be determined. Vickers indentation will be used to measure the toughness. The toughness results will be useful to compare to the results obtained by Barinek for C_2S in calcium zirconate (CZ). Calcium zirconate is a hard matrix compared to magnesia. A transformation zone will be looked for around the cracks initiated by the indenter using SEM.

TEM will be used to look at the C_2S grain interfaces to study the effect and method of constraint on both phases.

Acoustic emission can be used to help understand the transformation *insitu*. The properties of the transformation can be analysed while the particles of C_2S are completely constrained by the matrix and a crack is induced.

Many parameters such as higher temperature transformations (those above the β–γ transformation), twin size, residual thermal stresses and the effect of thermal cycling through the changing lattice correspondences affect control of the β–γ transformation in C_2S.

6. REFERENCES

1. E.A. Barinek, "The Development of Dicalcium-Silicate as aTransformation Toughener," M.S. Thesis, W.M. Kriven advisor, submitted Dec 1987.

2. C.J. Chan, "Effect of Phase Transformations, Chemical Doping and Matrix Constraint on the Microstructural Development of Dicalcium-Silicate," Ph.D. Thesis, W.M. Kriven advisor, submitted Feb 1989.

3. G.W. Groves, "Twinning in b Dicalcium-Silicate," Cem. Concr. Res. 12 619-624 (1982).

4 M. Cohen G.B. and Clapp, "On the Classification of Displacive Phase Transformations," Plenary Lecture, Proc. ICOMAT, MIT, Cambridge,MA, (1979)

5 A.G. King and P.J. Yarvorsky, "Stress Relief Mechanisms in Magnesia and Yttria-Stabilized Zirconia," J. Am. Cer. Soc., 51 [1] 38-42 (1968).

Appendix 1

Raw Materials
&
Processing Additives

MAGNESIUM OXIDE

Manufacture	Mallinckrodt
lot#	6015 KXDL
chemical analysis	Ammonium Hydrate Ppt...0.02%
	Barium(Ba).....0.005%
	Calcium(Ca).....0.05%
	Heavy Metals (as Pb).....0.003%
	Insoluble in HCl.....0.02%
	Iron (Fe).....0.01%
	Loss on Ignition.....2.0%
	Manganese(Mn).....0.0005%
	Nitrate (NO3).....0.005%
	Potassium (K).....0.005%
	Sodium (Na).....0.5%
	Soluble in Water.....0.4%
	Strontium (Sr).....0.005%
	Sulfate&Sulphite(as SO4)0.02%

CALCIUM CARBONATE

Manufacture	FISHER SIENTIFIC
lot #	874601
chemical analysis	Sodium (Na).....0.03%
	Strontium(Sr).....0.02%
	Insoluble in dilute
	Hydrochloric Acid.....0.002%
	Water-Soluble Titration
	Base.....0.0004meq/g
	Chloride (Cl)..... 0.0005%
	Oxidizing Substances
	(as NO3)..... 0.005%
	Sulphate (SO4)..... 0.008%
	Ammonium (NH4)..... 0.003%
	Barium (Ba)..... 0.001%
	Heavy Metals (as Pb).... 0.0002%
	Iron (Fe)..... 0.0005%
	Magnesium (Mg)..... 0.01%
	Ammonium Hydroxide ppt 0.01%
	Potassium (K)..... 0.002%
	Flouride (F)..... 0.0006%

SILICIC ACID

Manufacture	Mallinckrodt
lot #	2847 KMND
chemical analysis	Chloride (Cl)..... <0.01%
	Heavy Metals (as Pb).. <0.002%
	Iron (Fe)..... 0.0008%
	Nonvolatile with HF..... 0.04%
	Loss on Drying..... 6%
	Loss on Ignition..... 11.5%

RHOPLEX

Manufacture	Rohm and Haas
lot #	339044
Grade	B-60A
Code	6-5159
Chemical Analysis	Acrylic Resin

POLYVINYL BUTYRAL

Manufacturer	Monsanto
lot #	2929,Bulvar B-76

Appendix 2

SEM Micrographs of Dicalcium Silicate Powder

Figure 1 SEM micrograph of sieved -30 +20µm Ca_2SiO_4 particles after ultrasonication in isopropyl alcohol with "optimal" B60A.. Shows uniformity of particle size and morphology.

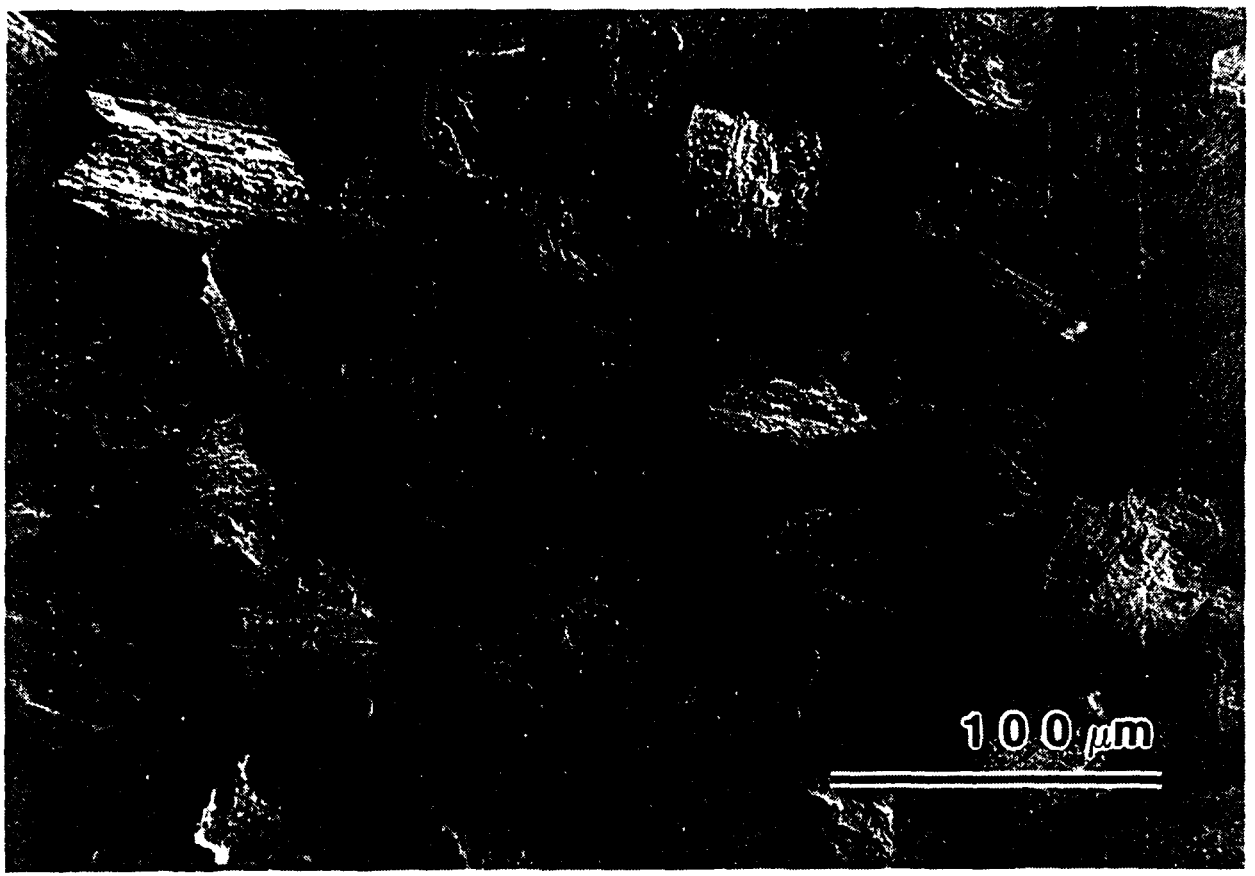

Figure 2 SEM micrograph of sieved -20 +10mm Ca_2SiO_4 particles after ultrasonication in isopropyl alcohol with "optimal" B60A. Shows uniformity of particle size and morphology. Note exposed lath structure.

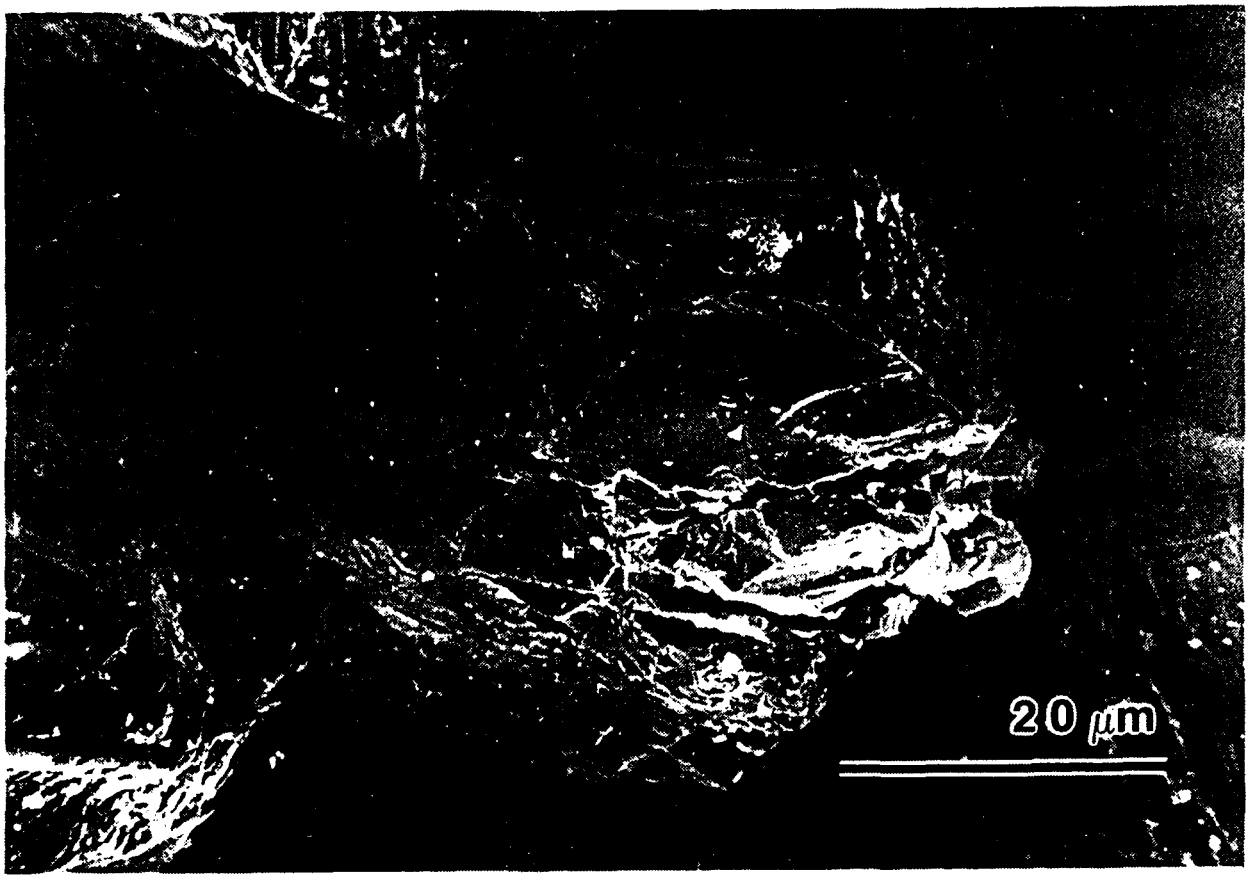

Figure 3 SEM micrograph of sieved -20 +10μm Ca_2SiO_4 particle after ultrasonication in isopropyl alcohol with "optimal" B60A. Severe cracking shows result of 12% volume expansion. Cracks extend along the c-axis parallel to lath length.

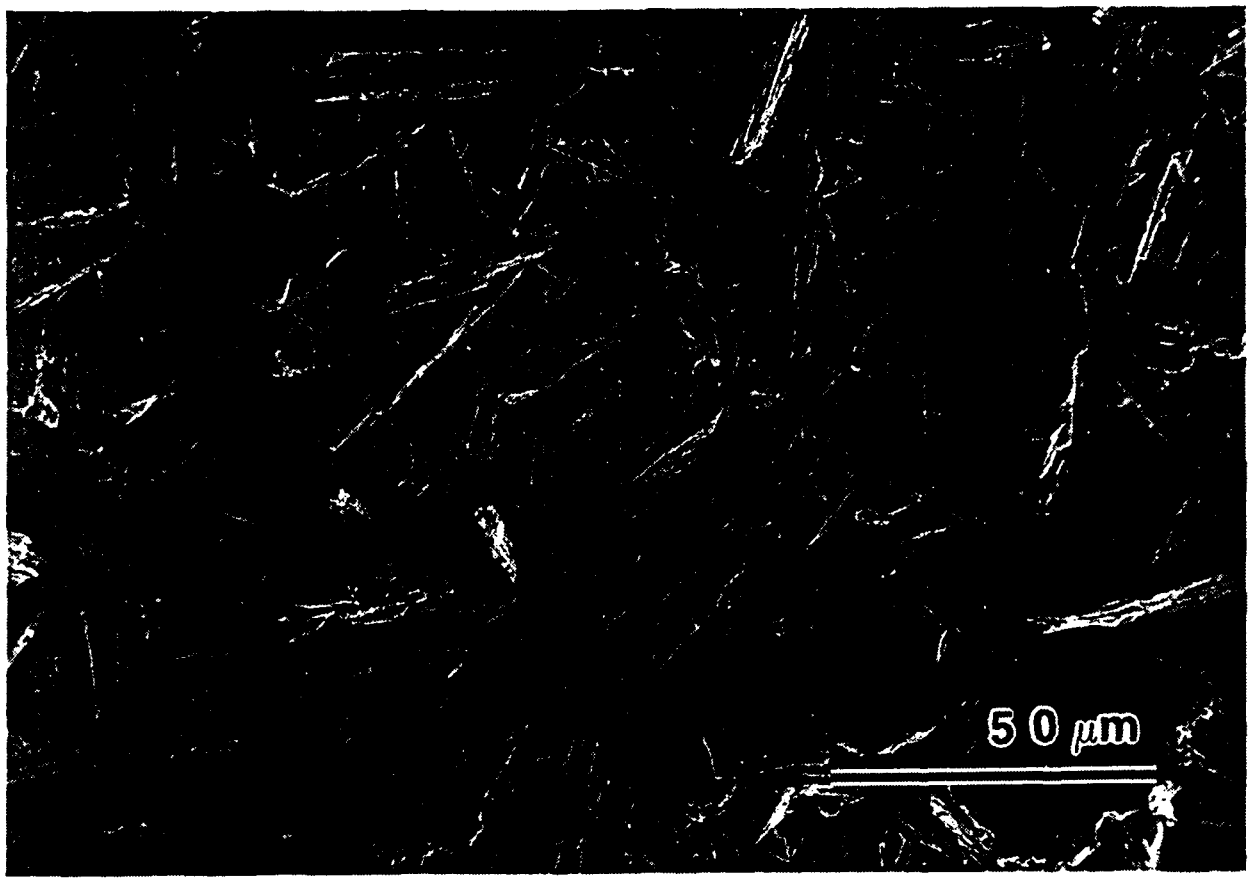

Figure 4 SEM micrograph of sieved -10µm Ca_2SiO_4 particles annealed at 900°C for two hours. Ultrasonicated in isopropyl alcohol with "optimal" B60A. Breaking up of lath bundles leaves particles with exagerated lath structure.

Appendix 3

Air Classifier Calibration Curve and Results

CALIBRATION CURVE FOR AIR CLASSIFIER

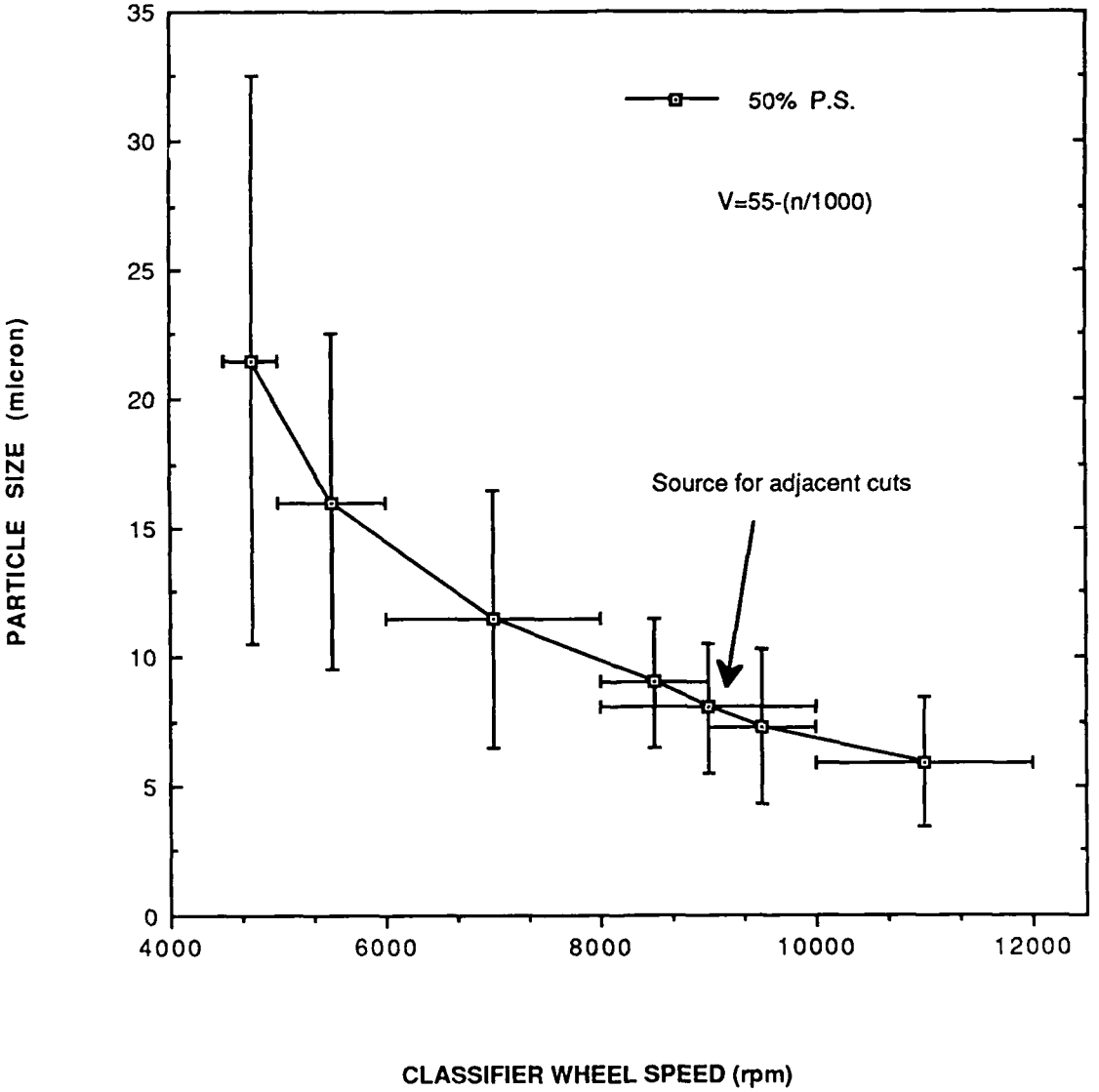

SEDIGRAPH ANALYSIS OF AIR CLASSIFIER DATA

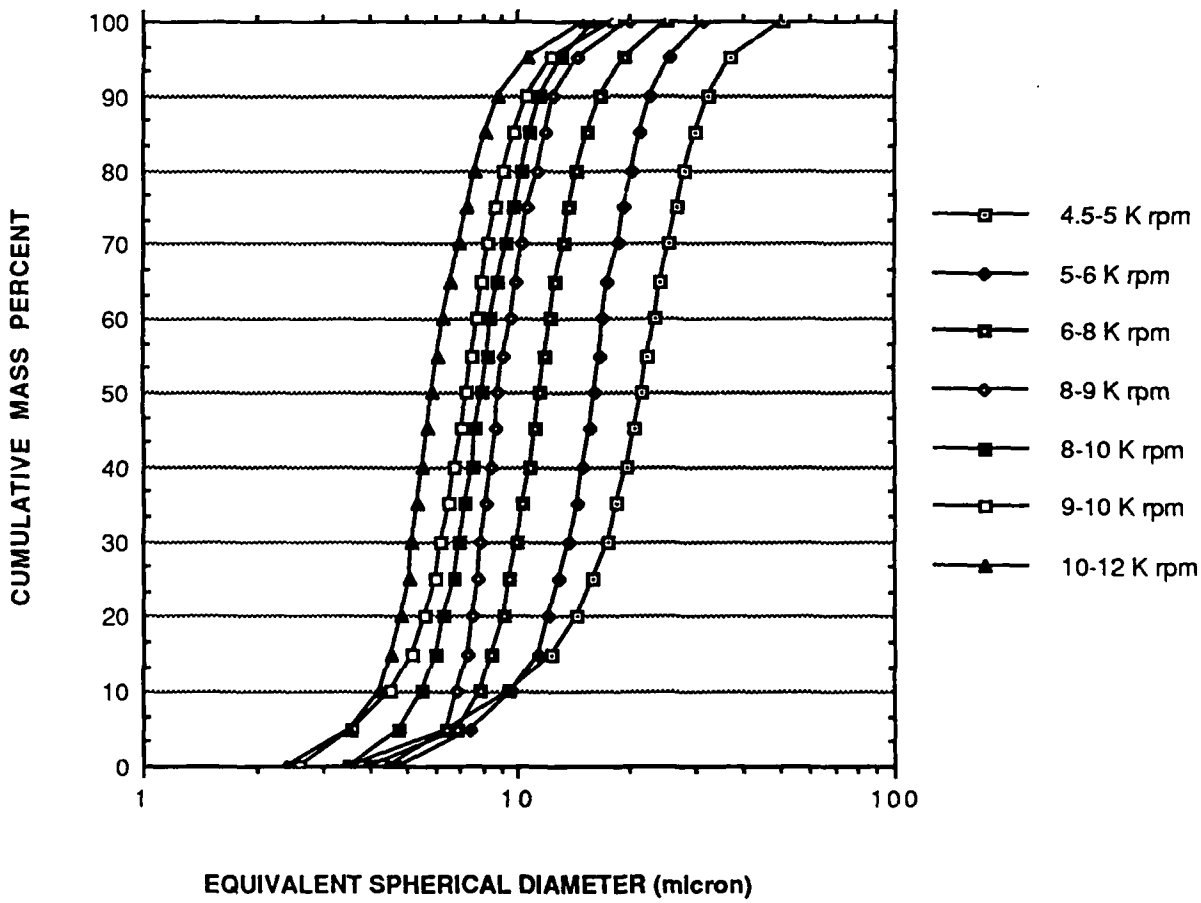

SEDIGRAPH ANALYSIS OF AIR CLASSIFIER DATA

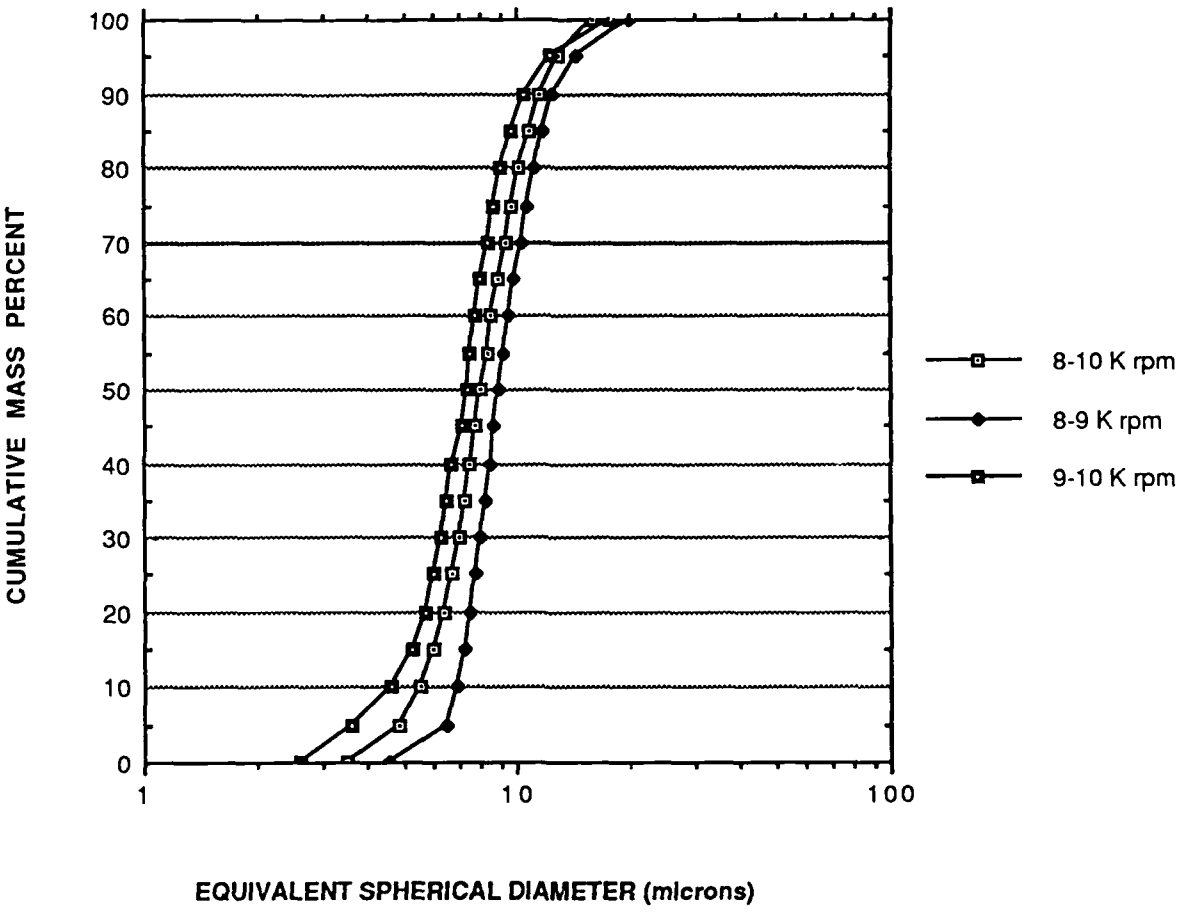

Appendix 4

Matrix Densification Surface Modifier Results

NH4OH DENSITY DATA

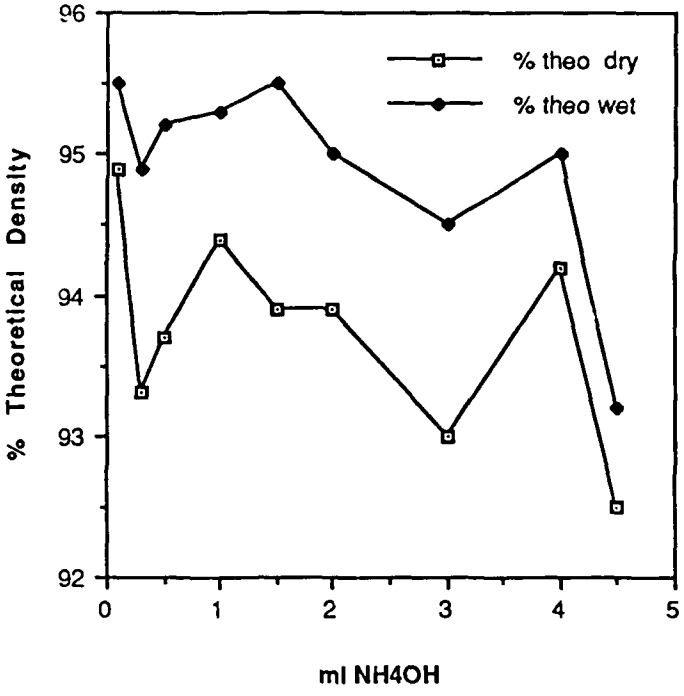

HNO3 DENSITY DATA

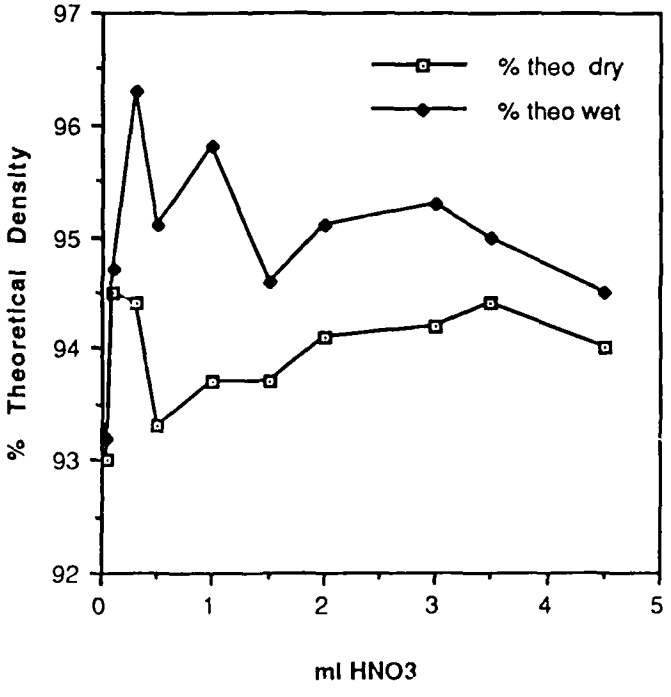

Polymer B60A Density Data

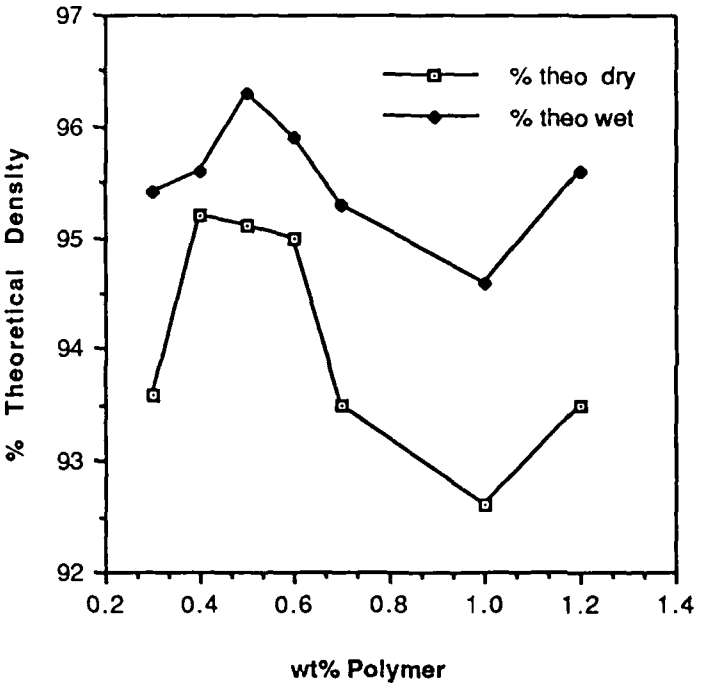

Polymar B76 Density Data

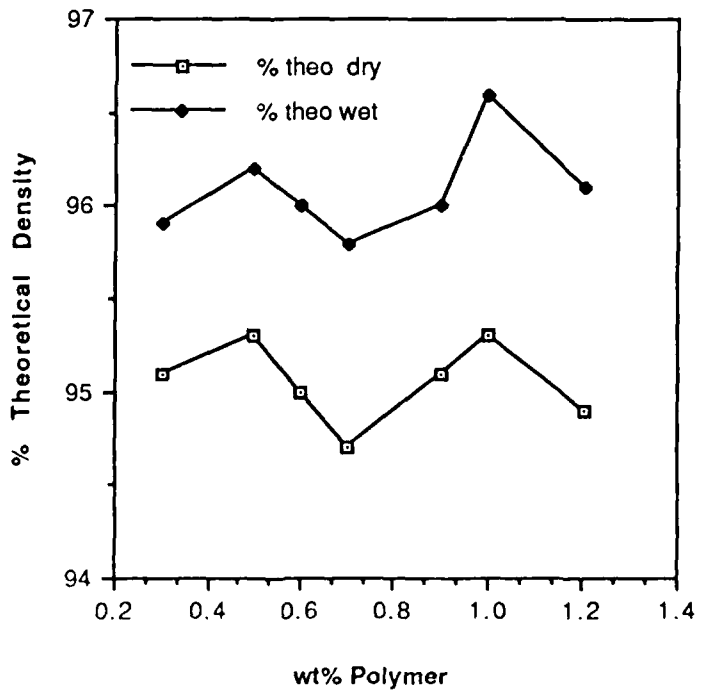

Appendix 5

Furnace Schedules

SAMPLE FIRING SCHEDULE

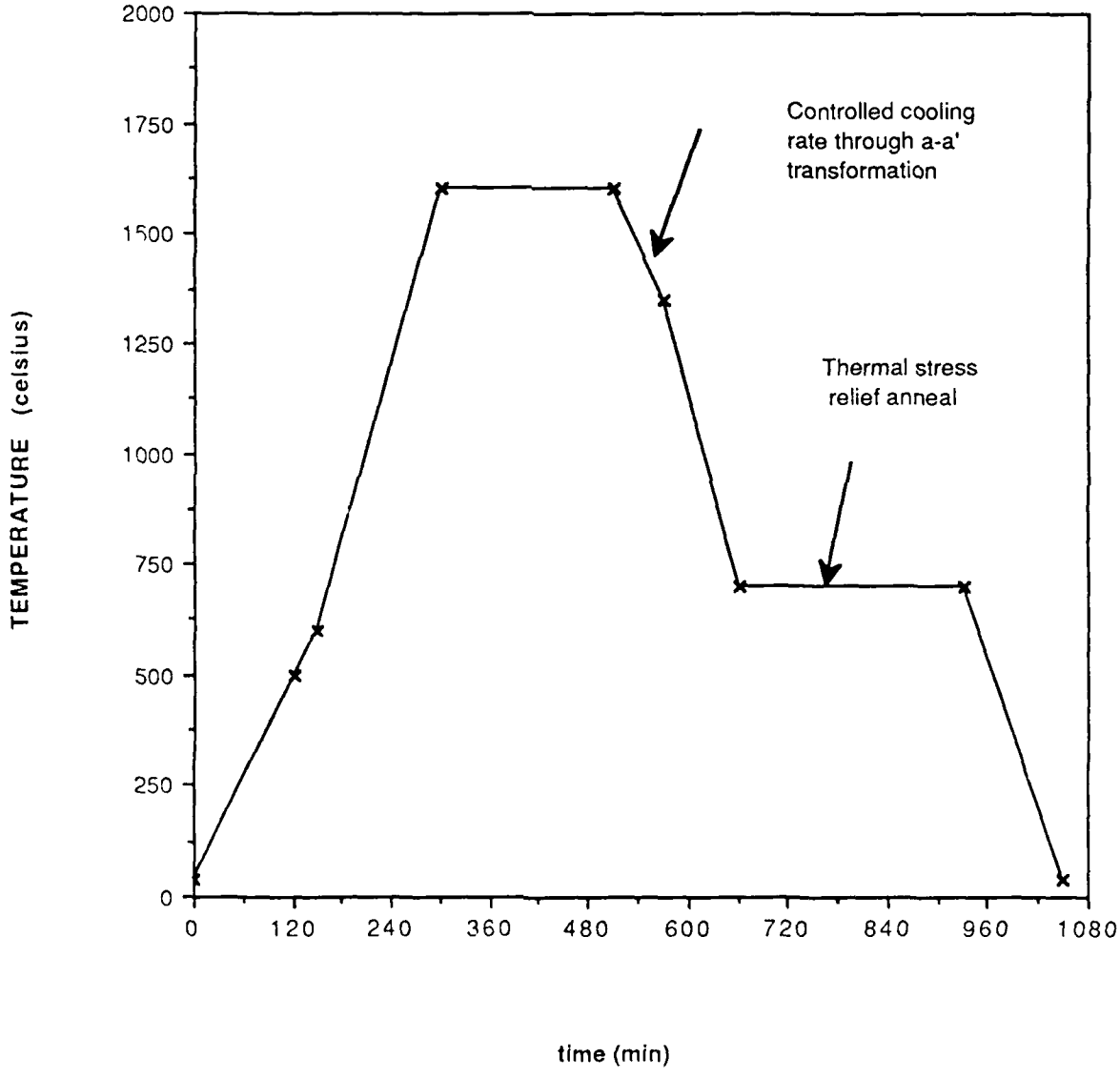

THERMAL ETCHING SCHEDULE

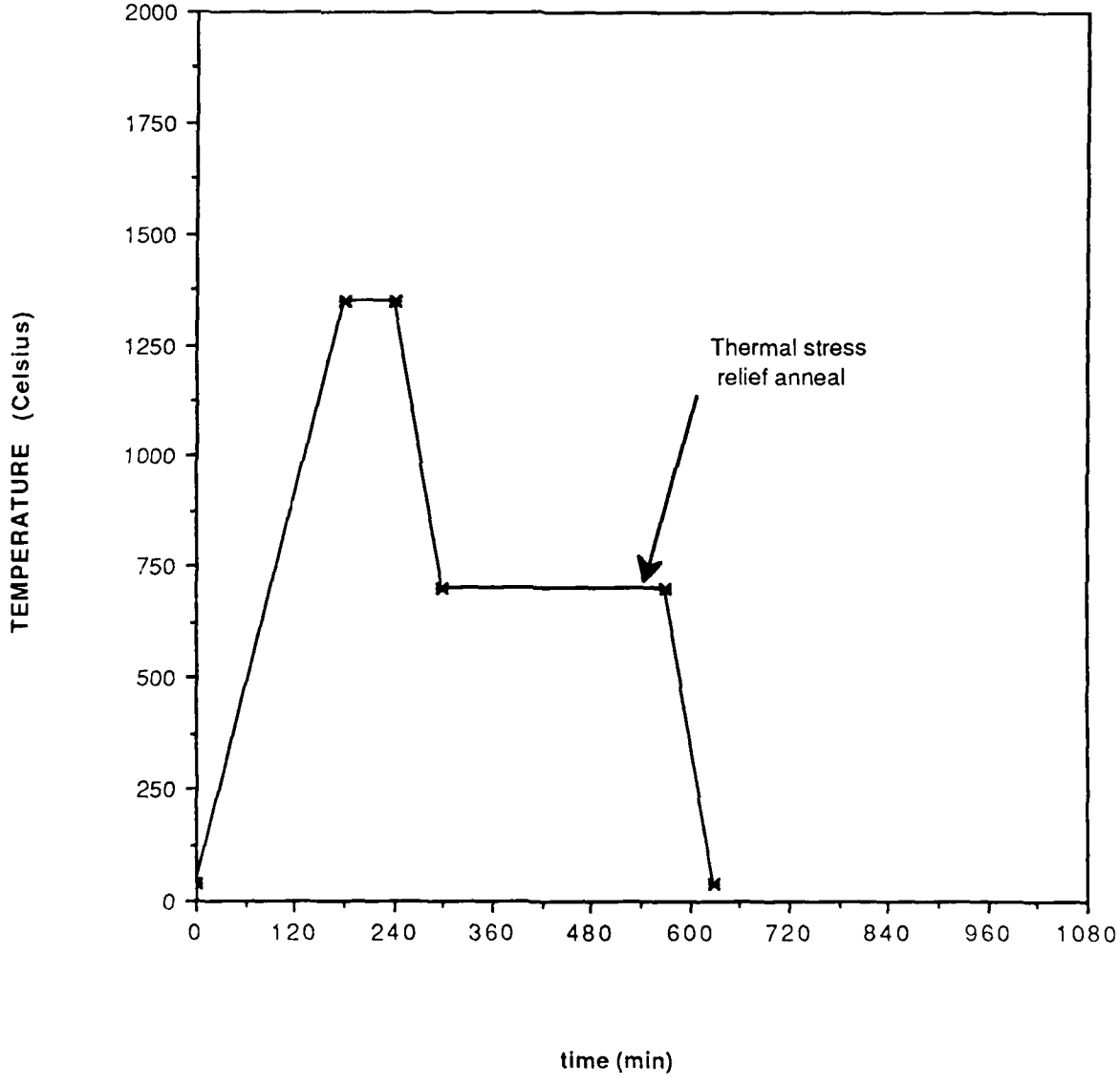

Appendix 6

SEM Micrographs of Composite Microstructures

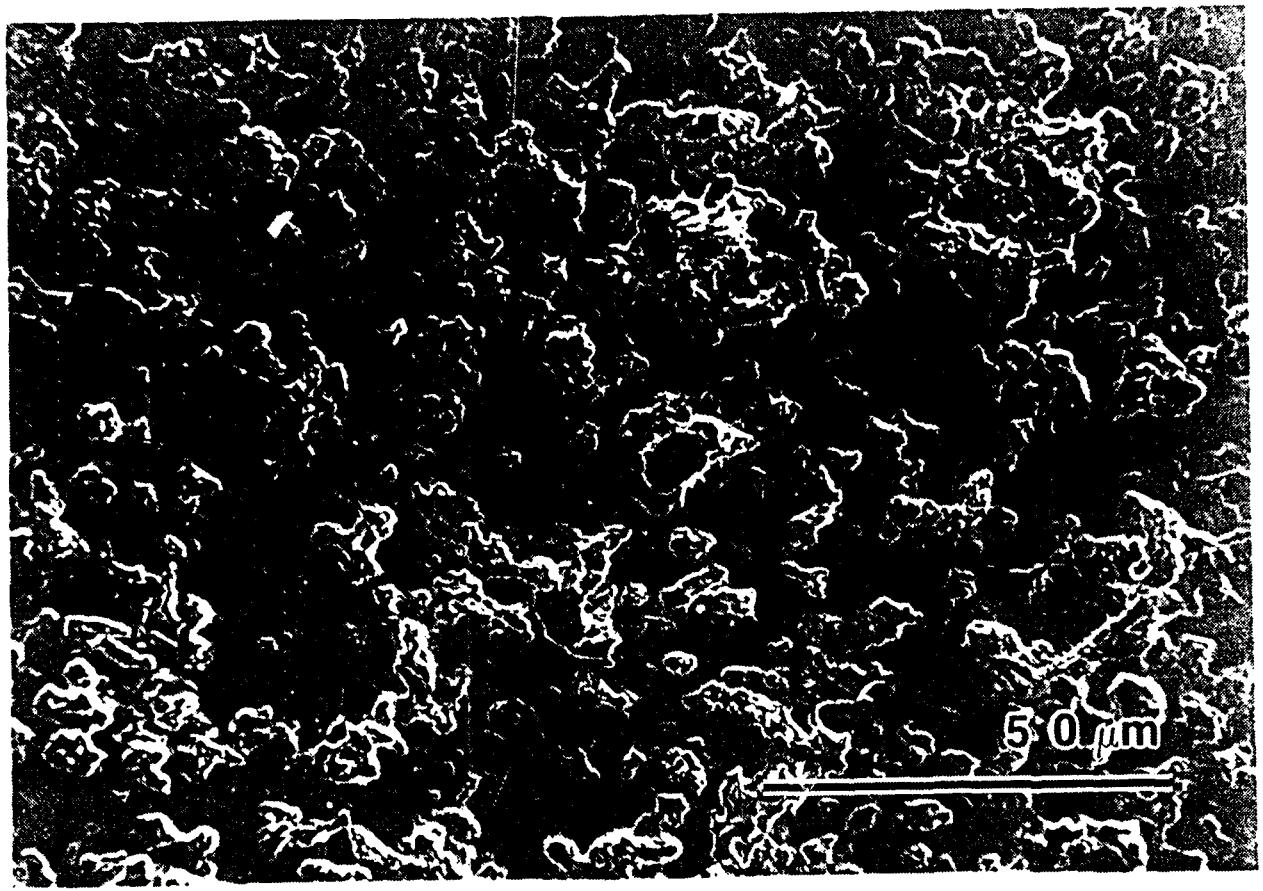

Figure 5 SEM micrograph of 15% (volume) Ca_2SiO_4-magnesia pellet surface. Air classified Ca_2SiO_4, 8000-10,000 rpm fraction. Fired at 1600°C for three hours. Polished to 6µm then etched in 1/2% nytol for five minutes. Ca_2SiO_4 etched away leaving structure of magnesia matrix, this shows former internal distribution of the dicalcium silicate.

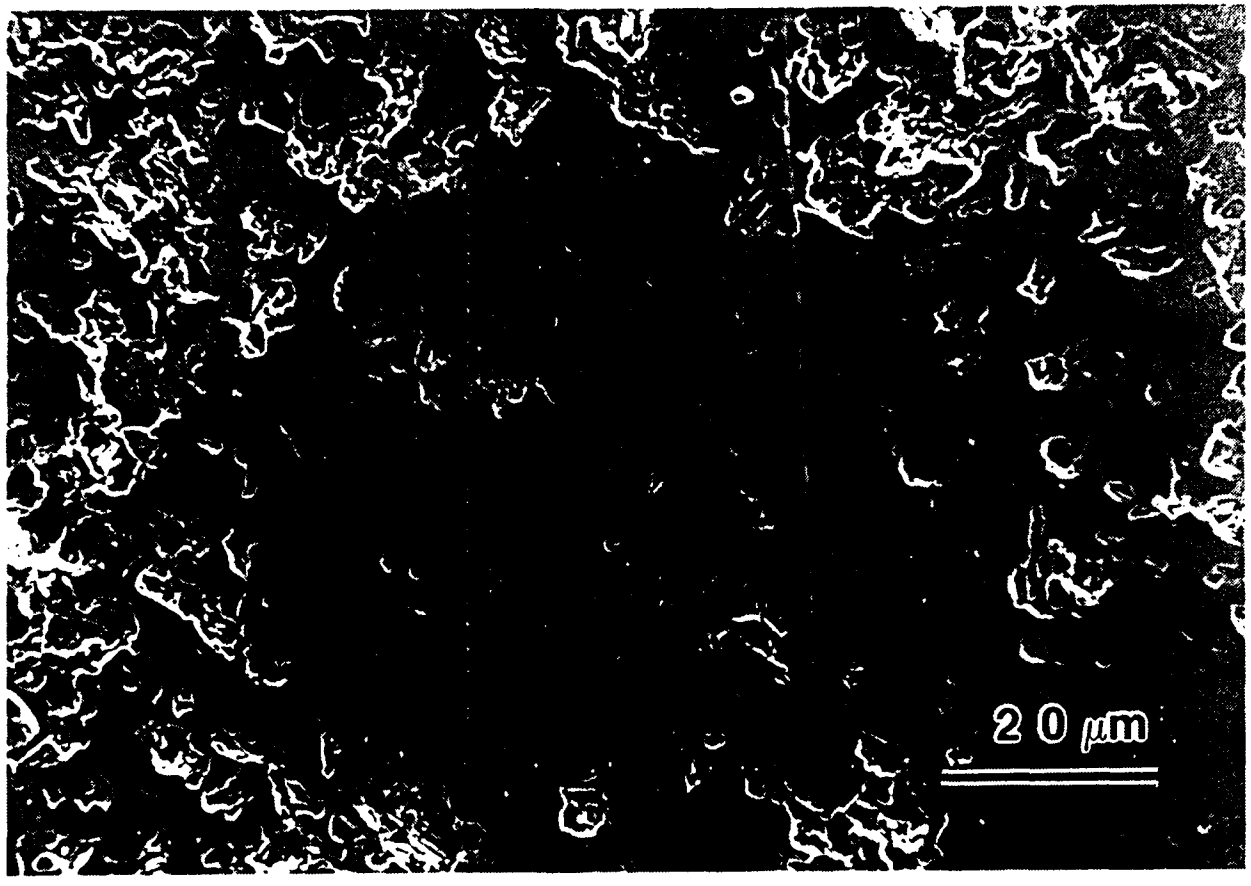

Figure 6 SEM micrograph of 15% (volume) Ca_2SiO_4-magnesia pellet surface. Air classified Ca_2SiO_4, 8000-10,000 rpm fraction. Fired at 1600°C for three hours. Polished to 6µm then etched in 1/2% nytol for five minutes. Ca_2SiO_4 etched away leaving structure of magnesia matrix, this shows former internal distribution of the dicalcium silicate. Some scratches remain from polishing.

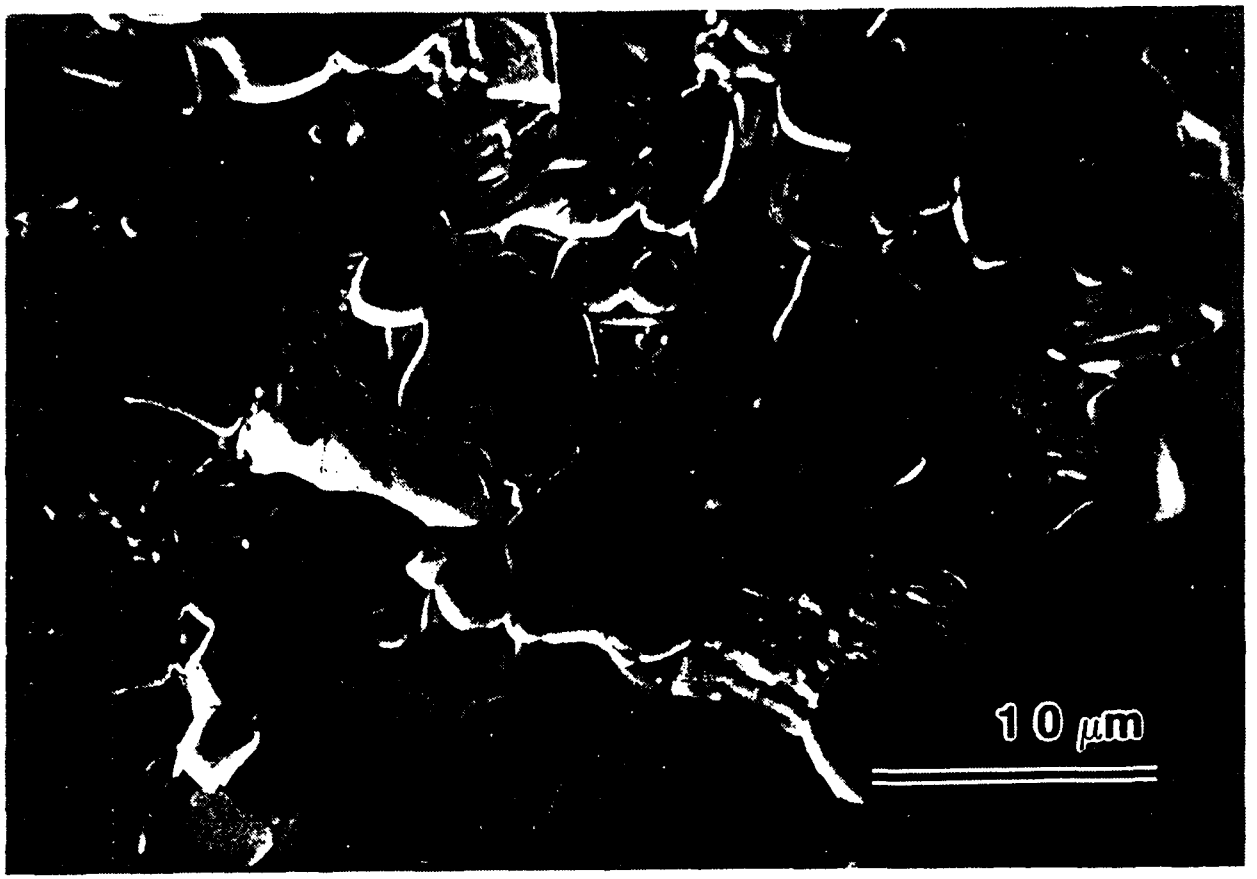

Figure 7 SEM micrograph of 15% (volume) Ca_2SiO_4-magnesia pellet surface. Air classified Ca_2SiO_4, 8000-10,000 rpm fraction. Fired at 1600°C for three hours. Polished to 6µm then thermally etched one hour at 1400°C. Both types of Ca_2SiO_4 grains (lighter grains) those with and without structure shown.

Figure 8 SEM micrograph of 15% (volume) Ca_2SiO_4-magnesia pellet surface. Air classified Ca_2SiO_4, 8000-10,000 rpm fraction. Fired at 1600°C for three hours. Polished to 6μm then thermally etched one hour at 1400°C. Ca_2SiO_4 structure easily discernable in this grain.

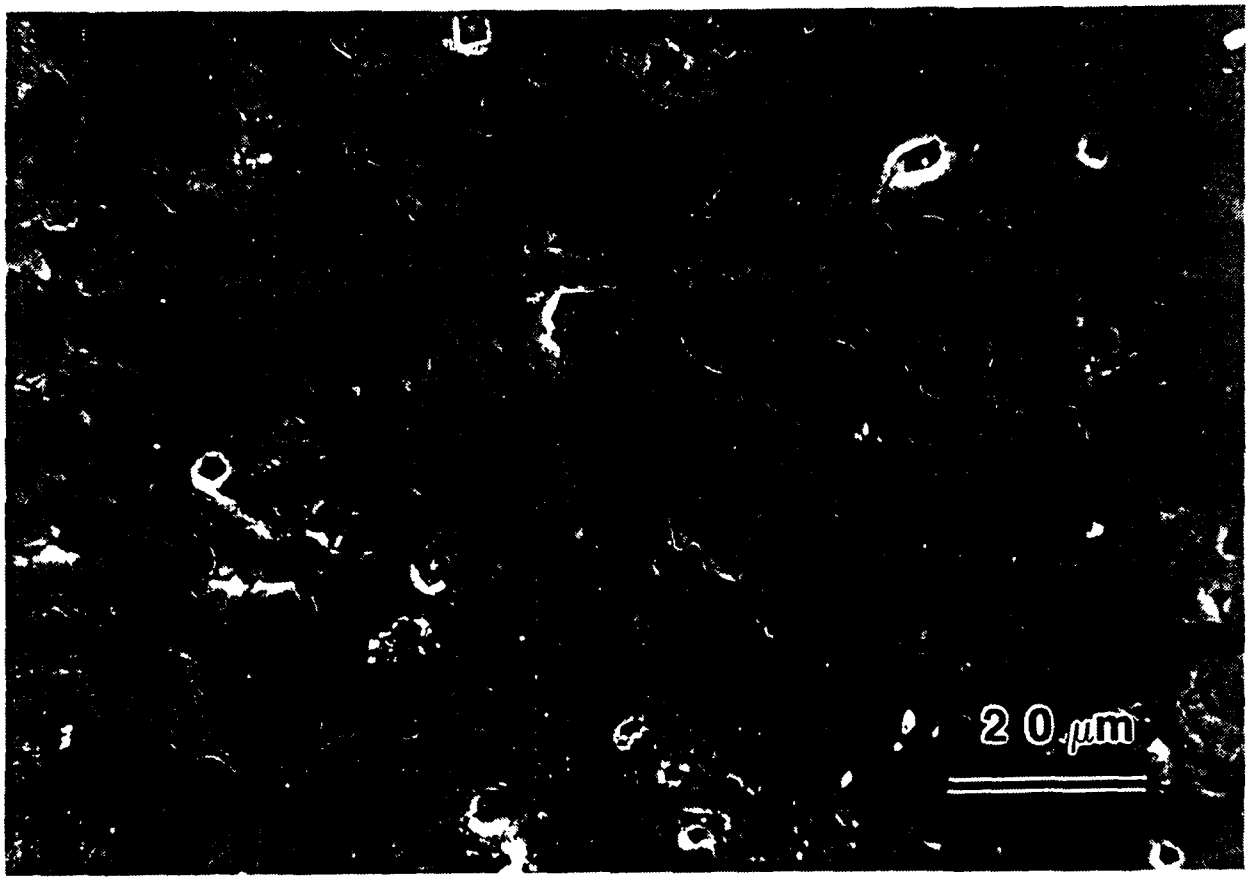

Figure 9 SEM micrograph of 15% (volume) Ca_2SiO_4-magnesia pellet surface. Air classified Ca_2SiO_4, 8000-10,000 rpm fraction. Fired at 1600°C for three hours. Polished to 6μm then thermally etched one hour at 1350°C.

Figure10 SEM micrograph of 15% (volume) Ca_2SiO_4-magnesia pellet surface. Air classified Ca_2SiO_4, 8000-10,000 rpm fraction. Fired at 1600°C for three hours. Polished to 6µm then thermally etched one hour at 1350°C. Image of dot map region.

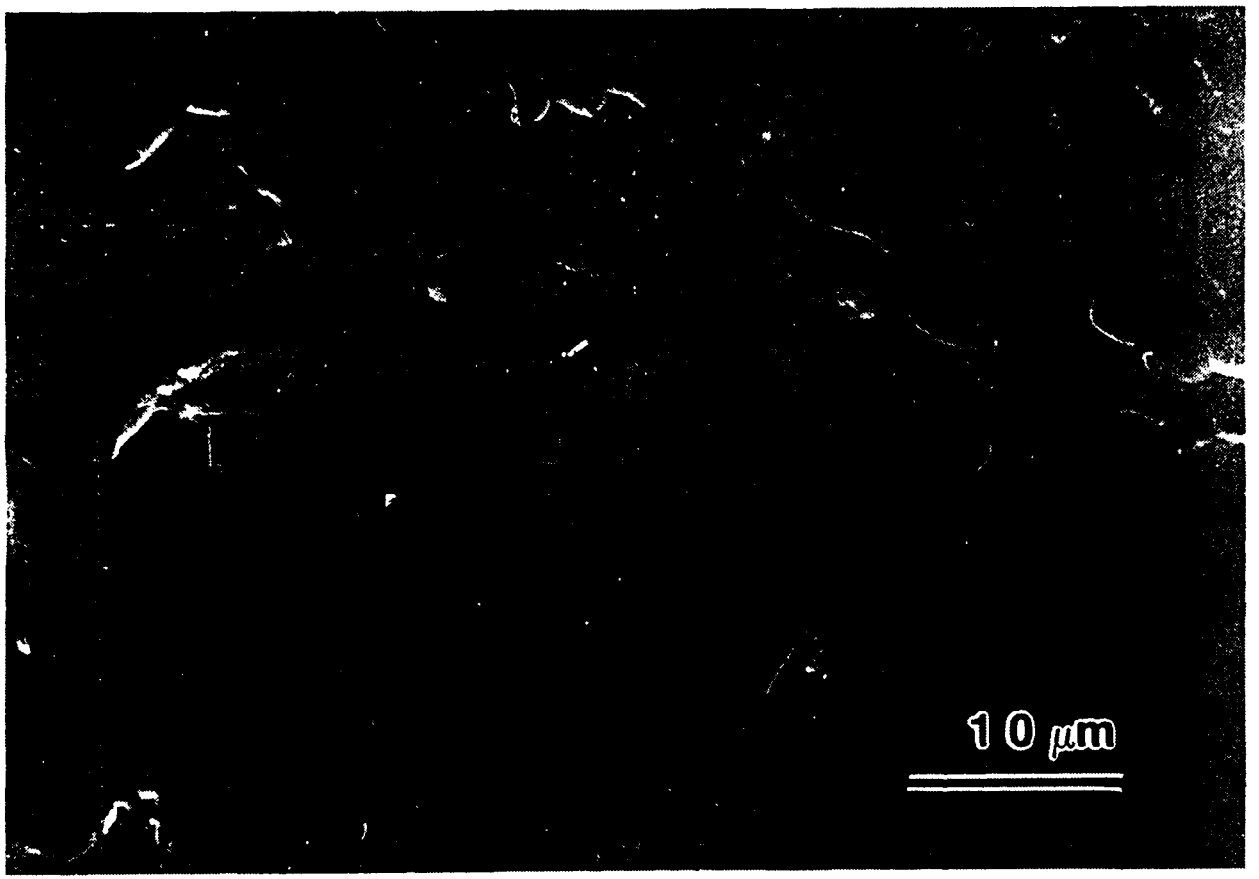

Figure11 SEM micrograph of 15% (volume) Ca_2SiO_4-magnesia pellet surface. Air classified Ca_2SiO_4, 8000-10,000 rpm fraction. Fired at 1600°C for three hours. Polished to 6µm then thermally etched one hour at 1350°C. Left grain shows only partial structuring, compared to the right grain.

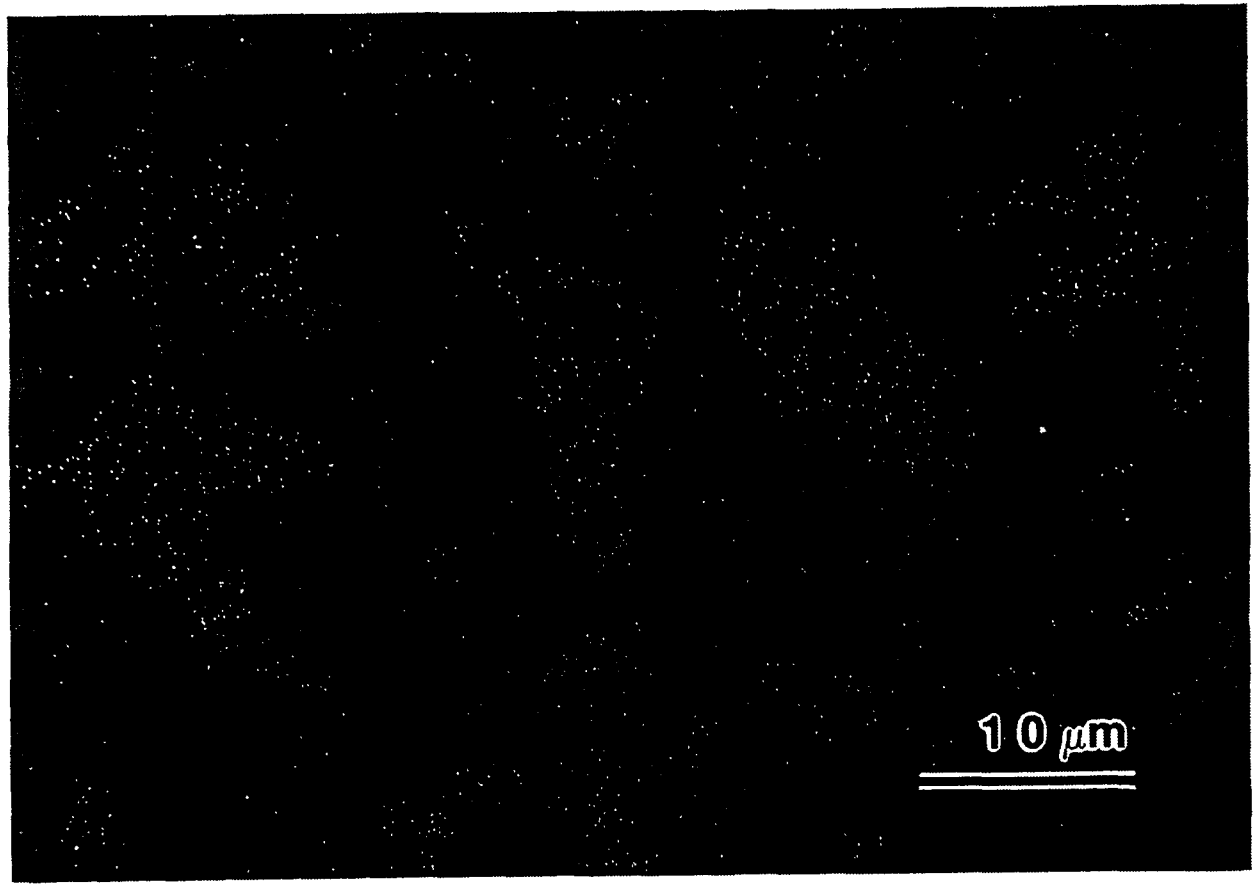

Figure12 SEM dot map of 15% (volume) Ca_2SiO_4-magnesia pellet surface, Ca and Si imaged. Air classified Ca_2SiO_4, 8000-10,000 rpm fraction. Fired at 1600°C for three hours. Polished to 6µm then thermally etched one hour at 1350°C.

Appendix 7

Acoustic Emission Curves

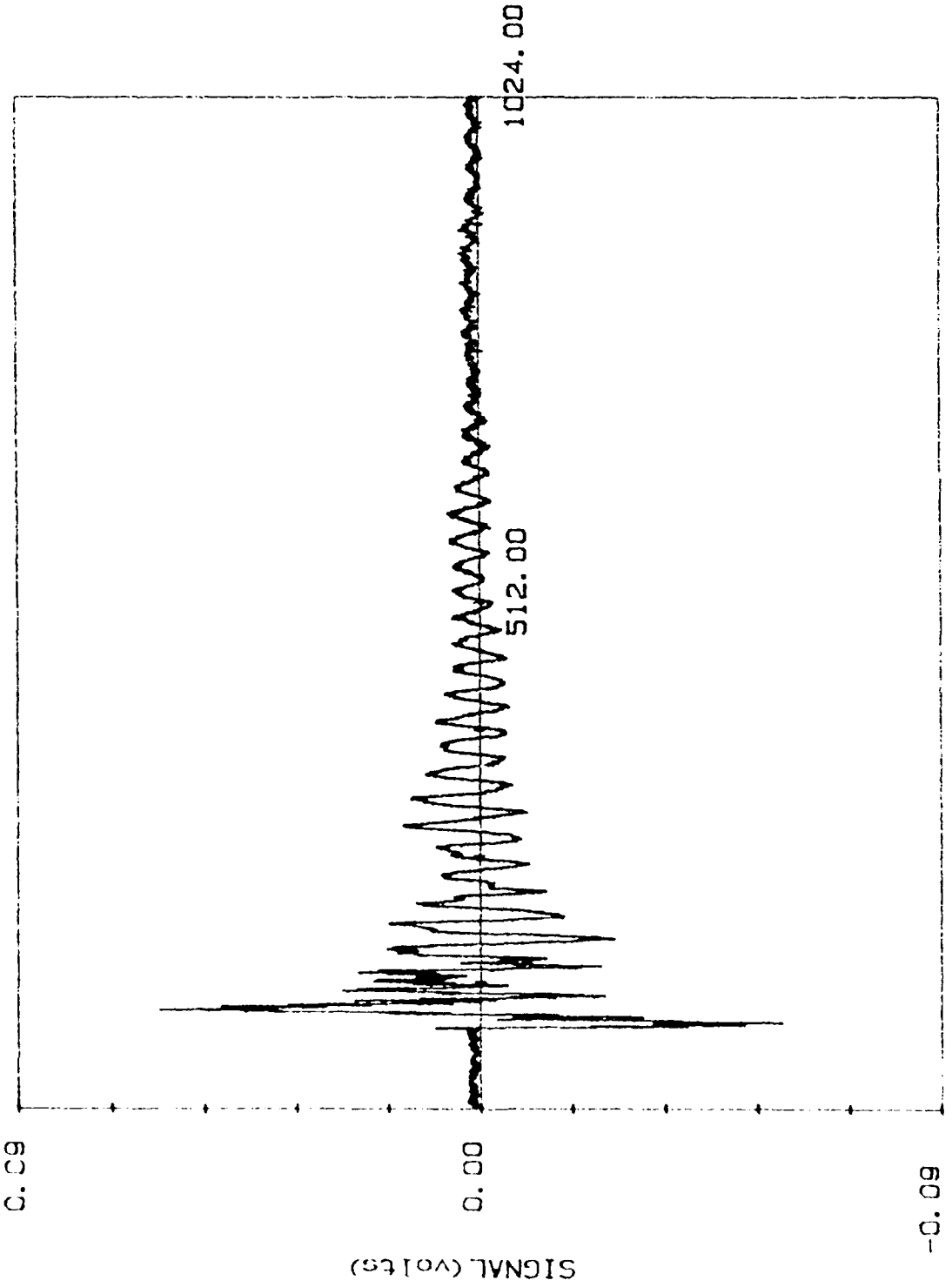
1024.00
512.00
TIME (usec)
0.09
0.00
-0.09
SIGNAL (volts)

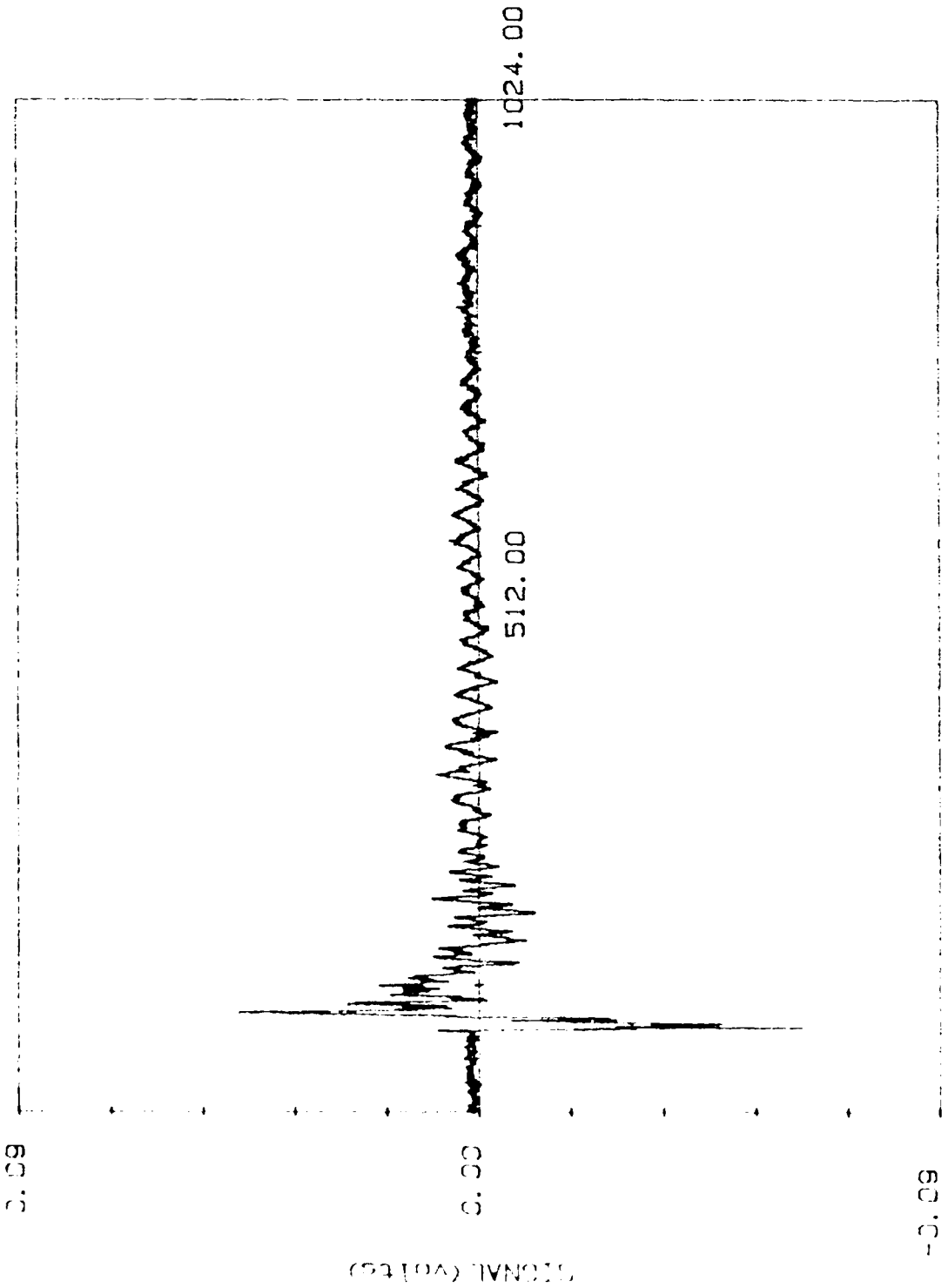
1024.00
512.00
0.00
TIME (usec)

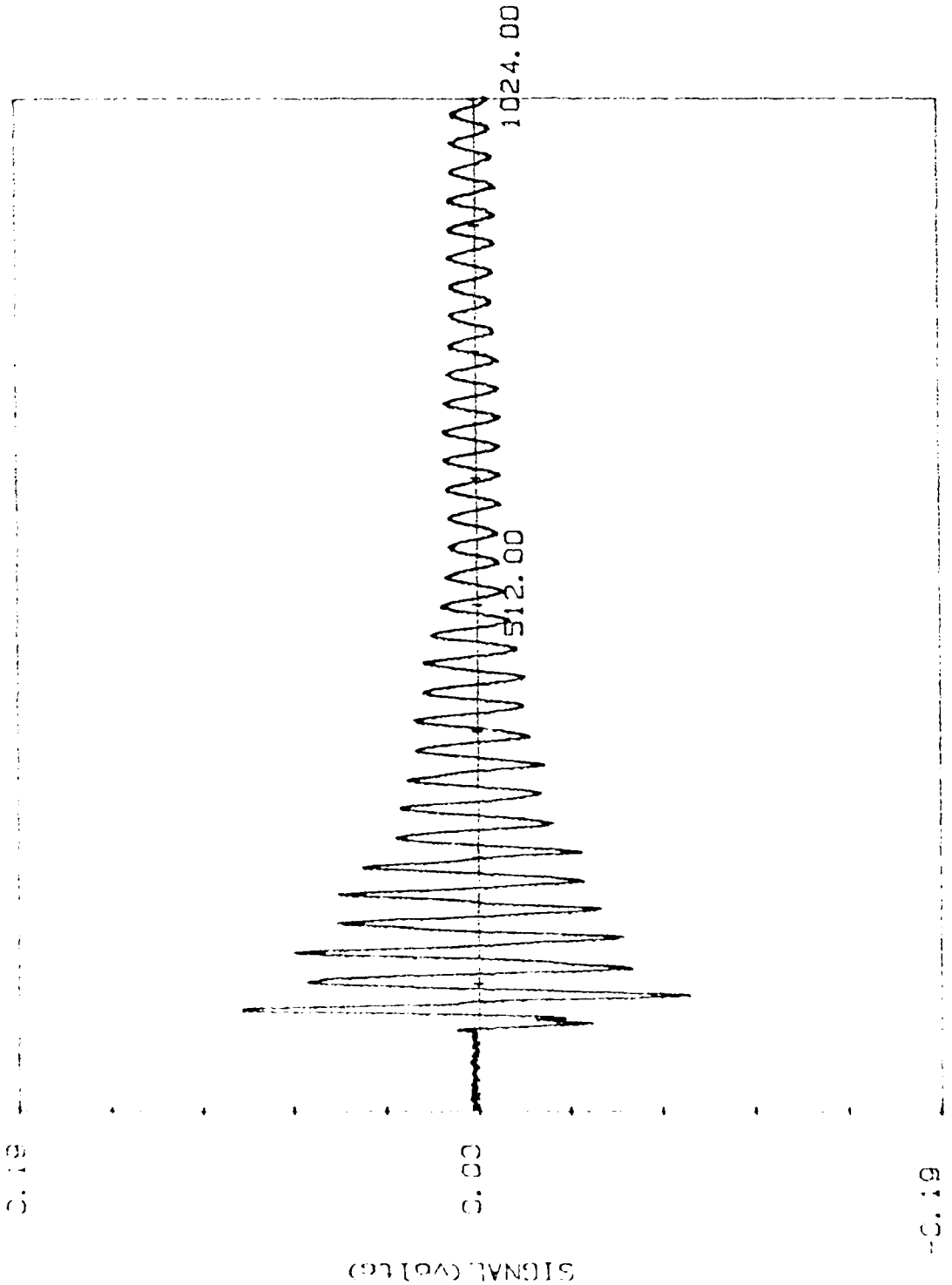
1024.00
512.00
0.00
TIME (usec)
SIGNAL (volts)

PROCESSING AND MICROSTRUCTURE OF DYSPROSIA IN SILICON CARBIDE MATRIX COMPOSITES

Annual Report

April 30th, 1989

S. Kim and W. M. Kriven

The high transformation temperature of dysprosia, coupled with its thermodynamic stability and low volatility at high temperatures suggests a high temperature transformation toughening agent in a suitable matrix. Several processing methods had been studied in order to disperse monoclinic (B) Dy_2O_3 into SiC matrix. This is intended to be an analogue to zirconia-toughened alumina in which 15 vol% of tetragonal zirconia particles are metastably dispersed in polycrystalline alumina.

The objectives of this research are to form a dense SiC -- B- Dy_2O_3 composites by optimizing processing variables and to understand the C $\leftrightarrow$ B transformation of Dy_2O_3 during densification and subsequent heat treatments and characterize the microstructure of SiC- Dy_2O_3 composite system.

Oxygen impurity is always present in SiC powders as thin surface oxide film. In SiC - Dy_2O_3 system, oxygen reduces the amount of free dysprosia at densification temperature and increases the amount of liquid phase. For SiC - 15 vol% Dy_2O_3 system, estimated equilibrium phases present at densification temperature (2000 C) are 94.6 m/o free SiC (solid), 1.7 m/o free Dy_2O_3(solid), and 3.7 m/o Dy_2O_3 - SiO_2 liquid which has a composition of 78 m/o Dy_2O_3 + 22 m/o SiO_2.

Processing variables include densification methods (hot pressing, hot ejection, hot isostatic pressing and pressureless sintering), additives (carbon and boron), cooling rate (quenching) and annealing treatments after densification.

Hot pressing was conducted at 2000 C using graphite as die and punch material. Hot isostatic pressing was done at 2000 C using tantalum metal encapsulation. The cooling rate was ~ 53 C/min. Pressureless sintering/quenching was conducted at 2050 C in argon gas (50.5 KPa). At the end of the hold time, the power of the heating element was turned off in order to get the highest cooling rate. Temperature dropped by 200 C in 10 seconds.

Table 1 lists the dysprosia phases and density of the composite after densification. Hot pressing or hipping (group 1) produced composites with C-dysprosia rather than B-dysprosia.Carbon and boron additions (group 2) help to get some dysprosia in the B-phase but the composites still have C-dysprosia. Hot ejection (group 3) also could not retain the B-dysprosia,

which suggests that the cooling rate was not high enough to retain the B-dysprosia.

Table 1. Dy_2O_3 Polymorphs and Density of SiC - Dy_2O_3 Composites.

Material	Densification/Heat Treatment	Dy_2O_3	%TD
	Group 1: No additives		
α15D*	HP (2000C, 28MPa, 20min)	C	88.4
β15D	HP (2000C, 28MPa, 20min)	C	88.6
β15D	HIP (2000C, 186MPa, 1hr)	C + B(tr)	98.1
β30D	HIP (2000C, 186MPa, 1hr)	C	92.2
	Group 2 ; C and B additives		
α30D1C1B	HIP (2000C, 186MPa, 1hr)	B + C	99.9
β30D1C1B	HIP (2000C, 186MPa, 1hr)	C + B	94.1
α10D2C1B	sinter-quench (2050C, 20min)	B	60.3
	Group 3: Hot Ejected (HE)		
α10D1C1B	HE (2050C, 28MPa, 20min)	B + C	97.5
α10D	HE (2050C, 28MPa, 20min)	C	93.6
	Group 4 :HE Followed by Heat and Quenching Treatments		
α10D1C1B	HE-quenching from 2050 C	B	
α10D	HE-quenching from 2050 C	B	

* α=α-SiC, β=β-SiC, 15D=15 vol% Dy_2O_3, 1C=1wt% C, 1B=1 wt% B

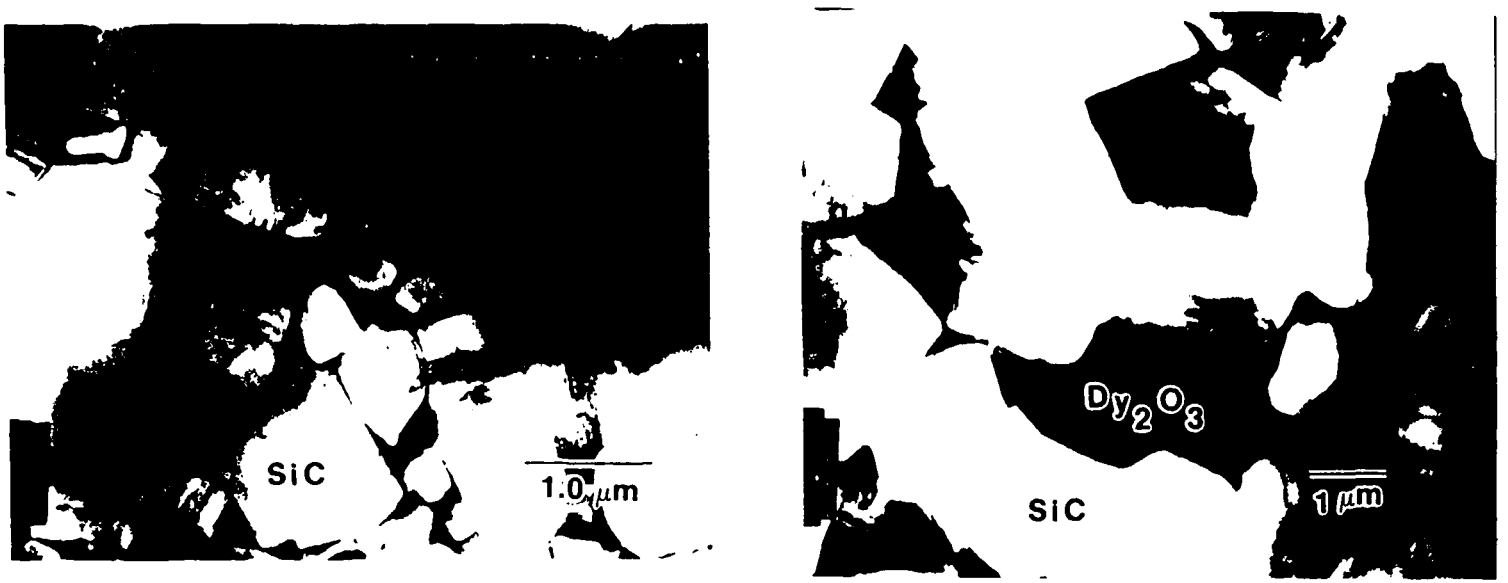

(a) (b)

Fig.1 Bright field TEM micrographs of α10D-HE
(a) as hot ejected (17 KX) (b) after quenching treatments (10.5 KX)

Heat and quenching treatment of hot ejected materials (group 4) was conducted by rapidly heating to 2050 C, 10min hold and quenching by turning off the power of heating element. Temperature dropped by 200 C in 10 seconds. Note that heat and quenching treatments could retain all the dysprosia in the B-phase, indicating that quenching is effective in retaining the B-dysprosia at room temperature.

Table 2. lists the comparison of d-spacings and relative intensities between pure B-dysprosia obtained by plasma spraying of dysprosia on aluminum substrate and B-dysprosia in SiC- Dy_2O_3 composites. The comparison shows a fairly good agreements in d-spacings with some differences in relative intensities. Bright field TEM micrographs of hot ejected α10D material is shown in Fig 1. The dysprosia grain wets SiC grain, suggesting that they formed a liquid phase during densification. Small crystallites were observed in dysprosia grain, the EDS analysis of which showed Si peak only, suggesting either SiC or SiO_2. Fig 2. shows SEM micrographs of hipped β15D material.

Table 2. Comparison of d-spacings and relative intensities.

Pure B- Dy_2O_3 Plasma Sprayed		B- Dy_2O_3 in SiC α10D-HE-Quenched	
d-spacing (A)	Intensity	d-spacing (A)	Intensity
3.116	84	3.118	92
3.000	38	3.062	43
2.937	72	------	---
2.837	40	2.841	43
2.788	73	2.757	100
2.72	100	2.716	59

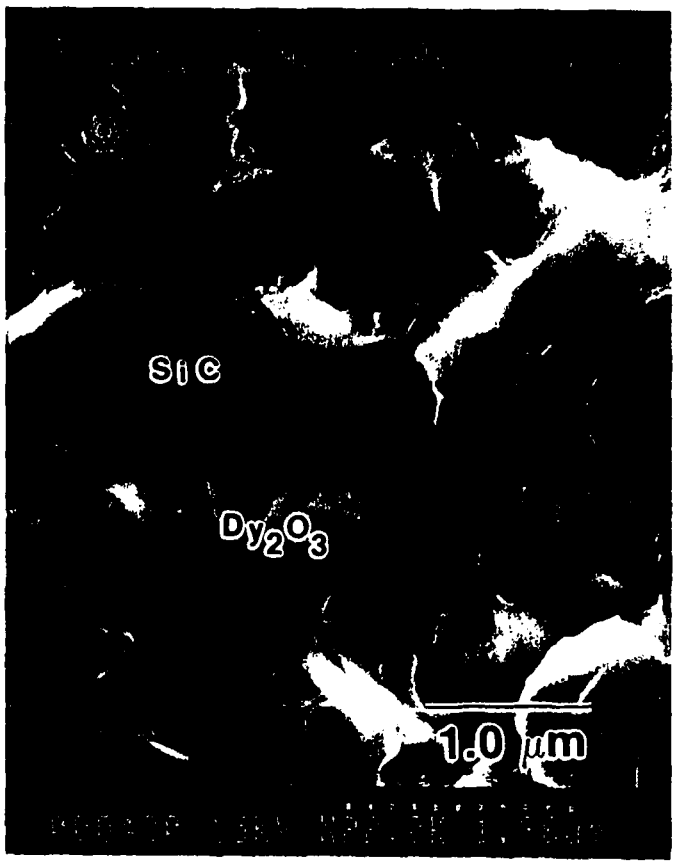

(a) (b)

Fig.2 SEM micrograph of as-hipped β15D-HIP.
(a) 2KX (b) 22KX

Annealing heat treatments

In order to find the effect of long term, high temperature annealing on the phase stability and microstructure of SiC- Dy_2O_3 composites, annealing heat treatments were conducted by heating at 1500 C for 50 hours. Some materials were also annealed at 1250 C. Static air and flowing argon gas atmosphere were used as annealing environments. As shown in Fig. 3, hot pressed or hot ejected materials annealed at 1500 C produced large amount of unknown phases (labeled X) on sample surfaces both in static air and in argon gas. The polished surface of hot ejected materials annealed at 1250 C in air did not show unknown phase (Fig. 4). In contrast to hot pressed materials, X-ray diffraction patterns of hipped materials (Fig.5) did not produce any unknown phase on annealing. This is due to the use of tantalum encapsulation which isolates the material from the environments. Annealing at 1500 C in air seems to produce B-dysprosia. Table 3. compares the d-spacings for pure B-dysprosia obtained by plasma spraying and dysprosia in SiC matrix after annealing in air. The relative intensities are different from each other. Bright field TEM micrographs of air annealed β15D-hip material is shown in Fig. 6. The microstructure of air annealed materials are similar to that of as-hipped material.

Table 3. Comparison of d-spacings and relative intensities.

Pure B- Dy_2O_3 Plasma Sprayed		B-Dy_2O_3 in SiC β15D-HIP-Air Annealed	
d-spacing (A)	Intensity	d-spacing (A)	Intensity
3.116	84	3.081	100
3.000	38	-------	---
2.937	72	2.933	43
2.837	40	2.850, 2.840	16
2.788	73	2.790	6
2.72	100	2.748	4

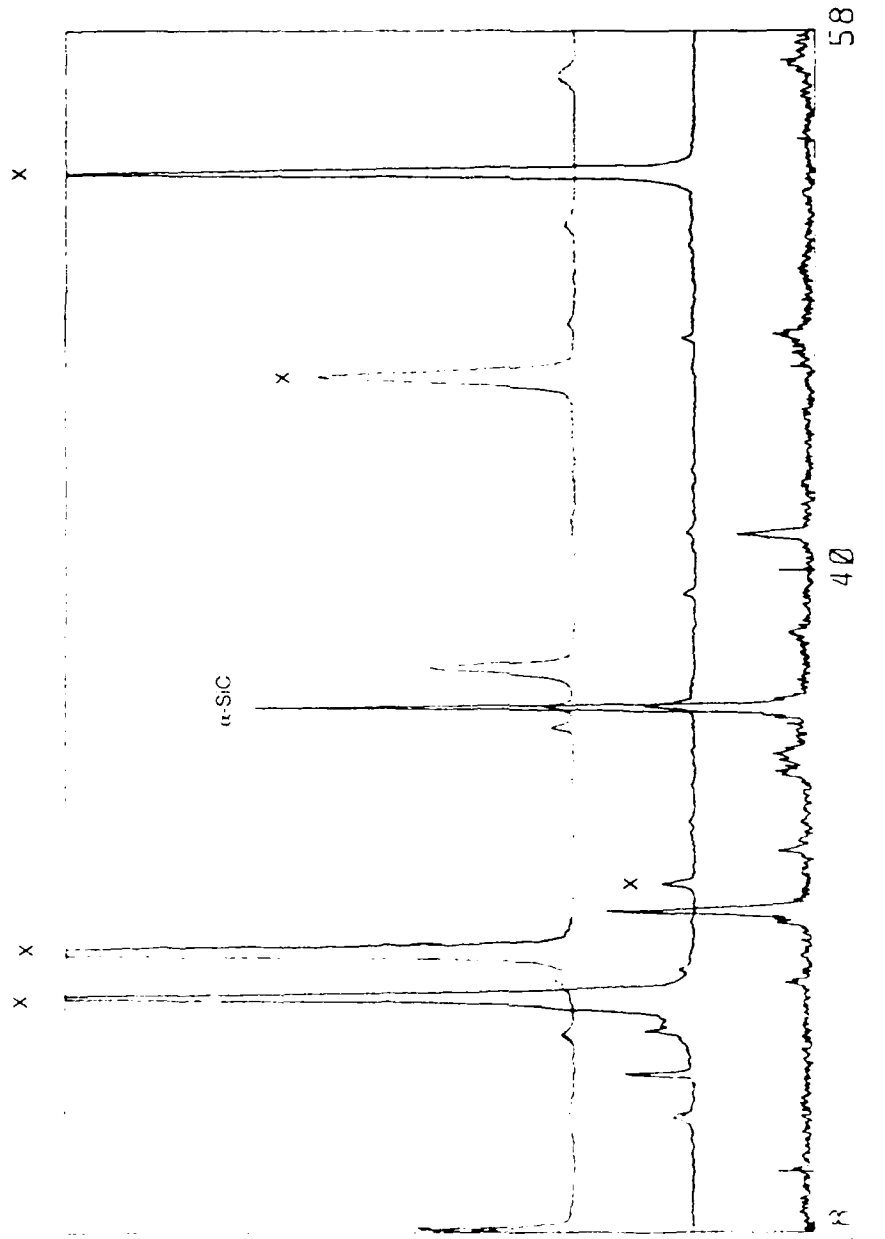

Fig.3 X-Ray diffraction patterns of β15D-HP after annealing treatment
(a) as-hot pressed (b) annealed in air at 1500 C (c) Annealed in argon

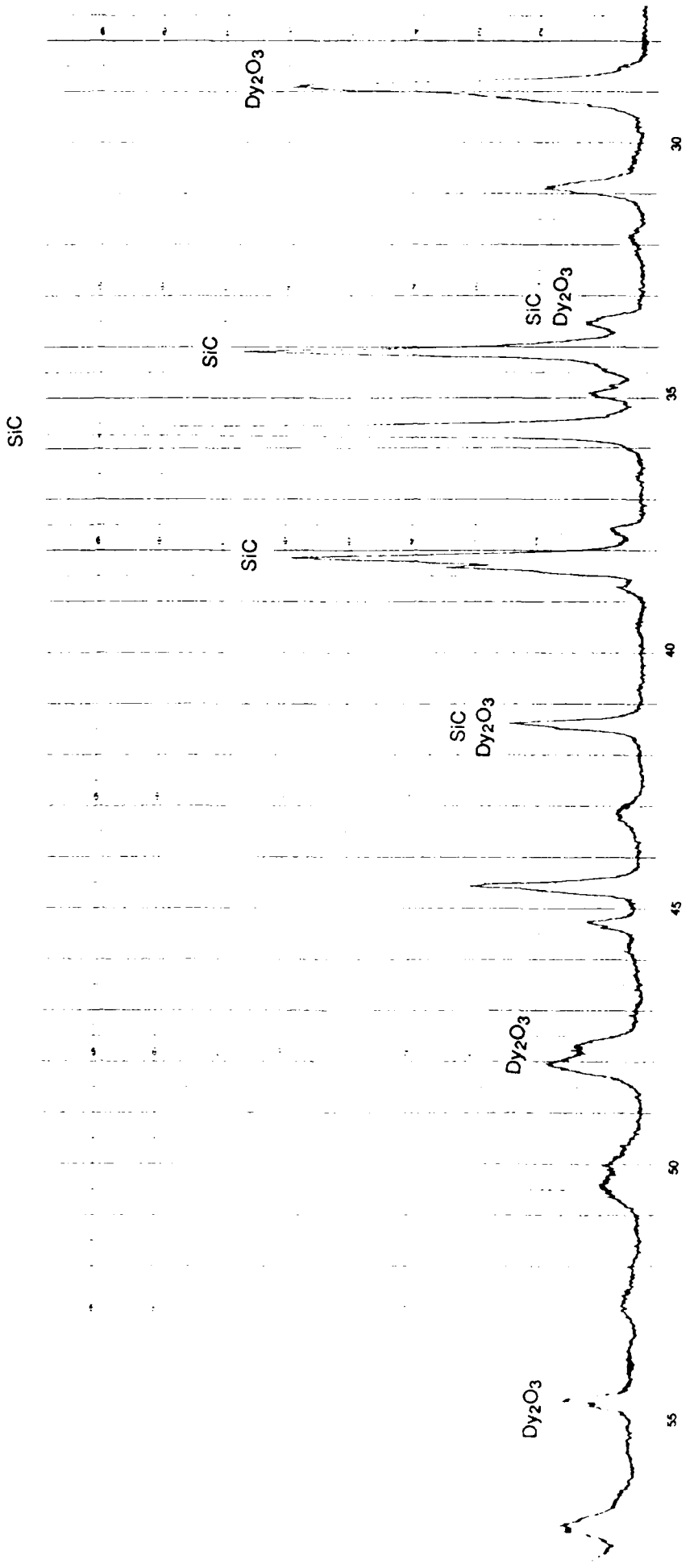

Fig.4 X-Ray diffraction patterns of α10D1C-HE after annealing at 1250 C for 50 hr in air

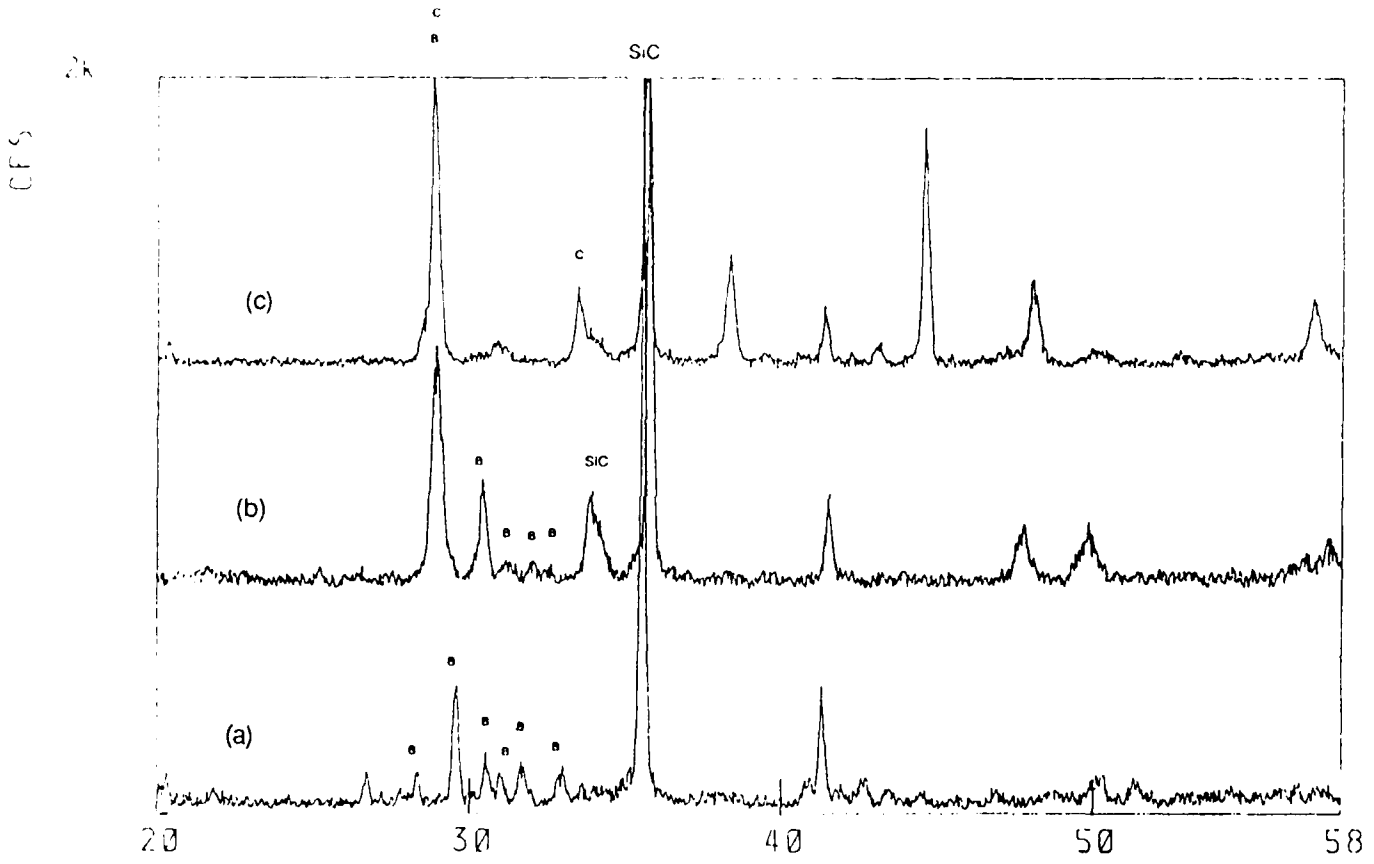

Fig.5 X-ray diffraction patterns of β15D-HIP after annealing heat treatment at 1500 C. (a) air-annealed surface (b)interior region of air-annealed specimen. (c)as-hipped (before annealing)

(a) (b)

Fig.6 Bright field TEM images of air-annealed β15D-HIP after annealing at 1500 C in air. (a) 13KX (b) 17KX

Because the presence of Si in dysprosia may affect the transformation behavior of dysprosia, TEM/EDS was taken in order to determine the Si content in dysprosia grain. Fig. 7 and 8 show the EDS plots for as-hipped and annealed materials, respectively, indicating the presence of Si in dysprosia grains. Several measurements were made on different dysprosia grains and the average Si content is listed in Table 4. Little difference in Si content is observed after annealing treatments.

Table 4. Average Si content in Dy_2O_3 grain in hipped specimens.
(Dy + Si=100%)

Material	Average Si Content (at%)
β15D-As Hipped	5.1%
β15D-HIP-Air Annealed	6.6 %

CONCLUSIONS

1. A dense SiC- Dy_2O_3 composite containing predominantly B-phase of Dy_2O_3 could be obtained.
2. Quenching was effective for retaining the B-phase of Dy_2O_3.
3. Chemical problems occurred with hot pressed or hot ejected sample surfaces after annealing at 1500C.
4. No new phases appeared in Ta encapsulated, hipped samples on annealing.
5. Long term high temperature annealing had little effect on the Si content in Dy_2O_3 grain.

AD-A208 714 HIGH TEMP TOUGHENING AND CREEP STUDIES(U) ILLINOIS UNIV 2/2
AT URBANA DEPT OF MATERIALS SCIENCE AND ENGINEERING
W M KRIVEN 11 MAY 89 AFOSR-TR-89-0688 AFOSR-85-0242
UNCLASSIFIED F/G 7/2 NL

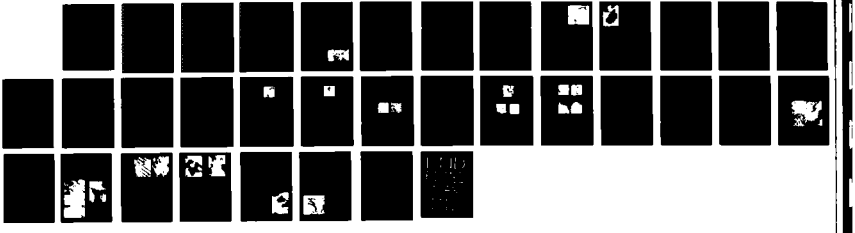

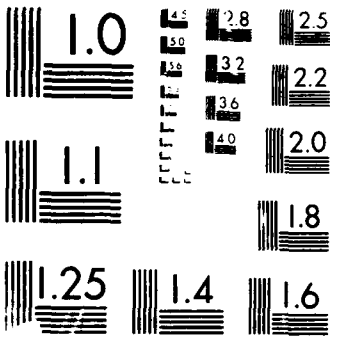
1.0
1.1
1.25
1.4
1.6
1.8
2.0
2.2
2.5
2.8
3.2
3.6
4.0
4.5
5.0
5.6

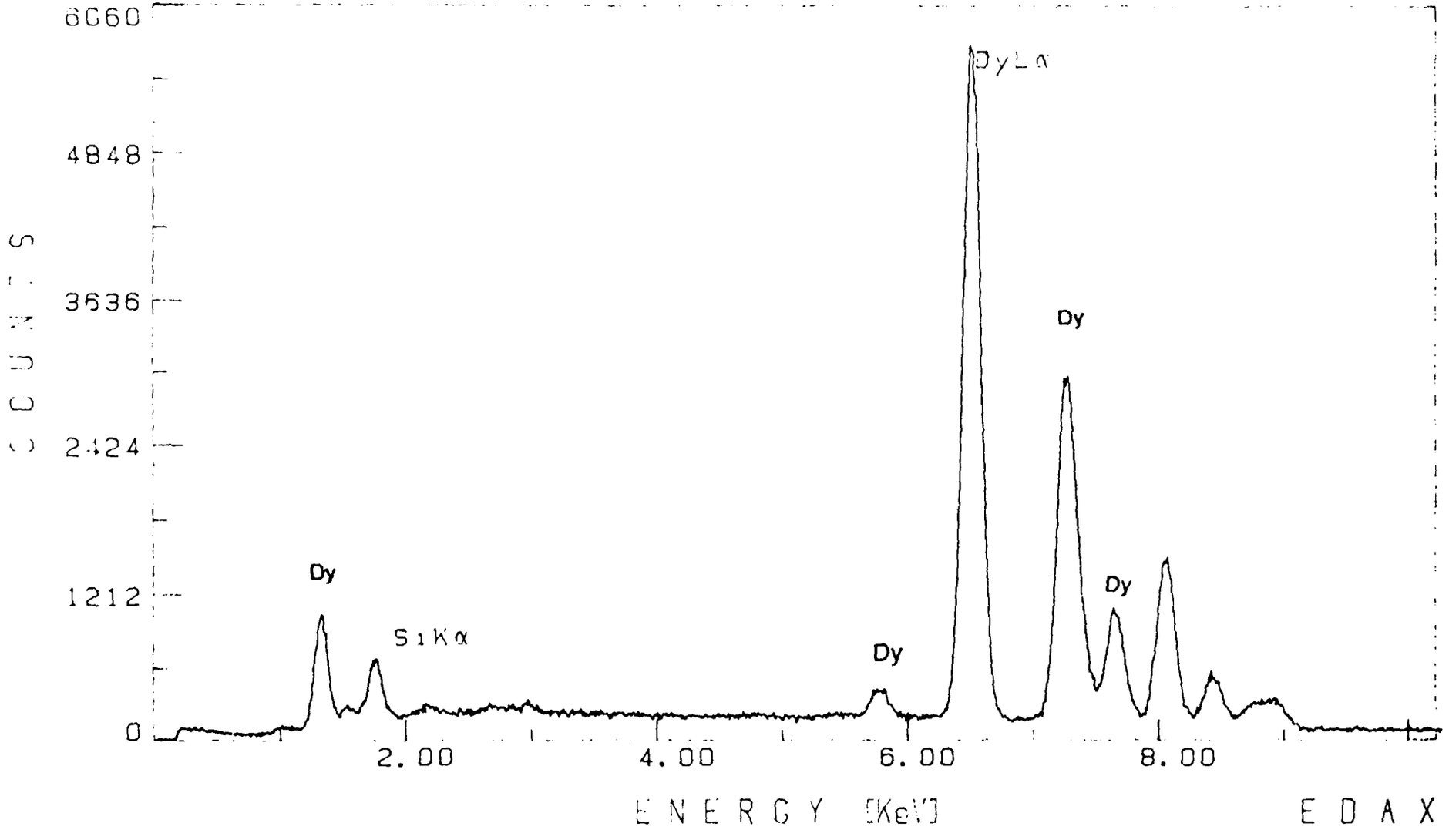

Fig.7 TEM/EDS plot of dysprosia grain in β15D-HIP (as-hipped)

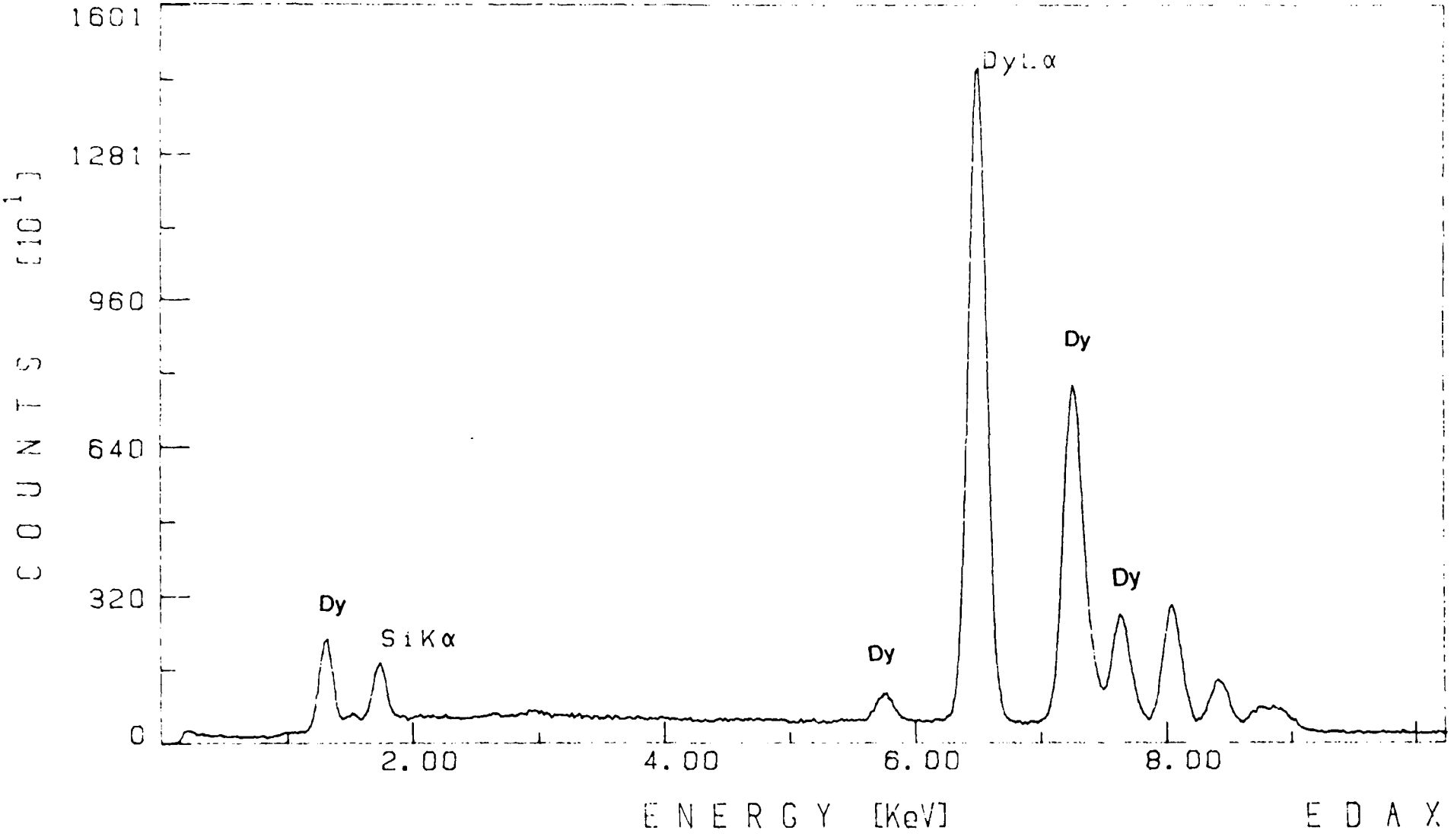

Fig.8 TEM/EDS plot of dysprosia grain in β15D-HIP (after annealing at 1500 C)

FUTURE WORK

1. Quenching treatment of hipped composites to optimize B-Phase content.
2. Prior hydrofluoric acid treatment of SiC powders to remove oxygen impurity.
3. Identify small Si containing precipitates in dysprosia grains.
4. Evaluate B → C transformation and mechanical properties.

JOURNAL

of the AMERICAN CERAMIC SOCIETY

Volume 71, No. 12 December 1988

J. Am. Ceram. Soc., 71 [12] 1021-30 (1988)

Possible Alternative Transformation Toughened to Zirconia: Crystallographic Aspects

WALTRAUD M. KRIVEN*

Department of Materials Science and Engineering and Materials Research Laboratory, University of Illinois at Urbana-Champaign, Urbana, Illinois 61801

Several new potential alternative transformation toughened to zirconia have been identified on the basis of crystallographic considerations and experimental observations. Examples can be found in ceramics, minerals, and components of glass and of cement. The displacive transformations exhibit martensitic characteristics of dusting or self-disintegration, and a critical particle size effect operates. Large positive volume changes (≤12%) accompany the transformations on cooling, in the lanthanide sesquioxides (Ln_2O_3), dicalcium silicate (Ca_2SiO_4), and nickel sulfide (NiS). High M_S temperatures (≤2000°C) in the Ln_2O_3 compounds also suggest the possibility of high-temperature transformation toughening. Detrimental negative volume changes are seen in composites with enstatite ($MgO \cdot SiO_2$) and the lanthanide borates ($LnBO_3$). The relative effects of volume change, X-ray unit-cell shape change, and the (martensitic) macroscopic shape change on the mechanical properties of a composite ceramic can thus be investigated.

I. Introduction

THE controlled application of the tetragonal (t) → monoclinic (m) transformation in zirconia (ZrO_2) to toughen a ceramic matrix has been extensively investigated, both scientifically and technologically.[1-7] Various types of transformation-toughened materials have been developed.[1-5] In large-grained, partially stabilized ZrO_2 (PSZ), tetragonal solid-solution particles are crystallographically precipitated from a cubic matrix. A fine-grained material, e.g., alumina, can be toughened by dispersions of randomly oriented, intergranular, irregularly shaped ZrO_2 particles (ZTA).[6] The Al_2O_3-ZrO_2 system is perhaps the most important of many examples to date of a variety of non-zirconia matrix materials toughened by ZrO_2 additions. In tetragonal zirconia polycrystalline (TZP) materials, very fine-grained Y_2O_3-ZrO_2 solid-solution particles act as their own matrix.[7]

Zirconia has the following polymorphs (CN is coordination number) under ambient pressures:[7]

$$\text{melt} \xleftrightarrow{2680\,^\circ\text{C}} \underset{\text{cubic}}{\text{I}} \xleftrightarrow{2370\,^\circ\text{C}} \underset{\substack{\text{tetragonal}\\ \text{CN: Zr}^{4+}\text{: 8}}}{\text{II}} \underset{1170\,^\circ\text{C}}{\overset{950\,^\circ\text{C}}{\rightleftharpoons}} \underset{\substack{\text{monoclinic}\\ \text{CN: Zr}^{4+}\text{: 7}}}{\text{III}}$$

The $t \rightarrow m$ transformation is considered to be martensitic in the bulk. It is accompanied by a volume increase of 3% at 950°C to 4.9% at room temperature. The transformation is notorious for causing unstabilized zirconia to shatter. The factors determining the stability of t-ZrO_2 particles confined in ceramic matrices are considered to be the matrix constraint, chemical composition, and the transformational nucleation barrier which is a function of ZrO_2 particle size.[7] The mechanical properties of ZrO_2 composites, such as toughness and thermal shock resistance, are significantly improved. Fracture of the material is retarded when the stress field of a moving crack tip nucleates the $t \rightarrow m$ transformation in ZrO_2 particles in a zone around the crack. As the crack propagates, the transformation zone (or wake), at its edges, absorbs its energy and constrains it (Fig. 1).

Fig. 1. High-voltage electron microscopy photograph (dark field) of a transformed zone in a thin specimen of Mg-PSZ near a Vickers indentation crack. The stress field of the propagating crack tip induced the transformation to twinned monoclinic particles in the "wake" of the crack, thereby constraining it.

Manuscript No. 199404. Received October 9, 1987; approved March 2, 1988.
Presented in part at the 88th Annual Meeting of the American Ceramic Society, Chicago, IL, May 1, 1986 (Basic Science Division, Paper No. 74-BP-86). Presented in part at the Advanced Ceramics II Lecture Meeting, Tokyo Institute of Technology, Nagatsuta Campus, Japan, September 1986.
Supported by the U.S. Air Force Office of Scientific Research under Contract No. AFOSR-85-0242.
*Member, the American Ceramic Society.

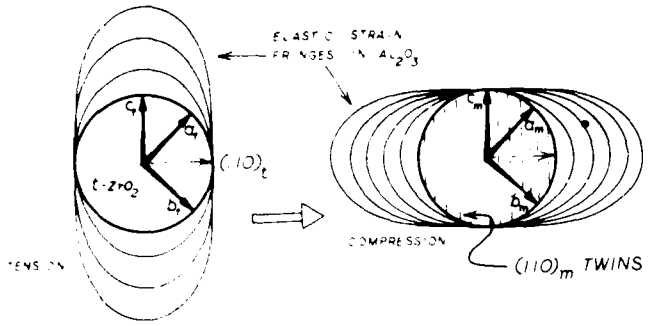

Fig. 2. Schematic representation of the $t \rightarrow m$ transformation mechanisms in spherical ZrO_2 particles confined in Al_2O_3.[5]

The transformational crystallography of confined spherical ZrO_2 particles dispersed in Al_2O_3 has been experimentally studied.[5] The relationship between elastic strain fields surrounding the t and m particles has been elucidated. As illustrated schematically in Fig. 2, the t-ZrO_2 particle existed in a state of tensile stress due to thermal expansion mismatch with the Al_2O_3 matrix. This arose during fabrication when the composite was cooled from the processing temperature of 1500°C to room temperature. The transformed monoclinic particle was twinned and exerted an anisotropic compressive stress on the matrix. It was much larger than the tetragonal field and perpendicular to it. Various theoretical studies have been made of the crystallography of the transformation mechanism in the bulk.[12-14] Their applicability to confined particle mechanisms has been questioned, however, since experimental observations suggest that matrix-constraining forces may also need to be considered in theoretical predictions.[5]

Martensitic transformation mechanisms have been recognized and confirmed both experimentally and theoretically in single-crystal studies of inorganic compounds by Kennedy and coworkers[15-17] during the past 25 years. Several such compounds underwent large volume changes. For example, a volume change of −16% occurred in NaCl-type → CsCl-type transformations in the alkali halides.[15-17] The zinc blende → NaCl-type and wurtzite → NaCl-type transformations in manganous sulfide (MnS) underwent 19% and 20% volume changes, respectively.[20-22] The transformations in the alkali and ammonium halides have been quantitatively proven to be martensitic.

Preliminary investigations have been made into the application of the wurtzite-type → graphite-type transformation in boron nitride (BN) which normally occurs under high pressures.[23] No stress-induced transformation at ambient pressures could be induced, however, presumably because of the extremely high nucleation barrier associated with such a large volume change. Allowing for high-pressure compressibility effects, we estimated the volume change as 31% (33% in the structurally analogous lonsdaleite → graphite transformation in carbon).[24] The volume change for BN (graphite-type → wurtzite-type transformation) under shock compression was measured as −19%.[23] Although hafnia (HfO_2) is isostructural with zirconia, no transformation toughening using HfO_2 has been reported to date.

Lattice deformational (displacive) transformations in nonmetals (including inorganic compounds, ceramics, minerals, and components of glass and portland cement) have been reviewed by Kriven.[25,26] Although nonmetals have not been extensively studied from the point of view of mechanisms, many exhibit characteristics and behavior analogous to zirconia (e.g., rapid kinetics and shattering). Such characteristics are also presumably common to martensitic transformations having large volume changes. When the structures are complex, or pure lattice strains are large, a choice of mechanism may operate for the same parent and product structures.[25] Examples have been observed where a mechanism may be diffusive, i.e., reconstructive,[26] or, under different nucleating conditions (e.g., rapid quenching, stress induced), displacive or lattice deformational.[27] Martensitic transformations are a subset of the latter category.[27]

Although there is no such choice of mechanism in zirconia, it can now be viewed as a model system for transformation toughening. However, since it has both a volume change *and* a shape change associated with the $t \rightarrow m$ transformation, it is not clear which is the more important component for toughening. Furthermore, the shape change can be subdivided into the unit-cell (angular) shape change (e.g., $\Delta\beta$, the change in monoclinic β angle is 9° in ZrO_2 in going from t to m symmetry) and the macroscopic shape change (m_1) associated with the martensitic mechanism.[2,28,29] In the quest for new alternative transformation tougheners to zirconia, therefore, a systematic study is necesssary in order to vary the components of the transformation. The relative effects on the mechanical properties of such composite ceramic systems can then be evaluated.

The aim of this review is to survey the literature for experimental and crystallographic evidence for displacive, possibly martensitic, phase transformations. This review will focus on those transformations having positive volume changes on cooling analogous to zirconia. Preliminary experimental observations and theoretical considerations will be presented. Table I summarizes these compounds and the relevant physical properties which can affect the mechanical properties of composite materials. The volume change in going from phase 1 to 2 is calculated as $(V_2 - V_1)/V_1$. The variety of chemical compositions brings to light a greater variety of chemically compatible matrices. The various combinations of volume and shape changes and crystallography open up an area in which little research has been done, but which has great potential scientific relevance and technological application.

II. Lanthanide Sesquioxides (Ln_2O_3)

(1) Lanthanide Sesquioxides

The rare-earth oxides have been comprehensively studied for many years,[30] and their transformations were reviewed.[31] The materials are among the most thermally stable known, melting from 2200° to 2500°C. The metal substructure is rigid up to the melting point, and temperatures of the order of 1200° to 1400°C are required before appreciable metal atom movement occurs. In contrast, there is high mobility in the oxygen sublattice, commencing above ~300°C. The sesquioxides are thermodynami-

Table I. Summary of Possible Alternative Transformation Tougheners to ZrO_2

Compound	Crystal symmetries	T, °C[a]	Change	
			ΔV, %	Angular, deg
ZrO_2	Tetragonal → monoclinic	950	−4.9	9
Ln_2O_3	Monoclinic → cubic	600–2200	−8 – −10	10
$2CaO \cdot SiO_2$	Monoclinic → orthorhombic	490	−12	4.6
NiS	Rhombohedral → hexagonal	379	−4	
$MgO \cdot SiO_2$	(PE) orthorhombic → (CE) monoclinic	865	5.5	18.3
$LnBO_3$	Hexagonal → hexagonal	550–800	−8.2	
$LuBO_3$	Hexagonal → rhombohedral	1310	−8	

[a] Transformation temperature. [b] Room temperature. [c] Transformation weakened.

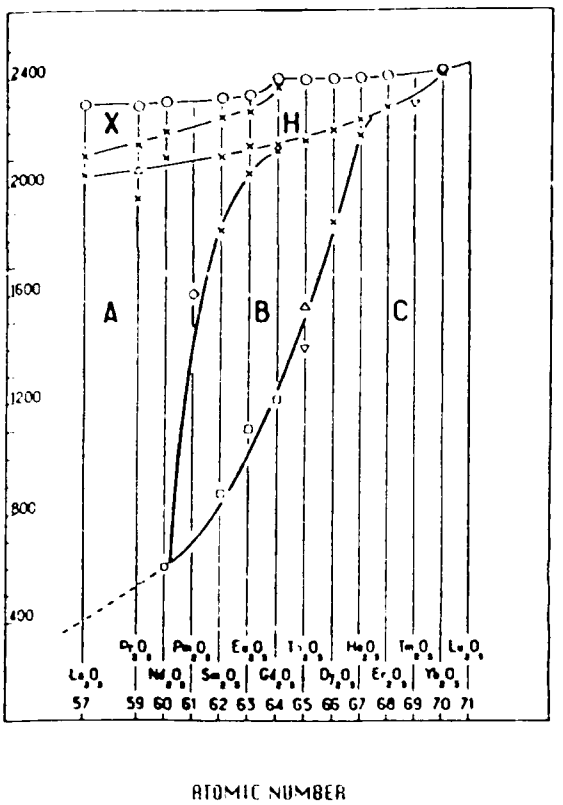

Fig. 3. Polymorphic forms and transformation temperatures of the lanthanide sesquioxides.[37]

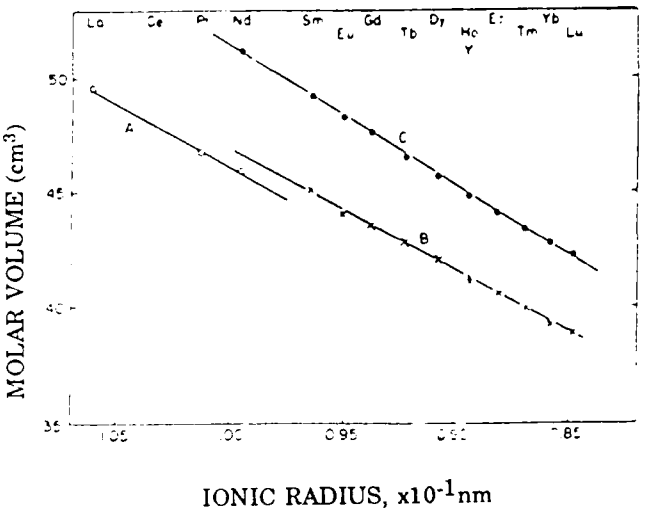

Fig. 4. Molecular volumes of the A, B, and C crystal structures in the lanthanide sesquioxides.[48]

cally very stable, so that vapor-transport reactions are negligible. Some oxides (e.g., Sm, Gd, Eu) have good nuclear irradiation stability and are potentially useful in nuclear reactors.

Most of the work on phase equilibria and crystal structures was done by Foex and co-workers[37-42] on samples crystallized from the melt in a solar furnace. The slightly lower temperature equilibria A ↔ B ↔ C were also studied in sintered pellets[43-45] and in materials prepared by chemical inorganic precipitation methods using hydroxides.[47]

The polymorphic transformations in lanthanide sesquioxides are summarized in Fig. 3.[37] Phase A is hexagonal, space group (SG) $P\bar{3}m1$, and contains 1 formula unit per unit cell ($Z = 1$). The cations are in sevenfold coordination with four close and three less-close oxygens. Phase B is monoclinic, SG $C2/m$, $Z = 6$, and has a sevenfold coordination of the cation.[48] Phase C is cubic and is fluorite derived, SG $Ia\bar{3}$, $Z = 16$, and CN = 6.[48,49] The high-temperature H and X phases are hexagonal and cubic, respectively. Thermal expansion coefficients and some kinetics for the A ↔ B ↔ C transformation oxides prepared from different starting compounds have been determined.[50-53]

(2) Hexagonal ↔ Monoclinic ↔ Cubic Transformation

Like ZrO_2, the A → B → C transformations are anomalous in that there is a volume increase on cooling. As shown in Fig. 4, the B → C volume change has been estimated as 8% to 10%, whereas that of A → B is much less.[37] The B phase was highly pressure sensitive and may be stabilized with respect to the C form on application of pressure.[37,54] Pellets of Eu_2O_3 underwent the C → B transformation during grinding on abrasive paper.[37] The B → C transformation in Dy_2O_3 was induced by grinding of splat quenched flakes.[55] Although there was some discussion of a reconstructive mechanism for B → C transformation,[37,55] Foex and Traverse[37] reported that the speed of B → C transformation grew very rapidly as one advanced along the series from Sm$_2$O$_3$ to Ho$_2$O$_3$, and the transformation temperature increased. The large volume increase on cooling caused the ceramic to shatter. However, at higher temperatures, e.g., in holmia, there was sufficient kinetic energy to permit posttransformational rearrangement to accommodate the drastic volume increase and, therefore, avoid fragmentation. By forming solid solutions, e.g., Gd_2O_3–Dy_2O_3, the B → C transformation may be made to occur over a continuous temperature range.[54] Chemical stabilization of the B form was achieved by the addition of CaO or SrO as dopants in combination with rapid quenching.[35,38] Substitution of Ca^{2+} ions for trivalent rare-earth ions caused oxygen vacancies and the destructive B → C transformation was suppressed. The amount of chemical stabilizer increased with increasing atomic number. The solid solutions were not stable, however, and reverted to Ln_2O_3 and CaO on prolonged annealing at 1200°C.[34] The CaO–Dy_2O_3 phase diagram is known and gives a solid-solution limit of CaO in B-phase dysprosia of ≈12 mol%.[55] Attempts to produce a partially stabilized dysprosia (PSD) analogue to PSZ have been under way in our laboratory using 8 mol% CaO–Dy_2O_3 compositions, and the work will be published separately.[56]

Current work in our laboratory by Jero and Kriven[57] has shown that the B → C transformations in the sesquioxides below Gd_2O_3 proceed with extremely slow, reconstructive kinetics and, therefore, do not appear to be viable choices for transformation toughening. However, the heavier members, in particular terbia and dysprosia, are viable, although the use of terbia is limited to inert atmospheres at elevated temperatures because of its tendency to disproportionate to Tb_4O_7. Dysprosia, with an M_s temperature of 1950°C on cooling, appears to be the most worthy of investigation at present. Having an even atomic number (66), it is more abundant than the odd-atomic-numbered members of the series.[58] No critical particle size analyses have been undertaken as yet. However, metastable retention of the high-temperature monoclinic phase is considered to depend also on the volume change and relative elastic moduli between the matrix and the toughening phase. Unlike ZrO_2 systems, rapid-cooling kinetics have been recognized to play a crucial role in retention of the high-temperature B phase.[37,54]

(3) Microstructure and Defects Associated with the A ↔ B ↔ C Transformations

Boulesteix *et al.*[59,60] and Caro[61,62] extensively studied the microstructure and defects produced in the A ↔ B ↔ C transformations. They grew thin films of the lanthanide sesquioxides in situ from rare-earth metal foils in the TEM. The oxides were generally large and thin crystallite grains, with a diameter of several micrometers and a thickness of ~50 nm. Transformations between polymorphs was achieved by strains induced by selective heating by the electron beam.

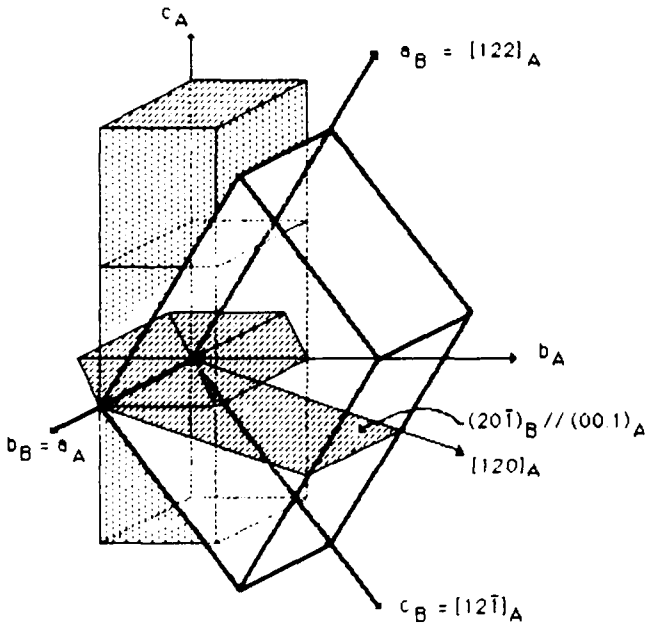

Fig. 5. Structural relationship between three stacked, primitive subcells of hexagonal A phase and the monoclinic ($Z = 6$) X-ray cell of the B-phase lanthanide sesquioxides.[71]

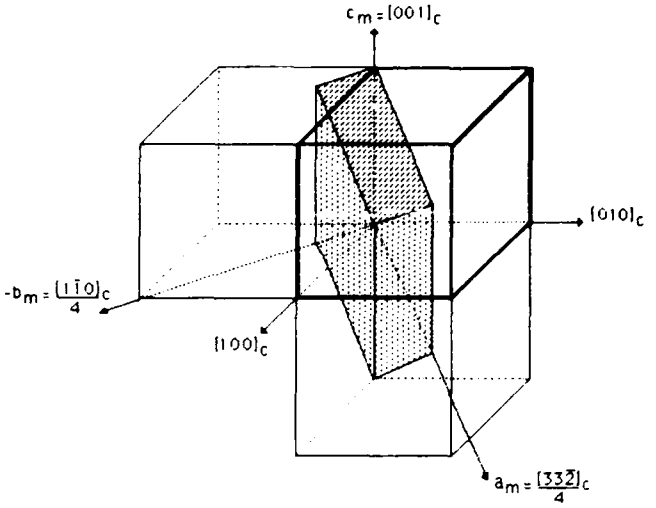

Fig. 6. Structural relationship between the monoclinic ($Z = 6$) (hatched) and cubic ($Z = 16$) X-ray unit cells of the lanthanide sesquioxides.[71]

Complex twinning was observed in the monoclinic B phase, as comprehensively reviewed by Boulesteix[67] and Caro.[65,70] Four different twinning systems were observed, viz., {313} and (132) (with magnitudes of shear, $s = 0.186$), and their combinations. The twins were mechanical in nature, produced by stresses associated with the heating and cooling of the electron beam. Transformation twins were also formed in the A → B transformation. The twin systems were either type 1 (reflection) or type 2 (rotation twins). Several preferred crystal orientations and unusual formations were observed and found to correlate well with the oxygen coordination scheme proposed by Caro.[69,70] For example, the A- and B-type grains usually formed in an epitaxial type of relationship such that the surface of the crystal (i.e., the large dimension) was parallel to the plane of the OLn_2 layers, i.e., $(0001)_A$ or $(20\bar{1})_B$.

A "martensitic character" has also been suggested for the B → A transformation.[70] Electron microscopy studies of the A → B transformation mechanism have indicated the orientation relation[71]

$$(0001)_A \; (20\bar{1})_B \quad \text{where} \quad (11\bar{2}0)_A \; [010]_B$$

This led to the postulation of a lattice correspondence between the hexagonal and monoclinic cells.[71] Figure 5 depicts this relationship in terms of three stacked, primitive hexagonal subcells and the monoclinic ($Z = 6$) cell.[71] The monoclinic structure is related to the hexagonal by a 3.2° shear of the basal hexagonal layers $(0001)_A$ and $(20\bar{1})_B$. Because of the pseudohexagonal symmetry of the B phase, there were 12 rotational variants of the twinning systems which could occur. A 13th variant could occur by double twinning.

Studies of the C phase found it to be more prone to slip than twinning, although one twin system was identified.[67] The B → C transformation was observed in the electron microscope with two different orientation relations being reported.[61,65] The structural relationship between B and C is complicated by having to compare X-ray unit cells of differing numbers of formula units. However, Fig. 6 illustrates a possible lattice correspondence postulated by Sudre and Kriven,[71] in which the cubic $Z = 16$ cell is related to the monoclinic $Z = 6$ cell.

In summary, the experimental observations implying the possibility of transformation toughening by the higher atomic number members of the lanthanide sesquioxides is presented in Table II. The high M_s temperatures (to 2200°C) in the higher atomic number Ln_2O_3 compounds indicate the possibility of high-temperature transformation toughening.

III. Dicalcium Silicate (Ca_2SiO_4)

Dicalcium silicate (belite) is one of the four major components of cement, the other constituents being tricalcium silicate ($3CaO \cdot SiO_2$), tricalcium aluminate ($3CaO \cdot Al_2O_3$), and tetracalcium aluminoferrite ($4CaO \cdot Al_2O_3 \cdot Fe_2O_3$) type phases.[72–75] In addition, minor amounts of calcium sulfate dihydrate (gypsum, $CaSO_4 \cdot 2H_2O$) are important in controlling the hydration of these components. The crystallography and polymorphism of

Table II. Comparison of the B → C Transformation in the Lanthanide Sesquioxides (Ln_2O_3) with the Tetragonal → Monoclinic Transformation in ZrO_2

	ZrO_2	Sm_2O_3–Dy_2O_3
Structure change	Tetragonal → monoclinic	Monoclinic → cubic
Coordination number	8 → 7	7 → 6
Volume change (%)*	+4.9, crystal shatters	+8 to +10, crystal shatters
Unit-cell shape change, $\Delta\beta$ (deg)	9	10
Transformation temperature, M_s (°C)	950	600–2200
Chemical stabilizers	CaO, MgO, Y_2O_3	CaO, SrO
Pressure stabilization	t-ZrO_2 in Al_2O_3	B phase stabilized by pressure
Transformable by grinding	Yes, in reverse direction	Yes, in reverse direction
Posttransformational rearrangement	Beginning	Yes, with increasing temperature

*Room temperature.

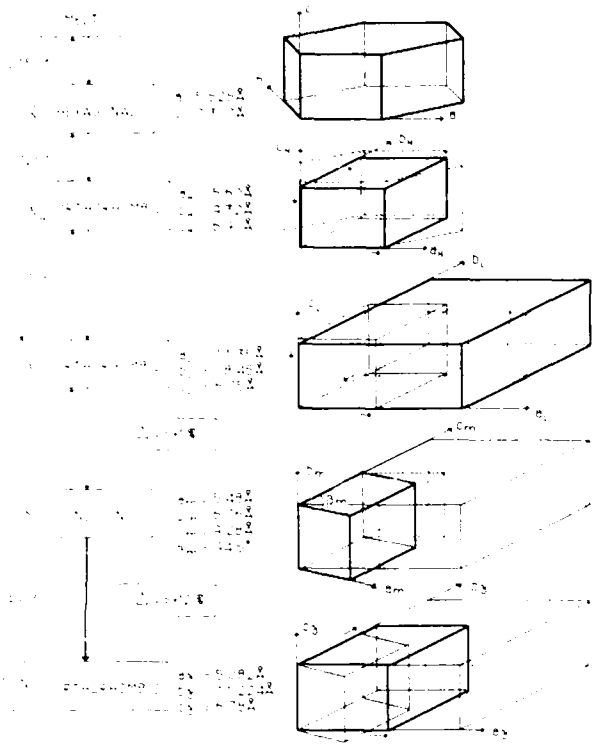

Fig. 7. Polymorphic transformations in Ca_2SiO_4.[93]

pure dicalcium silicate (abbreviated C_2S) have been extensively studied[93,94] and reviewed[95,96] and are summarized in Fig. 7. Udagawa *et al.*[97,98] conducted single-crystal X-ray experiments and determined the lattice correspondences as drawn. The widely known effect of "dusting" or self-disintegration of portland cement is due to the large, positive volume increase of 12% which accompanies the $\beta \rightarrow \gamma$ transformation in dicalcium silicate. Figure 8 shows the C_2S grains in the SEM which transformed to γ.[94]

The effect of chemical dopants in stabilizing the various polymorphs of C_2S down to room temperature has been extensively studied and reviewed[95,96,99–104] The exact role of the dopants, however, is unclear, since in some cases (e.g., K_2O), concentrations of the dopant were found in an intergranular, amorphous phase rather than in solid solution with the C_2S. Furthermore, recent experiments show that the stabilizing effect in K_2O-doped C_2S depends on the cooling rate or the annealing treatment after sintering.[105] In Al_2O_3-doped C_2S systems on the other hand, aluminum can be found both in the glassy phase and in solid solution with C_2S.[106]

The physical factors affecting the $\beta \rightarrow \gamma$ transformation have been studied by X-ray diffraction, optical microscopy, SEM, and electron probe microanalysis. A review of the cement chemistry literature[95,96,107–109] shows that the ratio of β to γ in repeatedly ground and sintered pellets of C_2S depended on the following parameters:

(i) Particle size. A large γ-C_2S particle size tended to produce γ phase for given annealing conditions of temperature, time, and a slow cooling rate. Small initial γ-C_2S size, however, stabilized the β phase. These observations were made both in sintered powders[107,110] and in dense pellets.[111,112,113]

(ii) Temperature. Increased annealing temperatures below the $\alpha_H' \rightarrow \alpha_L'$ transformation temperature of 1425°C produced more γ.[107,110,111] This was also the case for annealing above 1425°C, but there accelerated grain growth had occurred.[107,110]

(iii) Time. Longer annealing times produced more γ-C_2S, but this effect was secondary to the effect of temperature.[107,111]

(iv) Kinetics. The kinetics of cooling through the $\alpha_H' \rightarrow \alpha_H'$ transformation was very important. Slow cooling through 1425°C led to the formation of γ-C_2S whereas fast cooling tended to retain β-C_2S in the final microstructure.[106–108]

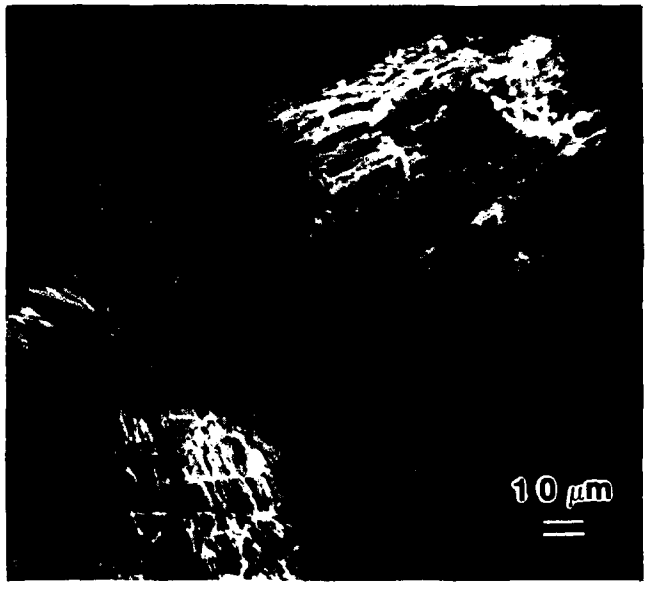

Fig. 8. SEM micrograph of C_2S grains which underwent $\beta \rightarrow \gamma$ transformation and "dusted" because of the accompanying large 12% molar volume increase.[94]

Thus, it was concluded that a particle size effect operated in controlling the $\beta \rightarrow \gamma$ transformation in C_2S.[94]

In contrast with zirconia, which is twinned *after* transformation to monoclinic, the parent, monoclinic β-C_2S, is twinned *before* transformation to orthorhombic γ-C_2S. This leads to an ambiguity in the definition of the critical particle size.[94] Specifically, a critical particle volume for transformation could be defined by the overall β-C_2S particle size, the twin thickness, or a combination of both the twin thickness and twin length.

The third condition occurs when C_2S pellets are very rapidly quenched from above the $\alpha_H' \rightarrow \alpha_L'$ transformation temperature at 1425°C. Work in progress by Chan *et al.*[94,105,113] indicates that this causes the β twins to undergo regular microcracking diagonally across the twins. It is hypothesized[105,113] that the $\alpha \rightarrow \alpha_H'$ transformation initiates a large shrinkage in unit-cell volume, which is intensified by the quenching of high-temperature, thermally expanded lattice parameters. It is estimated that −6.56% volume shrinkage needs to be accommodated. This causes stresses to be accumulated within the C_2S grains which are relieved by periodic microcracking of twinned β-C_2S particles or herringbone twinned microstructures.

However, quantitative values for the critical particle size for transformation were inconsistent, ranging from 5[107,110] to 7 μm[107,110] down to 0.2 to 0.3 μm.[107,108] The large values were obtained by optical microscopy and SEM and referred to overall C_2S particle size, whereas the submicrometer values obtained from X-rays and SEM referred to the width of individual transformed γ laths within C_2S particles, as seen, for example, in Fig. 8. TEM microstructural studies of the $\alpha' \rightarrow \beta$ and $\beta \rightarrow \gamma$ transformations found that γ-C_2S was formed by the growth of needles or laths whose long axes were *parallel* to [001] or [010].[113–116]

Recently, C_2S particles have been successfully mixed with a calcium zirconate phase to form a composite ceramic[95,96,117] with a microstructure similar to ZTA. Figure 9 is a TEM micrograph of a pure β-C_2S particle confined in a calcium zirconate matrix.[94] It is twinned on (100), as a result of the $\alpha' \rightarrow \beta$ transformation which is thought to be martensitic.[113,117] The metastable β-C_2S particles of suitable size and confined in a matrix can be induced to transform to γ by grinding.[95,96,118] Finally, the evidence for postulating C_2S as a transformation toughener is summarized in Table III.

Fig. 9. *TEM micrograph of a β-C_2S grain twinned on $(100)_m$ and metastably confined in a calcium zirconate (CZ) matrix.*[22]

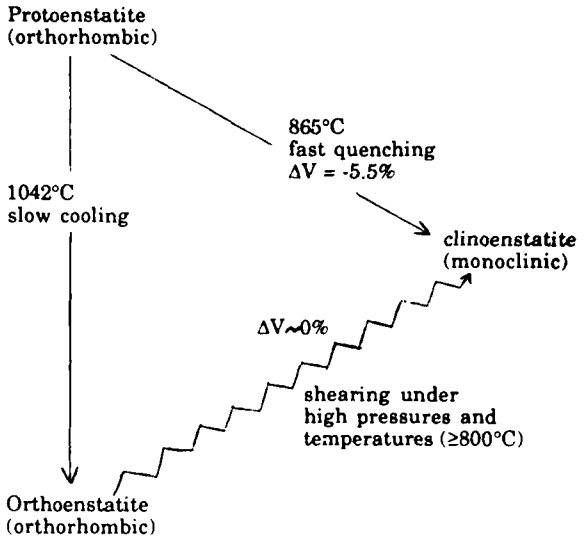

Fig. 10. Polymorphs of enstatite ($MgSiO_3$). Clinoenstatite is a metastable phase obtained by quenching of protoenstatite.

IV. Nickel Sulfide (NiS)

Nickel sulfide (millerite) exists as the following polymorphs at 1 atm:[119]

$$\underset{\text{rhombohedral}}{\beta} \xrightleftharpoons[\sim 396\,°C]{\sim 379\,°C} \underset{\text{hexagonal, NiAs-type}}{\alpha}$$

During processing of soda–lime plate glass, spherical or ellipsoidal NiS inclusions were metastably retained in the high-temperature α form down to room temperature. It was recognized[120-123] that spontaneous transformation of particles of α-NiS to β caused destruction of the glass when the particles were located in the internal stress field. Plate glass can be thermally toughened by quenching, which produces a compressive stress state in the surface region. The $\alpha \rightarrow \beta$ transformation is accompanied by a volume increase of +3.93%.[124] NiS is an IR radiation transmitter at 8 to 14 μm.

A critical particle size effect was theoretically predicted and calculated from fracture mechanics considerations of annealed glass.[124-125] Critical sizes for nucleation of the transformation and microcracks around the particles were estimated at 32 to 22 μm. However, in tempered glass, the critical size depended on the particle location because of different stress levels in surface versus bulk regions.

It was concluded that the $\alpha \rightarrow \beta$ transformation in NiS could be avoided by either of two methods:[125]

(i) The particles could be chemically doped with NiSe or NiAs.

(ii) The internal oxygen partial pressure could be altered during processing so as to produce nonstoichiometric Ni-S_x, Ni_3S_2, or elemental Ni.

V. Magnesium Metasilicate ($MgSiO_3$)

Enstatite ($MgO \cdot SiO_2$) is the major component of steatite ceramics which are used as electrical insulators. They have low power losses in the high-frequency range and good dielectric properties to elevated temperatures. The polymorphism of enstatite has been extensively reviewed[23,25,126] and is summarized in Fig. 10. At ambient pressures, enstatite exists as protoenstatite (proto) above 1042°C and orthoenstatite (ortho) on slow cooling to room temperature. Fast quenching of proto, however, produces metastable clinoenstatite (clino) at 865°C. The monoclinic β angle is 108.3°. The proto → clino transformation is accompanied by a −5.5% volume decrease, whereas the ortho → clino transformation volume change is negligible. The monoclinic β angle is 108.3°, which gives a unit-cell shape change $\Delta\beta = 18.3°$. This is approximately double that of ZrO_2 ($\Delta\beta = 9°$).

The transformation mechanisms between the three phases have been investigated.[127-137] The slow proto → ortho transformation mechanism is considered to be reconstructive.[26] Similarly, clino reverts to ortho on annealing at high temperatures and via the proto phase.[128] Prolonged annealing only, between 650° and 950°C, also produces ortho via a slow, apparently reconstructive mechanism.[136]

In contrast, the proto → clino transformation on quenching is very rapid and displacive. The mechanism has martensitic characteristics, being diffusionless, athermal, stress inducible, and having an orientation relation between parent and product phases.[135,136]

Clinoenstatite has an equilibrium stability field only above 566°C + (4.5°C/kbar)P, where P is applied hydrostatic pressure of geological magnitudes.[135] Under hydrostatic stresses, the ortho →

Table III. Comparison of the $\beta \rightarrow \gamma$ Transformation in Ca_2SiO_4 with the Tetragonal → Monoclinic Transformation in ZrO_2

	ZrO_2	Ca_2SiO_4
Structure change	Tetragonal → monoclinic	Monoclinic → orthorhombic
Transformation temperature, M_s (°C)	950	490[57]
Volume change (%)	+4.9	+11.96[57]
Coordination number change	8 → 7	Ca(I) 7, Ca(II) 8 } 6[57]
Unit-cell shape change, $\Delta\beta$ (deg)	9	4.6
Chemical stabilizers	MgO, CaO, Y_2O_3	B_2O_3, Al_2O_3, BaO, K_2O, Cr_2O_3, etc.
Transformation induced by grinding	Yes	Yes

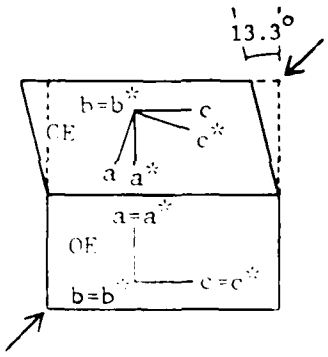

Fig. 11. Lattice correspondence adopted by orthoenstatite in transforming to clinoenstatite under 5×10^8 Pa (5 kbar) confining pressure and 800°C, and under a constant strain rate applied at 45° to the **a** and **c** axes.[77]

clino transformation is slow and sluggish, requiring the use of fluxes and long reaction times.[77] At elevated temperatures (below 1000°C) and under high pressures, particularly nonhydrostatic stress directed along the crystallographic $(100)[001]_o$ direction, the kinetics of the ortho → clino transformation can be accelerated.[77] Typical conditions required are 5×10^8 to 6×10^8 Pa (5 to 6 kbar) at 800°C, 5×10^8 Pa (50 kbar) at 920°C,[77] or high strain rates directed along $(100)[001]_o$ above 450° to 650°C. Under these conditions, the ortho → clino transformation appears to be displacive.[77] The lattice correspondence observed is illustrated in Fig. 11,[77] where the unit cell shape change of 18.3° is effectively reduced to 13.3° because of the lattice correspondence adopted. The suggestions of a martensitic mechanism for ortho → clino,[157,162] however, are refuted by TEM observations of partially transformed microstructures.[77,157] The coexistence of ortho and clino lamellae, controllable kinetics, and lack of any martensitic features (such as an interface or habit plane) indicate a nonmartensitic mechanism. Hence, the potential application of the ortho → clino transformation as a toughening mechanism is doubtful in the realm of conventional ceramic composites.

The proto → clino transformation which is apparently martensitic, however, has a large negative volume change on cooling. One might say that "transformation weakening" was first recognized in some $CaCO_3$-containing steatite ceramics which degraded and fractured after a period of storage at room temperature.[163] The problem was attributed to CaO in calcined powders which caused enhanced grain growth during sintering as compared with BaO under the same conditions. Careful experiments showed that a critical particle size effect operated.[30,159,160] Proto particles larger than 7 μm transformed spontaneously to clino, whereas those smaller than 7 μm metastably remained in the proto phase. The large negative volume change accompanying the proto → clino transformation was responsible for the deleterious effects on the steatite body.

Chemical stabilization of the enstatite polymorphs can be achieved by 1 to 2 mol% additions of MnO to proto[147] or by doping ortho with alumina.[152] MgF_2 and LiF act as mineralizers in proto formation and they affect the proto → clino transformation.[154]

Finally, the transformations in enstatite are arch types for other silicates, in particular, ferrosilite and wollastonite.[127,142] Ferrosilite ($FeO \cdot SiO_2$) is isostructural with enstatite, whereas the monoclinic ↔ triclinic transformations in wollastonite and parawollastonite ($CaO \cdot SiO_2$) are considered to be shear related, by analogy with enstatite.[77,78]

VI. Lanthanide Borates ($LnBO_3$)

The polymorphism of the RBO_3-type lanthanide borates has been studied by Levin *et al.*[144,145] Essentially, this type has the

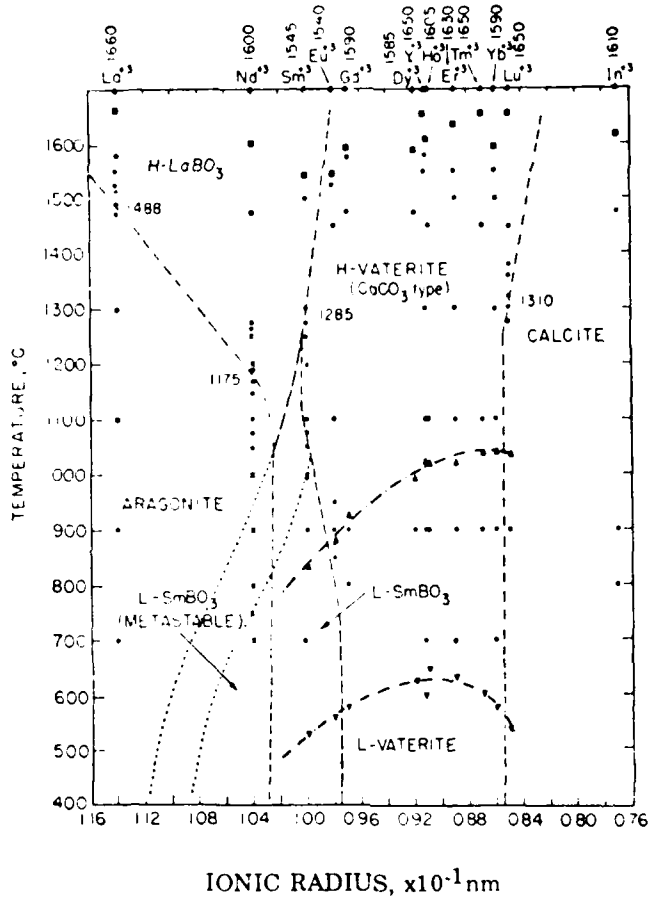

Fig. 12. *Stability relations of the ABO_3-type borates as a function of* temperature and ionic radius of the large cation.[145]

$CaCO_3$-type structure of aragonite, calcite, or vaterite. The equilibrium and metastable phase fields are shown in Fig. 12.[145] In the aragonite- and calcite-type phases, the CO_3^{2-} or BO_3^{3-} groups are trigonal planar in arrangement. However, in the vaterite-like borates, unlike the carbonates, the BO_3^{3-} groups have an unusual T shape, with one B–O bond longer than the other two.[145] The vaterite-type phases are hexagonal and have higher densities than the calcite-type phases for a given lanthanide compound. As seen in Fig. 12,[145] lutetium borate ($LuBO_3$) has the smallest ionic radius and is the only borate to undergo the vaterite-type → calcite-type transformation at 1310°C. It is accompanied by the anomalous volume increase of +8.1% on cooling and is reversible. The kinetics and nature of the transformation mechanism, however, are not known.

The vaterite-type phases themselves exist in high- and low-temperature modifications, where the high-temperature phase is most analogous to the $CaCO_3$-vaterite structure.[145] The transformation exhibits hysteresis which can be increased to 550°C by solid-solution formation with $LaBO_3$. On cooling, the high → low transformation causes cracking or "dusting" to a loose powder at room temperature. This is due to the large volume decrease of −8.2%. A large hysteresis of ~500°C accompanies the high → low vaterite-type transformation in $YbBO_3$, which has temperatures of ~550°C on cooling and ~1040°C on heating.[145] *Although these characteristics suggest that a martensitic* mechanism may be operating in the high → low vaterite-type transformation, the volume decrease on cooling indicates that it would not be useful as a transformation toughener.

In $LnBO_3$ solid solutions with $LaBO_3$, which also have vaterite-type structures, another transformation occurs from high $LaBO_3$ to low $SmBO_3$-type polymorphs.[145] The high $LaBO_3$ modification is unquenchable and the transformation also exhibits hysteresis of

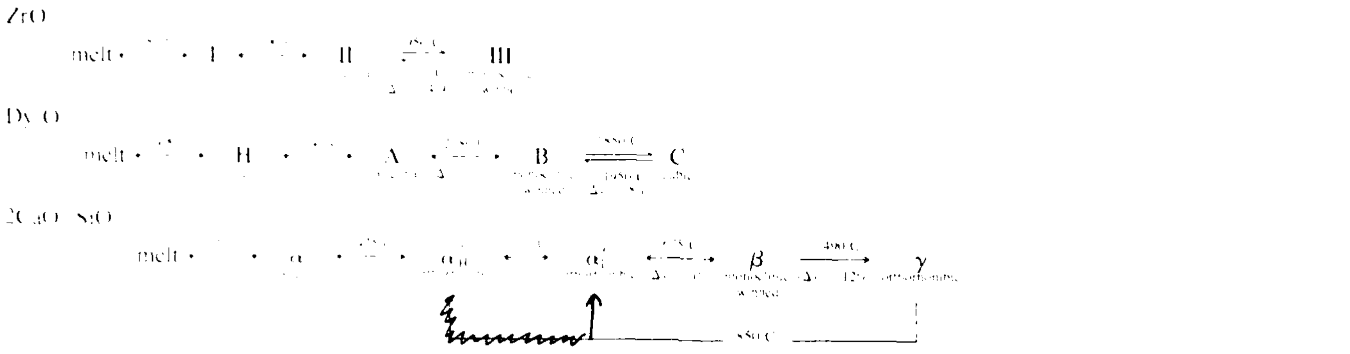

Fig. 13. Comparison of polymorphic transformations in ZrO_2, Dy_2O_3, and Ca_2SiO_4.

200°C and is accompanied by dusting. The volume change has not been determined, but the transformation may be chemically related to the high → low vaterite type transformation in pure LnBO systems.

VII. Discussion and Conclusion

Table I presents compounds which exhibit various combinations of volume and shape changes that accompany displacive phase transformations of interest in inorganic, ceramic, and mineral systems. Note that all the transformations accompanied by a volume increase on cooling are associated with a decrease in coordination number. Since the systems studied are not necessarily purely covalent or purely ionic, it is difficult to define the coordination number precisely. A common characteristic is that the transformations are sudden and explosive, causing "dusting," self-disintegration, or cracking of dense pellets. The challenge in transformation toughening is to design a composite ceramic material which controls and uses the energy of the martensitic mechanism in order to retard a propagating crack and, therefore, reduce brittleness. As in ZrO_2, a particle size effect appears to be operating in most systems (C S, N S, $MgSiO_3$), and our current work on the Ln O compounds also shows this effect.

Large volume changes are involved, as seen in Table I. In order to achieve a beneficial toughening effect, studies to date indicate that the volume change should be positive on cooling. Negative volume changes appear to be detrimental to a matrix. Note that various magnitudes of shape change are also involved. The shape change can be subdivided into an X-ray unit cell shape change (e.g., in ZrO_2 the unit cell changes from tetragonal to monoclinic [illegible] $\Delta\beta$ = 9°), an effective shape change (due to the lattice correspondence adopted (e.g., a 13.3° shape change in MgO·SiO as compared with the 18.3° change in the monoclinic β [illegible]), and a macroscopic shape change of a martensitic mechanism which results from the combination of a lattice variant deformation and a lattice invariant deformation such as slip or twinning.

Some interesting similarities exist between the phase transformations in ZrO_2, the lanthanide sesquioxides (e.g., Dy_2O_3), and the dicalcium silicate (Ca_2SiO_4) as summarized in Fig. 13.

[illegible] transformation toughening [illegible] of chemical compatibilities with [illegible]. However, compared with metals, the compounds have received negligible study and little is known about the transformation mechanisms. A systematic study of the various combinations of volume and shape changes and the role of relative elastic moduli between matrix and toughening phases can lead to a better understanding of the effects and applications of martensitic phase transformations to the mechanical properties of composite ceramics.

Acknowledgments: [illegible]

References

Advances in Ceramics, Vol. 3, Science and Technology of Zirconia I. Edited by A. H. Heuer and L. W. Hobbs. American Ceramic Society, Columbus, OH, 1981.

W. M. Kriven, W. L. Fraser, and S. W. Kennedy, "The Martensite Crystallography of Tetragonal Zirconia"; pp. 82–97 in Advances in Ceramics, Vol. 3, Science and Technology of Zirconia I. Edited by A. H. Heuer and L. W. Hobbs. American Ceramic Society, Columbus, OH, 1981.

Advances in Ceramics, Vol. 12, Science and Technology of Zirconia II. Edited by N. Claussen, M. Ruhle, and A. H. Heuer. American Ceramic Society, Columbus, OH, 1984.

(a) Proceedings of the 2d U.S.–Australian–West German Transformation Toughening Workshop, Lorne, Victoria, Australia, April 15–19, 1985, Part I, *J. Am. Ceram. Soc.*, **69** [3] 169–298 (1986); (b) Part II, *ibid.*, **69** [7] 511–84 (1986).

A. G. Evans and R. M. Cannon, "Toughening of Brittle Solids by Martensitic Transformations," *Acta Metall.*, **34** [5] 761–800 (1986).

Advances in Ceramics, Vol. 24, Science and Technology of Zirconia III. Edited by S. Somiya, N. Yamamoto, and H. Yanagida. American Ceramic Society, Westerville, OH, to be published in 1988.

A. H. Heuer, N. Claussen, W. M. Kriven, and M. Ruhle, "Stability of Tetragonal Zirconia Particles in Ceramic Matrices," *J. Am. Ceram. Soc.*, **65** [12] 642–50 (1982).

W. M. Kriven, "The Transformation Mechanism of Spherical Zirconia Particles in Alumina"; pp. 64–77 in Advances in Ceramics, Vol. 12, Science and Technology of Zirconia II. Edited by N. Claussen, *M. Ruhle, and A. H. Heuer*. American Ceramic Society, Columbus, OH, 1984.

(a) G. K. Bansal and A. H. Heuer, "On a Martensitic Phase Transformation in Zirconia (ZrO_2): Part I," *Acta Metall.*, **20** [11] 1281–89 (1972); (b) "Part II," *ibid.*, **22** [4] 409–17 (1974).

M. A. Choudrey and A. G. Crocker, "Theory of Twinning and Transformation Modes in Zirconia"; pp. 46–53 in Advances in Ceramics, Vol. 12, Science and Technology of Zirconia. Edited by N. Claussen, M. Ruhle, and A. H. Heuer. American Ceramic Society, Columbus, OH, 1984.

P. M. Kelly and C. J. Ball, "Crystallography of Stress-Induced Martensitic Transformations in Partially Stabilized Zirconia," *J. Am. Ceram. Soc.*, **69** [3] 259–64 (1986).

W. M. Kriven, "Martensite Theory and Twinning in Composite Zirconia Ceramics"; pp. 168–83 in Advances in Ceramics, Vol. 3, Science and Technology of Zirconia I. Edited by A. H. Heuer and L. W. Hobbs. American Ceramic Society, Columbus, OH, 1981.

S. W. Kennedy and J. H. Patterson, "Mechanism of Structure Transformations: Thallous Nitrate Crystals," *Proc. R. Soc. London, A*, **283**, 498–508 (1965).

W. L. Fraser and S. W. Kennedy, "The Crystal Structural Transformation NaCl Type → CsCl Type: Analysis by Martensite Theory," *Acta Crystallogr., Sect. A: Found. Crystallogr.*, **30**, 13–22 (1974).

S. W. Kennedy and W. M. Kriven, "Martensitic Transformation Cubic to Rhombohedral in Rubidium Nitrate," *J. Mater. Sci.*, **11**, [illegible] (1976).

S. W. Kennedy, W. M. Kriven, and W. L. Fraser, "Structural Transformations in KNO_3, $RbNO_3$, and NH_4Br"; pp. 208–13 in Proceedings of International Conference on Martensitic Transformations, ICOMAT. MIT Press, Cambridge, MA, 1979.

S. W. Kennedy and W. L. Fraser, "Martensitic Transformation I → II in NH_4Br"; pp. [illegible] in Proceedings of International Conference on Solid-to-Solid Phase Transformations. Edited by H. I. Aaronson, D. E. Laughlin, R. F. Sekerka, and C. M. Wayman. American Institute of Mining, Metallurgical, and Petroleum Engineers, Pittsburgh, PA, 1982.

S. W. Kennedy and W. M. Kriven, "Martensitic and Other Transformation Mechanisms and Relaxation in $RbNO_3$"; pp. 1848–49 in Proceedings of International Conference on Solid-to-Solid Phase Transformations. Edited by H. I. Aaronson, D. E. Laughlin, R. F. Sekerka, and C. M. Wayman. American Institute of Mining, Metallurgical, and Petroleum Engineers, Pittsburgh, PA, 1982.

[illegible] and S. W. Kennedy, "Martensitic Analysis of the [illegible]," [illegible] (unpublished work).

S. W. Kennedy, [illegible], and [illegible], "Mechanisms of [illegible] Transformation of Zinc Blende to NaCl in MnS Crystals," *J. Solid State Chem.*, **31**, [illegible] (1980).

S. W. Kennedy and [illegible], "Mechanisms of Transformation from the Wurtzite to the NaCl Structure in MnS"; pp. [illegible] in Proceedings of International Conference on Solid-to-Solid Phase Transformations. Edited by H. I. Aaronson, D. E. Laughlin, R. F. Sekerka, and C. M. Wayman. American Institute of Mining, Metallurgical, and Petroleum Engineers, Pittsburgh, PA, 1982.

[illegible] and N. Claussen, "Toughening of RN by Stress-Induced Phase Transformation," *Mater. Res. Bull.*, **13**, [illegible] (1978).

W. M. Kriven, "Shear Transformations in Inorganic Materials"; pp. 1507–[illegible] in Proceedings of International Conference on Solid-to-Solid Phase Transformations. Edited by H. I. Aaronson, D. E. Laughlin, R. F. Sekerka, and C. M. Wayman

American Institute of Mining, Metallurgical, and Petroleum Engineers, Pittsburgh, PA, 1982.

N. L. Coleburn and J. W. Forbes, "Irreversible Transformation of Hexagonal Boron Nitride by Shock Compression," *J. Chem. Phys.*, **48** [2] 555–59 (1968).

W. M. Kriven, "Displacive Transformation Mechanisms in Zirconia Ceramics and Other Nonmetals"; pp. 223–37 in Tailoring Multiphase and Composite Ceramics. Edited by R. E. Tressler, G. L. Messing, C. G. Pantano, and R. E. Newnham. Plenum Press, New York, 1986.

M. J. Buerger, "Crystallographic Aspects of Phase Transformations"; pp. 183–[illegible] in Phase Transformations in Solids. Edited by R. Smoluchowski, J. E. Mayer, and W. A. Weyl. Wiley, New York, 1951.

M. Cohen, G. B. Olson, and P. C. Clapp, "On the Classification of Displacive Phase Transformations"; pp. [illegible] in Proceedings of International Conference on Martensitic Transformations, ICOMAT. MIT Press, Cambridge, MA, 1979.

Z. Nishiyama, Martensitic Transformation; pp. 372–73. Edited by M. E. Fine, M. Meshii, and C. M. Wayman. Academic Press, New York, 1978.

C. M. Wayman, Introduction to Crystallography of Martensitic Transformations. [illegible] Macmillan, New York, 1964.

[illegible] "[illegible] in Steatite Ceramics," *J. Br. Ceram. Soc.*, **2**, 309–16 [illegible]

[illegible] "The Binary Rare Earth Oxides"; pp. 337–99 in Handbook on the Physics and Chemistry of Rare Earths, Ch. 27. Edited by K. A. Gschneidner, Jr., [illegible] North Holland, Amsterdam, Netherlands, 1979.

[illegible] "The Binary Rare Earth Oxides"; in Handbook on the Physics and Chemistry of Rare Earths, Vols. 3 and 4. Edited by K. A. Gschneidner, Jr., and L. [illegible] North Holland, Amsterdam, Netherlands, 1979.

M. Foex, "Measurement of the Points of Solidification of the Refractory Oxides," [illegible] *Hautes Temp. Refract.*, **3**, 309–26 (1966).

M. Foex, [illegible] the Allotropic Transformations of Rare Earth Ses[illegible] *C. R. Acad. Sci.*, **337** [illegible] (1965).

M. Foex [illegible] Traverse, "Comments on the Allotropic Transformations of [illegible]" *Rev. Int. Hautes Temp. Refract.*, **3**, 429–53 [illegible]

M. Foex [illegible] Traverse, "A Study of the Polymorphism of the Rare-Earth [illegible]" (in Fr.), *Bull. Soc. Fr. Mineral. Cristallogr.*, **89** [illegible]

M. Foex [illegible] Traverse, "[illegible] the Different Crystalline Transforma[illegible] High Temperatures of the Rare Earth Sesquioxides" (in Fr.), [illegible] C, **262** [illegible] (1966).

M. Foex [illegible] C–B Transformation in the Rare [illegible] *Bull. Soc. Fr. Mineral. Cristallogr.*, **77**, 521–22 [illegible]

[illegible] R. Verges, [illegible] M. Foex, "High Temperature Study of [illegible] Sesquioxide with the Lanthanide Sesquioxides [illegible]" *J. Solid State Chem.*, **17**, 171–82 [illegible]

[illegible] R. Verges, [illegible] M. Foex, "High Temperature Study of the System [illegible] Sesquioxide with the Sesquioxides of Yttrium and [illegible]" *Mater. Res. Bull.*, **9** [illegible] (1974).

[illegible] B. Granier, R. Renard, and M. Foex, [illegible] for the High Temperature Study of the [illegible] Refractory Oxides" (in Fr.), *Rev. Int. Hautes* [illegible] **15** [illegible]

[illegible] R. Verges, and M. Foex, "Comparison of the Values of Solidification [illegible] Different Rare Earth Sesquioxides: Influence of the [illegible]" *Rev. Int. Hautes Temp. Refract.*, **12** [illegible] (1975).

R. S. Roth [illegible] S. J. Schneider, "Phase Equilibria in Systems Involving the Rare Earth Oxides. Part I. Polymorphism of the Oxides of the Trivalent Rare Earth [illegible]" *J. Res. Natl. Bur. Stand., Sect. A*, **64** [illegible] (1960).

S. J. Schneider and R. S. Roth, "Phase Equilibria in Systems Involving the Rare Earth Oxides. Part II. Solid State Reactions in Trivalent Rare Earth Oxide Systems," *J. Res. Natl. Bur. Stand., Sect. A*, **64** [illegible] 317–22 (1960).

S. J. Schneider, R. S. Roth, and J. L. Waring, "Solid State Reactions Involving [illegible]" *J. Res. Natl. Bur. Stand., Sect. A*, **65** [illegible]

[illegible] and R. Roy, "[illegible] of the Rare Earth Sesquioxides," [illegible] **65** [illegible]

[illegible]

[illegible] "Study of Thin Layers of Type B Samarium Sesquioxide by Microscopy and Electron Diffraction Techniques" (in Fr.), *Acta Crystallogr., Sect. B: Struct. Crystallogr. Cryst. Chem.*, **27**, 216–20 (1971).

C. Boulesteix, P. E. Caro, M. Gasgnier, Ch. H. La Blanchetais, and G. Schiffmacher, "Phase Transformations in Rare-Earth Oxide Thin Films," *Proc. Rare Earth Res. Conf., 9th*, 777–85 (1971).

C. Boulesteix, P. E. Caro, Ch. Loier, and R. Portier, "Determination of Twinning Elements for Mechanical Twins in the Rare Earth Sesquioxides of Monoclinic Structure" (in Fr.), *Phys. Status Solidi A*, **11**, 771–82 (1972).

C. Boulesteix and Ch. Loier, "Electron Microscopy Study of the Interpretation of Mechanical Twinning in Crystalline Thin Films — Role of Microtwinning" (in Fr.), *Phys. Status Solidi A*, **18**, 553–66 (1973).

P. E. Caro, G. Schiffmacher, C. Boulesteix, Ch. Loier, and R. Portier, "Defects and Impurities Influences on Phase Transformation in Rare-Earth Oxides"; pp. 519–35 in Defects and Transport in Oxides. Edited by S. Seltzer and R. I. Jaffee. Plenum Press, New York, 1974.

B. Yangui and C. Boulesteix, "Domains and Interfaces Generated in the Course of a Cooperative Crystallographic Transformation — Application to the Case of the Hexagonal Monoclinic Transformation of Rare-Earth Sesquioxides" (in Fr.), *Phys. Status Solidi A*, **73**, 515–27 (1982).

C. Boulesteix, "Defects and Phase Transformation Near Room Temperature in Rare-Earth Sesquioxides"; pp. 321–86 in Handbook on the Physics and Chemistry of Rare Earths, Vol. 5. Edited by K. A. Gschneider, Jr., and L. Eyring. North Holland, Amsterdam, Netherlands, and New York, 1982.

M. Ben Salem, R. Dorbez, B. Yangui, and C. Boulesteix, "Ferroelastic Character and Study by HREM of the Mechanism of the Hexagonal Monoclinic Phase Transition of the Rare Earth Sesquioxides," *Philos. Mag. A*, **50** [5] 621–34 (1984).

P. E. Caro, "OM₄ Tetrahedron Linkages — An Important Feature in Rare Earth Oxide and Oxysalt Structures," *Proc. Rare Earth Res. Conf., 6th*, 329–40 (1967).

P. E. Caro, "OM₄ Tetrahedra Linkages and the Cationic Group (MO)ₙ in Rare Earth Oxides and Oxysalts," *J. Less-Common Met.*, **16**, 367–77 (1968).

O. Sudre and W. M. Kriven, unpublished work.

A. Guinier and M. Regourd, "Structure of Portland Cement Minerals," *Proc. Int. Symp. Chem. Cem., 5th*, **1**, 1–32 (1968).

G. Yamaguchi and S. Takagaki, "Analysis of Portland Cement Clinker," *Proc. Int. Symp. Chem. Cem., 5th*, **1**, 181–218 (1968).

M. Regourd and A. Guinier, "The Crystal Chemistry of the Constituents of Portland Cement," *Proc. Int. Symp. Chem. Cem., 6th*, 1–81 (1974).

B. Matkovic, "Doped Dicalcium Silicates," *God. Jugosl. Cent. Kristalogr.*, **17**, 67–88 (1982).

S. N. Ghosh, P. B. Rao, A. K. Paul, and K. Raina, "The Chemistry of Dicalcium Silicate Mineral," *J. Mater. Sci.*, **14**, 1554–66 (1979).

N. B. Singh and P. Rastogi, "Solid State Chemistry of Dicalcium Silicate," *Zement-Kalk-Gips* [illegible] **104**, 645–51 (1980).

H. Midgley, "The Polymorphism of Calcium Orthosilicate," *Proc. Int. Congr. Chem. Cem., 6th*, 1–14 (1974).

C. M. Midgley, "The Crystal Stucture of β Dicalcium Silicate," *Acta Crystallogr.*, **5**, 307–12 (1952).

D. W. Cruickshank, "Refinements of Structures Containing Bonds between Si, P, S, or Cl and O or N: β-Ca_2SiO_4," *Acta Crystallogr.*, **17**, 685–86 (1964).

H. Saalfeld, "X-ray Investigation of Single Crystals of β-Ca_2SiO_4 (Larnite) at High Temperatures," *Am. Mineral.*, **60**, 824–27 (1975).

K. H. Jost, B. Ziemer, and R. Seydel, "Redetermination of the Structure of β-Dicalcium Silicate," *Acta Crystallogr., Sect. B: Struct. Crystallogr. Cryst. Chem.*, **33** [6] 1696–1700 (1977).

P. Barnes, C. H. Fentiman, and J. W. Jeffery, "Structurally Related Dicalcium Silicate Phases," *Acta Crystallogr., Sect. A: Found. Crystallogr.*, **36**, 353–56 (1980).

D. K. Smith, A. J. Majumdar, and F. Ordway, "The Crystal Structure of γ-Dicalcium Silicate," *Acta Crystallogr.*, **18**, 787–95 (1965).

R. Czaya, "Refinement of the Structure of γ-Ca_2SiO_4," *Acta Crystallogr., Sect. B: Struct. Crystallogr. Cryst. Chem.*, **27**, 848–49 (1971).

S. Udagawa, K. Urabe, M. Natsume, and T. Yano, "Refinement of the Crystal Structure of γ-Ca_2SiO_4," *Cem. Concr. Res.*, **10**, 139–44 (1980).

N. Yannaquis and A. Guinier, "The Polymorphic [illegible] Orthosilicate" (in Fr.), *Bull. Soc. Fr. Mineral. Cristallogr.*, **82** [illegible]

K. Niesel, "The Importance of the [illegible] Dicalcium Silicate," *Silic. Ind.*, **37** [illegible] (1972).

S. Udagawa, K. Urabe, T. Yano, K. Takada, and M. Natsume, "[illegible] Distinct of Ca_2SiO_4 — The Crystal Structure of [illegible]" *Cem. Concr. Res.*, **33**, 58–[illegible] (1979).

S. Udagawa and K. Urabe, "The Crystal Structure of [illegible] Ca_2SiO_4 and Their Phase Transformations," *Rev. Gen. Meet. Tech. Sess. Cem. Assoc. Jpn.*, **32**, 31–33 (1978).

S. Udagawa, K. Urabe, T. Yano, and M. Natsume, "[illegible] of Ca_2SiO_4 by X-ray Single Crystal [illegible] High Temperature Apparatus," *J. Jpn. Ceram. Soc.*, **88** [illegible] (1980).

K. Urabe, T. Yano, [illegible] X-Ray Single Crystal Study of Ca_2SiO_4 [illegible] *Rev. Gen. Meet. Tech. Sess. Cem. Assoc. Jpn.*, **36** [illegible]

S. Udagawa, K. Urabe, and T. Yano, [illegible] of Ca_2SiO_4 [illegible]

W. M. Kriven, C. J. Chan, and E. A. Barinek, "The Particle Size Effect of Dicalcium Silicate in a Calcium Zirconate Matrix"; [illegible] Science and Technology of Zirconia III [illegible] Yamamoto, and H. Yanagida. American Ceramic Society, Westerville, OH, [illegible]

I. M. Pritts and K. E. Daugherty, "[illegible]" *Cem. Concr. Res.*, **6** [illegible]

A. Ghose and P. Barnes, "Electron Microscopic [illegible]" *Cem. Concr. Res.*, **9** [illegible]

A. I. Kurmanov, [illegible] R. Rebinder, "[illegible]" *Proc. Int. Symp. Chem. Cem.*, [illegible] **1** [illegible]

A. I. Kurmanov, [illegible] Zeitsch, [illegible]

A. Dubois, G. [illegible] Ca_2SiO_4 [illegible] **29** [illegible]

A. Dubois [illegible] **31** [illegible]

S. Chan, A. Ghose, and [illegible]

α- and β-Dicalcium Silicate," *Proc. Int. Conf. Cem. Microsc., 5th*, 11–22 (1983).

A. Ghose, S. Chopra, and J. F. Young, "Microstructural Characterization of Doped Dicalcium Silicate Polymorphs," *J. Mater. Sci.*, **18**, 2905–14 (1983).

C. J. Chan, A. Ghose, W. M. Kriven, and J. F. Young, "Microstructure of Nonstoichiometric Dicalcium Silicate Doped with Potassium Oxide"; pp. 11–23 in Proceedings of Beijing International Symposium on Cement and Concrete, Vol. 1, Beijing, China, 1985. China Building Industry Press, Beijing, China, 1986.

C. J. Chan, W. M. Kriven, and J. F. Young, "Microstructure Characterization of Nonstoichiometric Dicalcium Silicates Doped with Aluminum Oxide"; pp. 452–53 in Proceedings of the 44th Annual Meeting of Electron Microscopy Society of America (EMSA), Albuquerque, NM, 1986. San Francisco Press, San Francisco, CA, 1986.

C. J. Chan, W. M. Kriven, and J. F. Young, "Analytical Electron Microscopic Studies of Doped Dicalcium Silicates," *J. Am. Ceram. Soc.*, **71** [9] 713–19 (1988).

S. [illegible], "The Inversion of the Beta Gamma Modifications of Dicalcium Silicate" (in Ger.), *Zem.-Kalk-Gips*, **8**, 383–89 (1970).

M. Gawlicki and W. Nocun-Wczelik, "Influence of Thermal Treatment on the Transition β- to γ-C₂S" (in Fr.), *Proc. Int. Congr. Chem. Cem., 7th*, **II**, 161–65 (1980).

M. Gawlicki, "The Role of Thermal Treatment on Dicalcium Silicate Polymorphic Transitions"; pp. 67–73 in Proceedings of the 14th Conference on Silicate Industry and Silicate Science, Vol. 3, Budapest, Hungary, 1985. OMIKK Technoinform, Budapest, Hungary, 1985.

S. Shibata, K. Kishi, K. Asaga, and M. Daimon, "Effect of Thermal History on [illegible] Transformation of Pure Ca_2SiO_4" (in Jpn.), *Yogyo Kyokaishi*, **91** [11] [illegible] (1983).

S. Shibata, K. Kishi, K. Asaga, and M. Daimon, "Effect of Thermal History on [illegible] Transformation of Ca_2SiO_4 in Presence of Fe_2O_3" (in Jpn.), *Yogyo Kyokaishi*, **92** [illegible] (1984).

S. Shibata, K. Kishi, K. Asaga, and M. Daimon, "Preparation and Hydration of [illegible] Stabilized," *Cem. Concr. Res.*, **14**, 323–28 (1984).

K. [illegible] and F. Thorman, "The Stability Fields of Dicalcium Silicate Modifications" [illegible], **91** [9] 362–69 (1967).

[illegible] and W. M. Kriven, "Effect of Kinetics on Ca_2SiO_4 Microstructure [illegible]" (abstract 112-B-87), *Am. Ceram. Soc. Bull.*, **66** [3] 519 (1987).

G. W. Groves, "Portland Cement Clinker Viewed by Transmission Electron Microscopy," *J. Mater. Sci.*, **16**, 1063–70 (1981).

G. W. Groves, "[illegible] in β-Dicalcium Silicate," *Cem. Concr. Res.*, **12**, [illegible] (1982).

G. W. Groves, "Phase Transformations in Dicalcium Silicate," *J. Mater. Sci.*, **18**, [illegible] (1983).

[illegible] and S. de Aza, "Transformation Toughening in Composites [illegible] Dicalcium Silicate," *J. Am. Ceram. Soc.*, **68** [9] C-259–C-262 (1985).

[illegible] and W. M. Kriven, "Development of Dicalcium Silicate as a [illegible] Toughener" (abstract 272-B-87), *Am. Ceram. Soc. Bull.*, **66** [illegible] (1987).

[illegible] R. A. [illegible], "The NiS System and Related Minerals," [illegible] **3** [illegible] (1962).

[illegible] CSIRO Division of Building Research Report, Melbourne, Australia [illegible].

K. W. [illegible], H. W[illegible], and K. Konopicky, "Study of Spherical Inclusions [illegible] Electron Microscopy" (in Ger.), *Glastech. Ber.*, **39**, [illegible].

[illegible] Nickel Sulphide in Glass" (in Ger.), *Glastech. Ber.*, **47** [illegible].

[illegible] Nickel Sulfide in Glass" (in Fr.), *Glastech. Ber.*, **50** [11] 296–300 (1977).

[124]C. C. Hsiao, "Spontaneous Fracture of Tempered Glass," *Fracture 1977*, 985–90 (1977).

[125]M. V. Swain, "Nickel Sulfide Inclusions in Glass: An Example of Microcracking Induced by a Volumetric Expansion Phase Change," *J. Mater. Sci.*, **16**, 151–58 (1981).

[126]A. G. Evans, "The Role of Inclusions in the Fracture of Ceramic Materials," *J. Mater. Sci.*, **9**, 1145–52 (1974).

[127]W. E. Lee and A. H. Heuer, "On the Polymorphism of Enstatite," *J. Am. Ceram. Soc.*, **70** [5] 349–60 (1987).

[128]R. S. Coe, "The Thermodynamic Effect of Shear Stress on the Ortho–Clino Inversion in Enstatite and Other Coherent Phase Transition Characterized by a Finite Simple Shear," *Contrib. Mineral. Petrol.*, **26**, 247–64 (1970).

[129]R. S. Coe and W. F. Muller, "Crystallographic Orientation of Clinoenstatite Produced by Deformation of Orthoenstatite," *Science (Washington, D.C.)*, **180**, 64–66 (1973).

[130]R. S. Coe and S. H. Kirby, "The Orthoenstatite to Clinoenstatite Transformation by Shearing and Reversion by Annealing: Mechanism and Potential Applications," *Contrib. Mineral. Petrol.*, **52**, 29–55 (1975).

[131]S. H. Kirby, "The Role of Crystal Defects in the Shear-Induced Transformation of Orthoenstatite to Clinoenstatite"; pp. 465–72 in Electron Microscopy in Mineralogy. Edited by H. R. Wenk *et al.* Springer-Verlag, New York, 1976.

[132]F. J. Turner, H. Heard, and D. T. Griggs, "Experimental Deformation of Enstatite and Accompanying Inversion to Clinoenstatite"; pp. 399–408 in Proceedings of the International Geological Congress, Part 18, Structure of the Earth's Crust and Deformation of Rocks. Edited by A. Kvale and A. Metzger. Det Berlingske Bogtrykkeri, Copenhagen, Denmark, 1960.

[133]R. E. Riecker and T. P. Rooney, "Deformation and Polymorphism of Enstatite under Shear Stress," *Geol. Soc. Am. Bull.*, **78**, 1045–54 (1967).

[134]C. B. Raleigh, S. H. Kirby, N. L. Carter, and H. G. Ave Lallement, "Slip and Clinoenstatite Transformation as Competing Rate Processes in Enstatite," *J. Geophys. Res.*, **76** [17] 4011–22 (1971).

[135]R. Sadanaga, F. P. Okamura, and H. Takeda, "X-ray Study of the Phase Transformations of Enstatite," *Mineral. J.*, **6** [1–2] 110–30 (1969).

[136]J. R. Smyth, "Experimental Study on the Polymorphism of Enstatite," *Am. Mineral.*, **59**, 345–52 (1974).

[137]J. Murakami, Y. Takeuchi, and T. Yamanaka, "The Transition of Orthoenstatite to Protoenstatite and the Structure at 1080°C," *Z. Kristallogr.*, **160**, 299–312 (1982).

[138]F. R. Boyd and J. L. England, "The Rhombic Enstatite Clinoenstatite Inversion"; pp. 117–20 in Carnegie Institute of Washington Yearbook, Vol. 64. Carnegie Institute of Washington, Washington, DC, 1965.

[139]H. Thurnauer and A. R. Rodriguez, "Notes of the Constitution of Steatite," *J. Am. Ceram. Soc.*, **25** [15] 443–50 (1942).

[140]M. D. Rigterink, "Microscopic and X-ray Investigation of Some Steatite Bodies," *J. Am. Ceram. Soc.*, **30** [7] 214–18 (1947).

[141]J. F. Sarver and F. A. Hummel, "Stability Relations of Magnesium Metasilicate Polymorphs," *J. Am. Ceram. Soc.*, **45** [4] 152–56 (1962).

[142]H.-R. Wenk, W. F. Muller, N. A. Liddell, and P. P. Phakey, "Polytypism in Wollastonite"; pp. 324–31 in Electron Microscopy in Mineralogy. Edited by H. R. Wenk *et al.* Springer-Verlag, New York, 1976.

[143]E. M. Levin, R. S. Roth, and J. B. Martin, "Polymorphism of ABO_3-type Rare-Earth Borates," *Am. Mineral.*, **46**, 1030–55 (1961).

[144]S. F. Bartram and F. J. Felton, "The Crystal Structure of the Vaterite Type Rare-Earth Borates," *Rare Earth Res., Proc. Conf., 2nd*, 329–38 (1961).

[145]R. S. Roth, J. L. Waring, and E. M. Levin, "Polymorphism of ABO_3-type Rare Earth Borate Solid Solutions," *Rare Earth Res., Proc. Conf., 3rd*, 153–63 (1963).

Reprinted from the Advances in Ceramics, Volume 24, Science and Technology of Zirconia III

The Particle-Size Effect of Dicalcium Silicate in a Calcium Zirconate Matrix

W. M. Kriven, C. J. Chan and E. A. Barinek

University of Illinois at Urbana-Champaign
Department of Ceramic Engineering
Urbana, IL 61801

Dicalcium silicate (Ca_2SiO_4), abbreviated C_2S, undergoes a monoclinic (β)-to-orthorhombic (γ) transformation at ≈490°C, which is accompanied by a 12% volume increase and a 4.6° unit cell shape change. These analogies to ZrO_2 make C_2S a potential transformation toughener. Previous work in pure or doped C_2S systems indicates that a particle-size effect controls the β-to-γ transformation. In this study, the critical size effect of C_2S in a confining calcium zirconate (CZ) matrix was investigated as a function of high-temperature annealing and time. Dense pellets of CZ-30 vol% C_2S were hot-pressed or sintered and yielded microstructures of intergranular, irregularly shaped C_2S particles. SEM and TEM grain size analyses and β twin width analyses by TEM revealed a correlation between twin width and grain size. Results suggested that the critical particle size may be determined by (1) overall C_2S grain size, (2) β twin thickness, or (3) both twin thickness and twin length. A characteristic "herringbone" type or parallel banded twin structure resulting from fast quenching through the $\alpha \leftrightarrow \alpha'_H$ transformation is believed to modify the β twin length and width. Further investigation of cooling kinetics and processing conditions on the critical size effect is suggested.

Dicalcium silicate, 2 CaO · SiO_2 (abbreviated C_2S) has five polymorphs at atmospheric pressure:

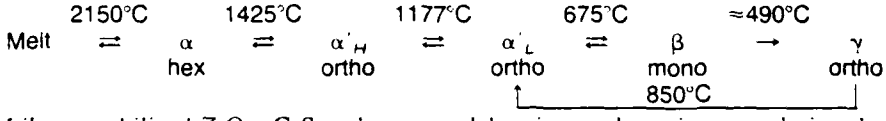

Like unstabilized ZrO_2, C_2S undergoes a deleterious volume increase during the monoclinic (β)-to-orthorhombic (γ) transformation, causing "dusting" or fragmentation of the solid body. This suggests that C_2S may be a possible transformation toughener alternative to ZrO_2.[1] Table I lists comparable properties of ZrO_2 and C_2S. On cooling, the β-to-γ transformation in C_2S has essentially double the volume increase (≈12%) and half the unit cell shape change ($\Delta\beta = 4.6°$) of ZrO_2.

As in ZrO_2, a particle-size effect is believed to control the $\beta \rightarrow \gamma$ transformation.[3,6-14] The impetus for this finding came from the fact that the β phase was more reactive to water than the γ phase. Hence, in cement chemistry, stabilization of β phase was desirable. In general, experimental studies were of the

Advances in Ceramics, Vol. 24: Science and Technology of Zirconia III

Table I. Comparison of the Ca_2SiO_4 β-to-γ Transformation with the Tetragonal-to-Monoclinic Transformation of ZrO_2

Compound	ZrO_2	Ca_2SiO_4
Structure change	$t \rightarrow m$	$m \rightarrow o$
Transformation temperature	950°C	490°C*
Volume change	+4.9%	+11.96%†
Coordination number change	8 → 7	(Ca I) 7 } (Ca II) 8 } → (Ca)6‡
Unit cell shape change (Δβ)	9°	4.6°
Chemical stabilizers	MgO	Cr_2O_3, K_2O§
	CaO	B_2O_3, Al_2O_3
	Y_2O_3	Na_2O, BaO, etc.
Transformation induced by grinding	Yes	Yes

* H. Midgley (1974) (Ref. 2).
† Data for pure C_2S (Refs. 2 and 3).
‡ K. H. Jost (Ref. 4).
§ Role of dopant unknown, possible glass formation occurred; K_2O found concentrated in intergranular glass phase by TEM-EDS (Ref. 5).

following type. Mixtures of pure calcium carbonate or calcia, and silica in the ratio 2:1 were made, with and without excess CaO or SiO_2 or additives. After calcination, powders or dense pellets were sintered at 1450° to 1550°C for one to three times, and cooled or quenched to room temperature. The resulting phase was usually γ-C_2S. Specimens were examined or recompacted and annealed at various temperatures, times, and quench rates. The β-to-γ ratios and C_2S particle size were determined by X rays, optical microscopy, and scanning electron microscopy (SEM) with electron probe microanalysis (EPMA).

Hence, a review of experimental observations and conclusions reported in the cement literature[3,6–14] indicates that the ratio of β-to-γ content depends on the following parameters:

1. Particle Size: For fixed annealing conditions of temperature, time, and a slow cooling rate, a large initial γ-C_2S particle size favored the formation of γ phase. However, a small initial γ-C_2S size stabilized the β phase. These observations were made both in final powders[3,6,9] or dense pellets.[3,6,7,10–12]

2. Temperature: Below 1425°C (the $\alpha \leftrightarrow \alpha'_H$ transformation temperature), increasing annealing temperatures produced more final γ phase.[7–14] Above 1425°C, accelerated grain growth occurred.[7,10,11]

3. Time: Longer annealing times produced more γ-C_2S, but this effect was secondary to temperature.[7,10–14]

4. Kinetics: The kinetics of cooling through the $\alpha \leftrightarrow \alpha'_H$ transformation were very important. Slow cooling through 1425°C led to the formation of γ-C_2S, while fast cooling tended to retain β-C_2S in the final microstructure.[7,10–14]

An inconsistency was noticed in the previous literature in the values and definition of critical particle size. Particle sizes ranging from 5 μm[3,6] or 7 μm[12,13] down to 0.2 to 0.3 μm[10,11] have been reported. The large values obtained by optical microscopy and SEM referred to overall C_2S particle size, whereas the submicrometer values obtained from X rays and SEM referred to the width of transformed γ needles within a C_2S particle. Microstructural studies of the $\alpha'_L \rightarrow \beta$ and $\beta \rightarrow \gamma$ transformation by TEM[15–17] found that γ-C_2S was formed by growth of needles or laths whose long axes were parallel to $[001]_\gamma$ or $[010]_\beta$.[17]

The studies referred to above dealt mainly with pure or doped C_2S systems.

Recently, C_2S particles have also been dispersed in a calcium zirconate (CZ) matrix in an attempt to demonstrate transformation toughening by C_2S.[18] The aim of our research was to investigate and define more precisely the critical size effect of C_2S particles confined in a calcium zirconate matrix. The microstructures of specimens with various thermal histories are characterized by XRD, SEM, TEM, and TEM/EDS techniques.

Experimental Procedure

Specimen Preparation

Composites of 30 vol% C_2S in a calcium zirconate (CZ) matrix were prepared from A.R. grade $CaCO_3$,* ZrO_2,† and silicic acid $(SiO_2 \cdot xH_2O)$‡ and either hot-pressed or sintered. For hot-pressing, the raw materials were attritor-milled in isopropyl alcohol, calcined at 1100°C, and hot-pressed at 1450°C under 34.5 MPa (5000 psi) pressure for 10 minutes. The density of the resulting specimen was measured as 95.4% of theoretical density by the immersion method. The composites were polished and X-rayed and then annealed at 1400°C for 10, 17, 40, 80, and 160 hours. Some specimens were also heated at 1450°C (above the $\alpha'_H \leftrightarrow \alpha$ transformation) for five hours, and then either slowly cooled to room temperature in the furnace, or fast quenched into liquid nitrogen. The purpose was to observe the effect of cooling kinetics through $\alpha \leftrightarrow \alpha'_H$ on the $\beta \rightarrow \gamma$ transformation.

For sintered specimens, silicic acid was first calcined at 1000°C before mixing with CaO and ZrO_2 in an attritor mill. The raw mix was dried, cold isostatically pressed, and sintered at 1650°C for one hour. The resulting specimen was 88.0% of theoretical density. The sintered pellets were then annealed at 1500°C for 5, 10, 20, and 40 hours, followed by slow cooling at 5°C/min to 1000°C, and then furnace cooled to room temperature.

X-Ray Diffractometry

A standard polishing procedure starting from 600 grit to a 1 μm diamond paste finish was routinely applied prior to X-ray diffraction (XRD) examination, in order to eliminate any possible surface transformation or relaxation effects. Each specimen was examined by XRD§ to determine its polymorphism before and after annealing. The relative ratios of $\beta/(\beta + \gamma)$ were also determined by integrating the peak areas of (130) of γ-C_2S and (103) of β-C_2S.

Microstructure Characterization

The general microstructure was studied by scanning electron microscopy (SEM).¶ To reveal grain size, shape, and distribution, polished samples were thermally etched at 1350°C for various times. Average grain sizes of both C_2S particles and the CZ matrix were analyzed according to the Jeffries-Saltykov method.[19] Typically, at least 300 particles were measured per sample.

Transmission electron microscopy (TEM)** was used to monitor twin widths

---

*Baker Chemical Co., Phillipsburg, NJ.
†Z-83 from Fisher Scientific, Fair Lawn, NJ.
‡100-mesh powder from Mallinckrodt, Paris, KY.
§Philips XRG-3100 diffractometer equipped with a computerized PW1710 controlling unit, Philips Electronic Instruments, Inc., Mount Vernon, NY.
¶DS-130 SEM, International Scientific Instruments, Milpitas, CA.
**Model 430, Philips Electron Instruments.

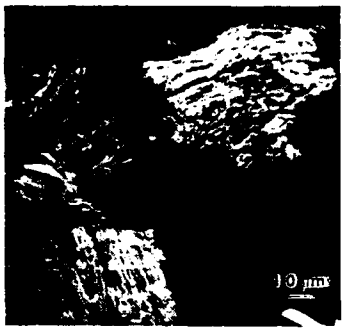

Fig. 1. Scanning electron micrograph of a γ-Ca_2SiO_4 fragment transformed from the β phase and shattered into needle or lath shapes separated by parallel cracks.

and grain-size variation of β-C_2S particles after different annealing temperatures and hold times. The TEM specimens were prepared by standard ceramic polishing, dimpling, and ion-milling techniques.

At the microscope, the average twin widths were obtained by tilting β-C_2S grains until twin planes were parallel to the incident beam direction. The twin width was defined as the length of a C_2S particle in the direction perpendicular to the twin planes, divided by the number of twins in the particle. The average twin width was obtained by averaging the values from all the particles analyzed. Typically, 30 to 50 particles were measured per sample.

Results

The dusting phenomenon of a pure C_2S pellet sintered at 1450°C for 90 minutes and air quenched, is illustrated in Fig. 1. Typically, the γ phase appeared as parallel needles or lath shapes bundled within a fragment. The same effect was also observed in a CZ-30 vol% C_2S sample which was hot-pressed at 1500°C under 34.5 MPa (5000 psi) for 30 minutes and found to be shattered several hours after removal from the hot press. Similarly, another CZ-30 vol% C_2S mixture sintered at 1600°C for two hours underwent some β-to-γ transformation when the surface was ground and polished (Fig. 2). It is seen that extensive cracking was induced in the adjacent area.

To investigate the effect of various parameters on the C_2S particle size and hence on control of the β-to-γ transformation, the processing conditions were modified as described earlier.

X-Ray Diffraction

Figure 3 is a plot of integrated X-ray peak intensity ratios of γ(130)/[γ(130) + β(103)] as a function of annealing time. It is evident that prolonged annealing at 1400° and 1500°C did not increase the amount of γ present, which is contrary to what was observed in pure C_2S systems.

Scanning Electron Microscopy

Figures 4(*a*) and 5(*a*) show the general microstructure of hot-pressed and sintered samples. C_2S particles are irregularly shaped, and intergranularly dis-

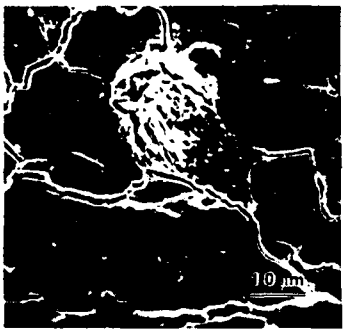

Fig. 2. Scanning electron micrograph of a CZ matrix containing a γ-C_2S particle transformed during grinding and polishing. Extensive microcracking occurred in the surrounding areas.

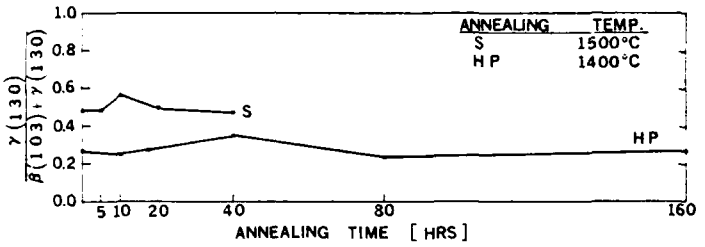

Fig. 3. Integrated X-ray peak intensity ratios of γ(130)/[γ(130) + β(103)] as a function of annealing time at high temperatures for both hot-pressed (HP) and sintered (S) samples.

persed in the CZ matrix. A certain degree of agglomeration was also observed in both specimens. The sintered specimen generally had a coarser CZ grain size. Prolonged annealing did not change the phase distributions in both types of specimens (Figs. 4(*a*), (*b*), and 5(*a*), (*b*)).

Grain-Size Analysis

The sintering process generally resulted in a coarser grain size than hot-pressing. In particular, the average CZ grain size of sintered samples was about an order of magnitude larger than that of hot-pressed samples. In both types of samples the average CZ and C_2S grain sizes showed an increase on annealing, reaching an almost constant value in a short time. Longer annealing times only slightly increased the grain sizes (Figs. 6(*a*), 7(*a*). The final CZ and C_2S grain sizes in hot-pressed samples were about twice their initial sizes, respectively, while sintered samples grew by only a factor of 1.2. It was interesting to note that the average CZ grain size of hot-pressed samples was slightly smaller than the average C_2S grain size. In contrast, in sintered samples, average CZ grain sizes were three times larger than the average C_2S grain sizes.

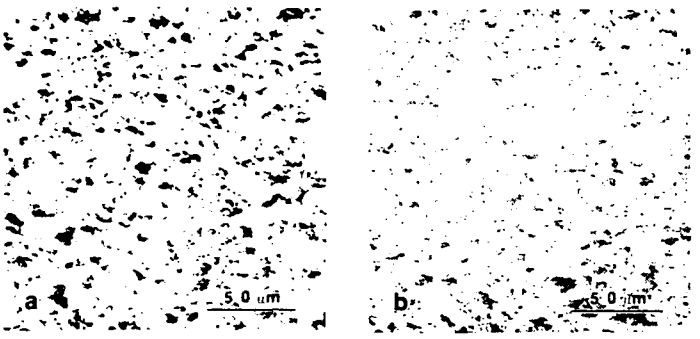

Fig. 4. Scanning electron micrographs of (*a*) typical microstructure of a hot-pressed specimen before annealing; (*b*) microstructure of the same type of specimen after annealing at 1400°C for 160 hours.

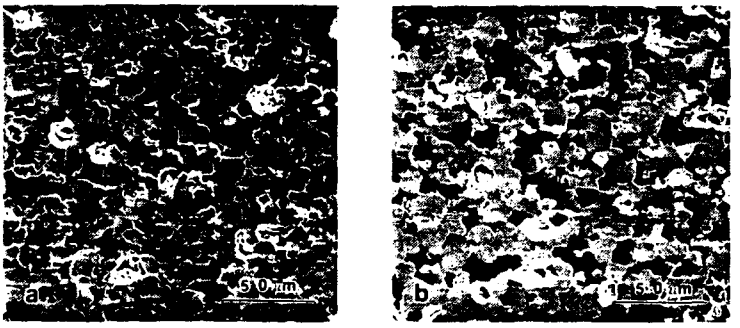

Fig. 5. Scanning electron micrographs of (*a*) typical microstructure of an as-sintered specimen; (*b*) microstructure of the same type of specimen after annealing at 1500°C for 40 h and slow cooling.

Transmission Electron Microscopy

Transmission electron microscopy studies confirmed that irregularly shaped C_2S particles were intergranularly dispersed in a polycrystalline CZ matrix (Fig. 8). β-C_2S particles were typically twinned on the (100) monoclinic plane,[15–17] and some agglomeration was also observed. Extensive microcracking was noticed at β-matrix and β-β grain boundaries (Fig. 8). A transformed γ-C_2S crystal containing numerous dislocation tangles and surrounded by a microcrack was found (Fig. 9).

Twin width analysis of hot-pressed specimens showed an average value of 0.09 μm for unannealed samples, which became 0.18 μm after 10 hours at 1400°C. Further annealing caused a slight decrease in twin width (Fig. 6(*b*)). Similarly, for sintered specimens, the initial average twin width of 0.11 μm increased very slightly to 0.12 μm after 40 hours at 1500°C (Fig. 7(*b*)). The standard deviation of the twin width analysis for both types of specimens was large, approximately 30 to 50%. Nevertheless, it is interesting to note that the twin

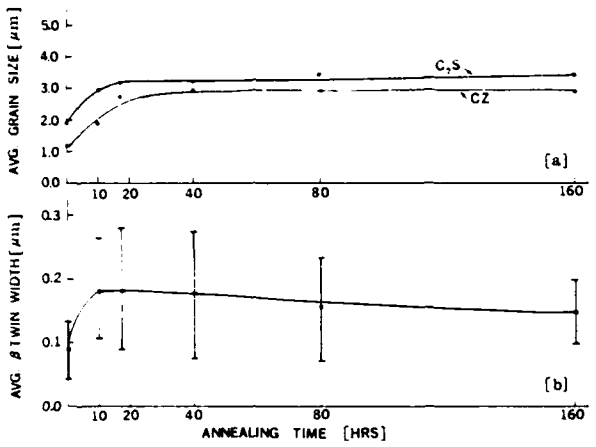

Fig. 6. (*a*) Plot of average grain sizes (determined from SEM micrographs) of C_2S and CZ for hot-pressed samples annealed at 1400°C, as a function of annealing time; (*b*) corresponding plot of twin widths (determined from TEM micrographs) of β-C_2S as a function of annealing time.

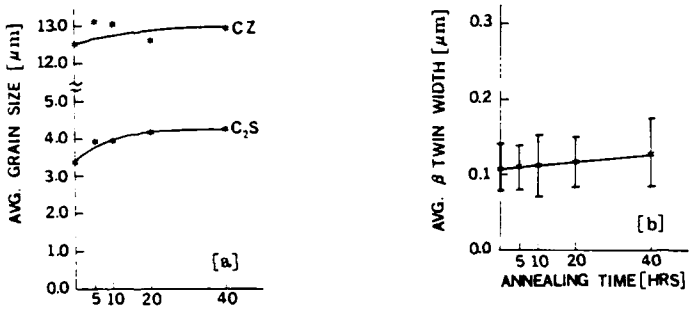

Fig. 7. (*a*) Plot of average grain size (determined from SEM micrographs) of C_2S and CZ for sintered samples annealed at 1500°C, as a function of annealing time. (*b*) Corresponding plot of twin widths (determined from TEM micrographs) of β-C_2S as a function of annealing time.

width increases of 2 and 1.1 observed by TEM parallel the grain-size increases of 2 and 1.2 observed by SEM, in hot-pressed and sintered samples, respectively.

Effect of $\alpha \rightarrow \alpha'_H$ Cooling Rate on Microstructure

The kinetics of cooling through the $\alpha \rightarrow \alpha'_H$ transformation is believed to have a strong influence on the β-to-γ transformation.[7,10–14] The SEM microstructural differences between fast-quenched and slowly cooled samples is illustrated in Fig. 10. Irregular, wrinkled features were observed in C_2S particles

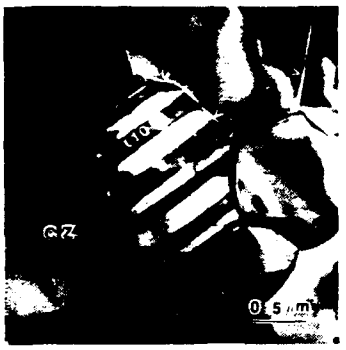

Fig. 8. Bright-field TEM micrograph of the hot-pressed CZ-30 vol% C_2S microstructure showing an irregularly shaped, intergranular β-C_2S particle. Typically, it was twinned on the (100) monoclinic plane. Interfacial microcracks were frequently observed (arrows).

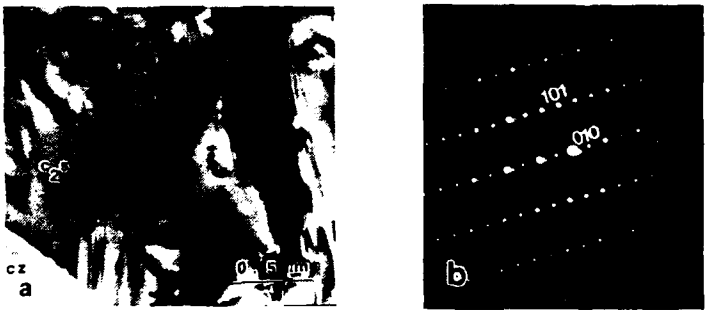

$\bar{B} = [1\,0\,\bar{1}]$

Fig. 9. (*a*) Transmission electron micrograph of a confined γ-C_2S particle containing numerous dislocations; (*b*) the corresponding single-crystal SAD pattern in the [101] orthorhombic zone axis projection.

of fast-quenched specimens, which were absent in slowly cooled specimens. Further investigation by TEM revealed a "herringbone" microstructure of internal twins (Fig. 11 (*a*)) or parallel bands (Fig. 11(*b*)) in rapidly quenched specimens. These are similar to microstructures seen in chemically doped C_2S samples.[5,20–22]

Discussion

As reviewed earlier, a particle-size effect operates in controlling the occurrence of the β-to-γ transformation in C_2S. This is analogous to ZrO_2-toughened systems. However, in ZrO_2 a single-crystal tetragonal particle transforms a twinned monoclinic phase, whereas in C_2S the starting β particle is already twinned before transforming to γ. This gives rise to an ambiguity in definition of critical particle size. Specifically, a critical volume of particle for transformation could be derived from either: (1) the overall particle size, (2) the twin thickness,

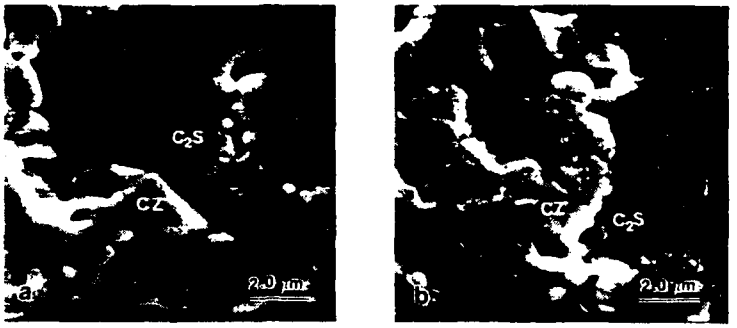

Fig. 10. Scanning electron micrograph of polished specimens of (*a*) a hot-pressed sample annealed at 1450°C for 5 h and slowly cooled at 5°C/min through the $\alpha \leftrightarrow \alpha'_H$ transformation; (*b*) a hot-pressed sample annealed at 1450°C for 5 h, but quenched into liquid nitrogen.

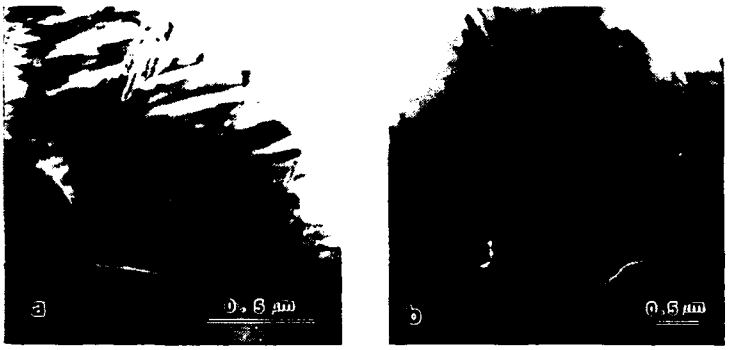

Fig. 11. (*a*) Transmission electron micrograph of a hot-pressed sample annealed for 5 h at 1450°C and rapidly quenched into liquid N_2. (*a*) A "herringbone" type of twinned structure was usually observed in β-C_2S grains; (*b*) alternatively, a parallel banded structure sometimes crossed the β twins.

or (3) both twin thickness and twin length. In this light, it should be noted that the β-C_2S twins actually formed during the α'_L to β transformation on cooling at 675°C, which is far below the annealing temperatures of 1400° to 1500°C.

Detailed evaluations of TEM micrographs were made in terms of twin thickness (t) and particle size as defined by the lengths (L and L'), parallel and perpendicular to the twin plane, respectively. In both hot-pressed and sintered samples a general trend of increasing twin thickness with increasing particle size was observed. This is consistent with the correlation between average values of particle size determined by SEM and twin thickness. However, as seen in Figs. 6(*a*) and 7(*a*), the absolute values of twin width differ between hot-pressed and sintered samples.

With respect to (3) above, twin lengths may also be relevant in determining the critical particle size. Twin lengths were shortened by cross twins in the

herringbone pattern (Fig. 11) or by the parallel bands (Fig. 12) both of which resulted from fast cooling through the $\alpha \rightarrow \alpha'_H$ transformation.

Conclusion

The particle-size effect of dicalcium silicate in a matrix has been investigated. The definition of the critical particle size of the β-to-γ transformation may depend on: (1) the overall C_2S particle size, (2) the β twin thickness, or (3) both the β twin thickness and twin length. Microstructural observations by SEM and TEM suggest a correlation between (1) and (2). Furthermore, fast cooling kinetics through the $\alpha \leftrightarrow \alpha'_H$ transformation modify the β microstructure by forming a herringbone pattern of twins or parallel bands, thereby reducing the twin length (parameter (3)).

The CZ matrix constraint retains β-C_2S under conditions where normally γ-C_2S would be expected in single-phased C_2S systems. This may be due to β-C_2S particles being below the critical particle size for transformation. Prolonged annealing at 1400° and 1500°C, followed by slow cooling, essentially (*a*) did not increase the γ content and (*b*) did not change the C_2S distribution. Microstructures containing β-C_2S particles of the critical particle size may be developed by optimizing the processing conditions used.

Acknowledgment

This work was supported by the U.S. Air Force Office of Scientific Research, Contract No. AFOSR 85-0242. The use of the facilities of the Center for Microanalysis of Materials in the Materials Research Laboratory, and of the Center for Electron Microscopy at the University of Illinois at Urbana-Champaign, are gratefully acknowledged.

References

[1]W. M. Kriven, "Displacive Transformation Mechanism in Zirconia Ceramics and Other Non-metals"; pp. 223–37 *in Tailoring Multiphase and Composite Ceramics*. Plenum, New York, 1985.

[2]H. Midgley, "The Polymorphism of Calcium Orthosilicate"; 6th International Congress on the Chemistry of Cement; Supplementary paper, Section I, pp. 1–16. Stroiisdat, Moscow, 1974.

[3]N. Yannaquis and A. Guinier, "Polymorphic β → γ Transition of Calcium Orthosilicate," *Bull. Soc. Franc. Mineral. Crist.*, **82**, 126–36 (1959).

[4]K. H. Jost, B. Ziemer, and R. Seydel, "Redetermination of the Structure of β-Dicalcium Silicate," *Acta Crystallogr.*, **B33**, 1696–1700 (1977).

[5]C. J. Chan, A. Ghose, W. M. Kriven, and J. F. Young, "Microstructure of Non-Stoichiometric Dicalcium Silicate Doped with Potassium Oxide," *Proc. Beijing Int. Symp. Cement Concrete, Beijing*, **1**, 11–23 (1986).

[6]A. Guinier and M. Regourd, "Structure of Portland Cement Minerals," Principal paper I, pp. 1–41 *in Proceedings of the 5th International Symposium on the Chemistry of Cement*, Vol. 1. Cement Association of Japan, Tokyo, 1969.

[7]S. Chromy, "The Inversion of the β → γ Modifications of Dicalcium Silicate," *Zement-Kalk-Gips*, **8**, 382–89 (1970).

[8]K. Niesel and P. Thormann, "The Stability Fields of Dicalcium Silicate Modifications," *Tonind.-Ztg.*, **91** [9] 362–69 (1967).

[9]K. Niesel, "The Importance of the α'_L-α'_H transition in the Polymorphism of Dicalcium Silicate," *Silicate Ind.*, **37** [5] 136–38 (1972).

[10]M. Gawlicki and W. Nocun-Wczelik, "Influence of Thermal Treatment on the Transition β → γ-C_2S,"; pp.161–65 in Proceedings of the 7th International Congress on the Chemistry of Cement, Vol. II. Editions Septima, Paris, 1980.

[11]M. Gawlicki, "The Role of Thermal Treatment on Dicalcium Silicate Polymorphic Transitions,"; pp. 67–73 in Proceedings of the XIV Conference on the Silicate Industry and Silicate Science, Vol. III. OMIKK-Technoinform, Budapest, 1985.

[12]S. Shibata, K. Kishi, K. Asaga, and M. Daimon, "Effect of Thermal History on β → γ Transformation of Pure Ca_2SiO_4," *Yogyo-Kyokai-Shi*, **91** [11] 497–502 (1983).

[13]S. Shibata, K. Kishi, K. Asaga, and M. Daimon, "Effect of Thermal History on β → γ Transformation of Ca_2SiO_4 in Presence of Fe_2O_3," *Yogyo-Kyokai-Shi*, **92** [2] 71–92 (1984).
[14]S. Shibata, K. Kishi, K. Asaga, and M. Daimon, "Preparation and Hydration of β-C_2S Without Stabilizer," *Cem. Conc. Res.*, **14**, 323–28 (1984).
[15]G. W. Groves, "Portland Cement Clinker Viewed by Transmission Electron Microscopy," *J. Mater. Sci.*, **16**, 1063–70 (1981).
[16]G. W. Groves, "Twinning in β-Dicalcium Silicate," *Cem. Conc. Res.*, **12**, 619–24 (1982).
[17]G. W. Groves, "Phase Transformations in Dicalcium Silicate," *J. Mater. Sci.*, **18**, 1615–24 (1983).
[18]J. S. Moya, P. Pena, and S. DeAza, "Transformation Toughening in Composites Containing Dicalcium Silicate," *J. Am. Ceram. Soc.*, **68** [9] C-259–C-262 (1985).
[19]R. T. DeHoff and F. N. Rhines, Quantitative Microscopy. McGraw-Hill, New York, 1968.
[20]B. Matkovic, V. Carin, T. Gacesa, R. Halle, I. Jelenic, and J. F. Young, "Influence of $BaSO_4$ on the Formation and Hydration Properties of Calcium Silicates: I. Doped Dicalcium Silicates," *Am. Ceram. Soc. Bull.*, **60** [8] 825–29 (1981).
[21]S. Chopra, A. Ghose, and J. F. Young, "Electron-optical Studies of Stabilized γ- and β-Dicalcium Silicate"; pp. 11–22 in Proceedings of the 5th International Conference on Cement Microscopy. International Cement Microscopy Association, Duncanville, TX, 1983.
[22]A. Ghose, S. Chopra, and J. F. Young, "Microstructural Characterization of Doped Dicalcium Silicate Polymorphs," *J. Mater. Sci.*, **18**, 2905–14 (1983).

G. W. Bailey, Ed., *Proceedings of the 46th Annual Meeting of the Electron Microscopy Society of America*

MICROSTRUCTURAL CHARACTERIZATION OF LASER-MELTED/ROLLER-QUENCHED DICALCIUM SILICATE

C. J. Chan, K. R. Venkatachari, W. M. Kriven and J. F. Young

Department of Materials Science and Engineering, Ceramics Division, University of Illinois at Urbana-Champaign, Urbana, IL 61801

Dicalcium silicate (Ca_2SiO_4) is a major component of portland cement. It has also been investigated as a potential transformation toughener alternative to zirconia.[1-3] It has five polymorphs: α, α'_H, α'_L, β and γ. Of interest is the β-to-γ transformation on cooling at about 490°C. This transformation, accompanied by a 12% volume increase and a 4.6° unit cell shape change, is analogous to the tetragonal-to-monoclinic transformation in zirconia[4]. Due to the processing methods used, previous studies into the particle size effect were limited by a wide range of particle size distribution. In an attempt to obtain a more uniform size, a fast quench rate involving a laser-melting/roller-quenching technique was investigated.

The laser-melting/roller-quenching experiment used precompacted bars of stoichiometric γ-Ca_2SiO_4 powder, which were synthesized from AR grade $CaCO_3$ and $SiO_2 \cdot xH_2O$. The raw materials were mixed by conventional ceramic processing techniques, and sintered at 1450°C. The dusted γ-Ca_2SiO_4 powder was uniaxially pressed into 0.4 cm × 0.4 cm × 4 cm bars under 34 MPa and cold isostatically pressed under 172 MPa. The γ-Ca_2SiO_4 bars were melted by a 10 KW-CO_2 laser. A laboratory-built twin roller quencher with titanium rollers was placed about 15 cm under the bar. The quench rate was estimated to be of the order of 10^7°C·sec^{-1}.

The as-quenched flakes had a thickness of about 60~70 μm. X-ray diffraction revealed broad peaks corresponding to those of the β phase. SEM observations showed only surface striations from the rollers (Fig. 1). By TEM, no amorphous phase was found. The Ca_2SiO_4 tended to form elongated grains with a β twinned structure (Fig. 2). A high density of dislocations was observed inside each grain together with modulated fringes (periodicity = 2 nm), as indicated in Fig. 3. Upon annealing at 650°C for 10 hours and furnace cooling, X-ray diffraction showed more well-defined β phase peaks. The dislocations and modulated fringes were not apparent after annealing (Fig. 4). Grain size analyses of the TEM microstructure of as-quenched specimens revealed a narrow size distribution.

This work indicates that it was impossible to obtain Ca_2SiO_4 in an amorphous form even with the fastest quenching rate. However, the

narrow grain size distribution and preliminary annealing experiment at 650°C suggest that it may be possible to study the critical particle size effect in Ca_2SiO_4 by a combination of laser-melting/roller-quenching and systematic annealing experiments.

References

1. J. S. Moya et al., J. Am. Ceram. Soc., 1985(68), C259.
2. W. M. Kriven et al., Proc. 3rd Int. Conf. Science and Technology of Zirconia, Tokyo, 1986, in press.
3. E. A. Barinek and W. M. Kriven, to be published.
4. W. M. Kriven, J. Am. Ceram. Soc., 1988, in press.

5. This work was supported by the Air Force Office of Scientific Research under contract numbers AFOSR F49620-87-C-0023 and AFOSR 85-0242.

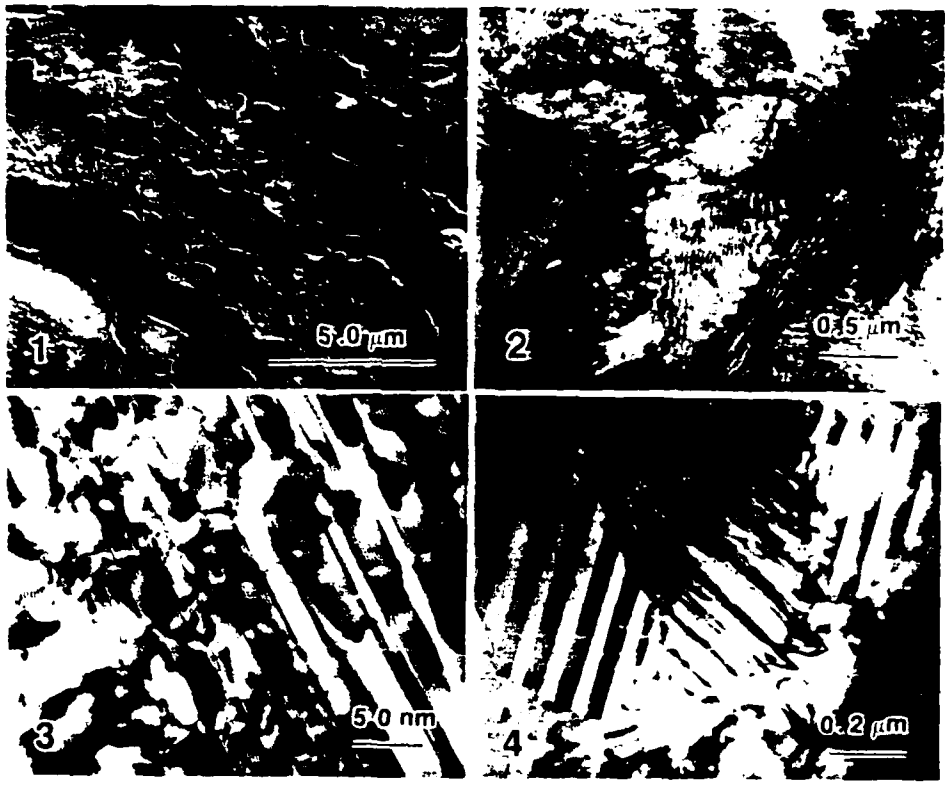

FIG. 1.--SEM micrograph of an as-quenched Ca_2SiO_4 flake.
FIG. 2.--TEM BF image of an as-quenched specimen showing elongated β-Ca_2SiO_4 grains.
FIG. 3.--Higher magnification of the as-quenched Ca_2SiO_4 showing a high dislocation density and the modulated fringes in each twin.
FIG. 4.--TEM BF image of laser-melted/roller-quenched Ca_2SiO_4 after annealing at 650°C for 10 hours.

JOURNAL

of the AMERICAN CERAMIC SOCIETY

Volume 71, No. 9 September 1988

J. Am. Ceram. Soc., 71 [9] 713-19 (1988)

Analytical Electron Microscopic Studies of Doped Dicalcium Silicates

CHIN-JONG CHAN,* WALTRAUD M. KRIVEN,* and J. FRANCIS YOUNG*

Department of Materials Science and Engineering, University of Illinois at Urbana–Champaign, Urbana, Illinois 61801

Dicalcium silicates having CaO/SiO$_2$ molar ratios of 1.8 to 2.2 were sintered at 1450°C for 90 min with or without small quantities of dopants (K$_2$O or Al$_2$O$_3$) and were air quenched. The microstructures of the fired samples were characterized using electron microscopy (SEM and TEM) and associated microanalytical techniques. There was no evidence for the existence of Ca$_{1+x}$SiO$_{3+x}$ or Ca$_{2+x}$SiO$_{4+x}$. Amorphous grain-boundary phases were observed between grains and as inclusions within the grains; the amounts decreased as CaO/SiO$_2$ ratios increased. The compositions of the amorphous phases were always rich in dopants and had a CaO/SiO$_2$ ratio close to that of wollastonite. High levels of Al$_2$O$_3$ were observed to enter the β-Ca$_2$SiO$_4$ grains under lime-rich conditions (CaO/SiO$_2$ = 2.2) up to a saturation level of about 3.0 wt%. Some additional crystalline phases were observed to form depending on stoichiometry and dopant level.

I. Introduction

DICALCIUM SILICATE (Ca$_2$SiO$_4$) can exist in five polymorphic forms — γ, β, α'_L, α'_H, and α. Only the γ form is stable at room temperature, the others being stable at increasingly higher temperatures. The monoclinic (β) → orthorhombic (γ) polymorphic transformation, which involves a significant increase (~12%) in specific volume and a 4.6° unit-cell shape change, fractures the material to a fine powder. This transformation has characteristics similar to those of the tetragonal → monoclinic transformation in zirconia and has been shown to have the potential for transformation toughening. β-Ca$_2$SiO$_4$ is an important component in portland cement and reacts readily with water, whereas the γ-Ca$_2$SiO$_4$ is essentially unreactive. The β polymorph is known to be stabilized by the presence of various ions,[5-8] which also affect its reactivity with water to some degree.

There are reports[9-13] that Ca$_2$SiO$_4$ can take up excess lime in solid solution, thereby stabilizing the β form and increasing its reactivity. Up to 6 wt% CaO (corresponding to a CaO/SiO$_2$ molar ratio of 2.2) can be taken up with[12] or without[9] other dopants being present. On the other hand, excess silica (2.0 wt% of SiO$_2$) has been reported to stabilize the γ form.[14] In the light of recently reported complexities in the microstructures of doped dicalcium silicate preparations,[15-17] we have reexamined these claims using K$_2$O and Al$_2$O$_3$ as dopants. Preliminary results[18,19] indicated that these claims could not be substantiated. It was found that the presence of amorphous glassy phases and additional crystalline phases accounted for the apparent departure from stoichiometry and caused a variable distribution of the dopant in fired samples. Complete details are reported here.

II. Experimental Procedure

The Ca$_2$SiO$_4$ samples under study were prepared from reagent-grade CaO, K$_2$CO$_3$, Al(OH)$_3$, and hydrated silica (SiO$_2$·xH$_2$O), using three different CaO/SiO$_2$ molar ratios (1.8, 2.0, and 2.2), to which different amounts of K$_2$O or Al$_2$O$_3$ were added. Dopant contents were 0.2, 0.5, 1.0, and 1.5 wt% for K$_2$O, and 0.5, 1.5, 2.3, 3.0, and 4.5 wt% for Al$_2$O$_3$. The CaO/SiO$_2$ ratios were calculated taking into account the dopant substitutions (assuming 2K$^+$ replaced Ca^{2+} and Al^{3+} replaced Si^{4+}).

The raw materials were wet ground and homogenized with isopropyl alcohol in a ball mill, followed by drying at 100°C, dry milling, calcining at 1000°C for 90 min, sintering at 1450°C for 90 min, and air quenching. Each fired sample was routinely examined by X-ray diffractometry† (XRD) to determine its polymorphism.

The stabilized Ca$_2$SiO$_4$ samples were further examined using a number of methods. Electron probe microanalysis (EPMA)‡ was employed to estimate the extent of actual dopant uptake and the stoichiometry of the stabilized Ca$_2$SiO$_4$ grains and to analyze any second phases present. Determination of free lime by ethylene glycol extraction was made to check the completeness of the firing process. Scanning electron microscopy (SEM)§ was used to study the overall microstructure of polished and 0.5% Nital etched¶ bulk specimens. Specimens for SEM and EPMA studies were mounted in epoxy and polished to 0.25 μm using standard metallographic techniques.

Manuscript No. [illegible]. Received December [illegible], 1987; approved March [illegible], 1988.
Presented at the [illegible] Annual Meeting of the American Ceramic Society, Pittsburgh, PA, April [illegible], 1987 (Cements Division, Paper No. 27-C-87).
Supported by the National Science Foundation under Grant No. CEE-83-00265. The work of C.-J. Chan was partially supported by the U.S. Air Force Office of Scientific Research (AFOSR) under Contract No. F49620-87-C-0023. The work of W. M. Kriven was supported by AFOSR under Contract No. 88-0242.
*Member, the American Ceramic Society.
†Model [illegible], Rigaku USA, Inc., Danvers, MA, and Model XRG 3100, Philips Electronic Instruments, Inc., Mt. Vernon, NY.
‡Model 50X, JEOL, Inc., Tokyo, Japan; microprobe (probe size estimated to be [illegible]) equipped with an energy dispersive spectrometer from Tracor Northern Co., Middleton, WI.
§Model ISM [illegible], JEOL, Inc., and Model EDS 130, ISI, Inc., Milpitas, CA, equipped with [illegible] spectrometer from Tracor Northern Co.
¶Prepared [illegible], Anachemia Chemicals Ltd., Montreal, Canada.

Table I. Polymorphism of Samples as Determined by X-ray Diffractometry

Dopant	Dopant content (wt%)	Molar ratio CaO/SiO_2* 1.8	2.0	2.2
K_2O	0.0	γ	γ	γ + (β)
	0.2	γ	γ	γ + (β)
	0.5	γ + (β)	γ	γ + β
	1.0	β + γ	β + γ	β + γ
	1.5	β + R + (γ)	β + γ	β + γ
Al_2O_3	0.0	γ	γ	γ + (β)
	0.5	β + γ[†]	β	γ + (β)
	1.5	β[†]	γ	β + γ[†]
	2.3	β + (γ)[†]	β + (γ)	β + (γ)[†]
	3.0	β + (G)[†]	β	β + (C_3A)
	4.5	β + G + γ[†]	γ[†]	β + C_3A

*Molar ratios were calculated from atomic ratio (Ca + 0.5K)/(Si + Al), where Ca, K, Si, and Al are concentrations of each atomic species. Major phase is given first; polymorphs in parentheses are present only in trace amounts. R is $Ca_3Si_2O_7$, G is $Ca_2Al_2SiO_7$, and C_3A is $Ca_3Al_2O_6$. †Delayed transformation observed.

Table II. Formation of Crystalline Phases on Annealing*

Annealing temperature (°C)	Sample annealed 1.8K1	1.8A2.3
1400	W + (R)[§]	(G)
1300	W + R	W + (G)
1200	W + (R)	G + W
1100	W + (R)	G + W
1000	W + (R)	G + W

*Phases listed are in addition to Ca_2SiO_4, as detected by XRD. G is gehlenite ($Ca_2Al_2SiO_7$); W is wollastonite (α-$CaSiO_3$); and R is rankinite ($Ca_3Si_2O_7$). Sample in which CaO/SiO_2 = 1.8 and doped with 1.0 wt% K_2O. Sample in which CaO/SiO_2 = 1.8 and doped with 2.3 wt% Al_2O_3. §Major phase is given first; polymorphs in parentheses are present only in trace amounts.

[*]Models EM-400T and EM-420, Philips Electronic Instruments, Inc., Mahwah, NJ; electron microscopes equipped with energy dispersive spectrometer from EDAX International, Inc., Prairie View, IL.

[**]Single crystal grown by the Czochralski method by S. B. Austerman, Rockwell International, Autonetics Marine Systems Division, Anaheim, CA.

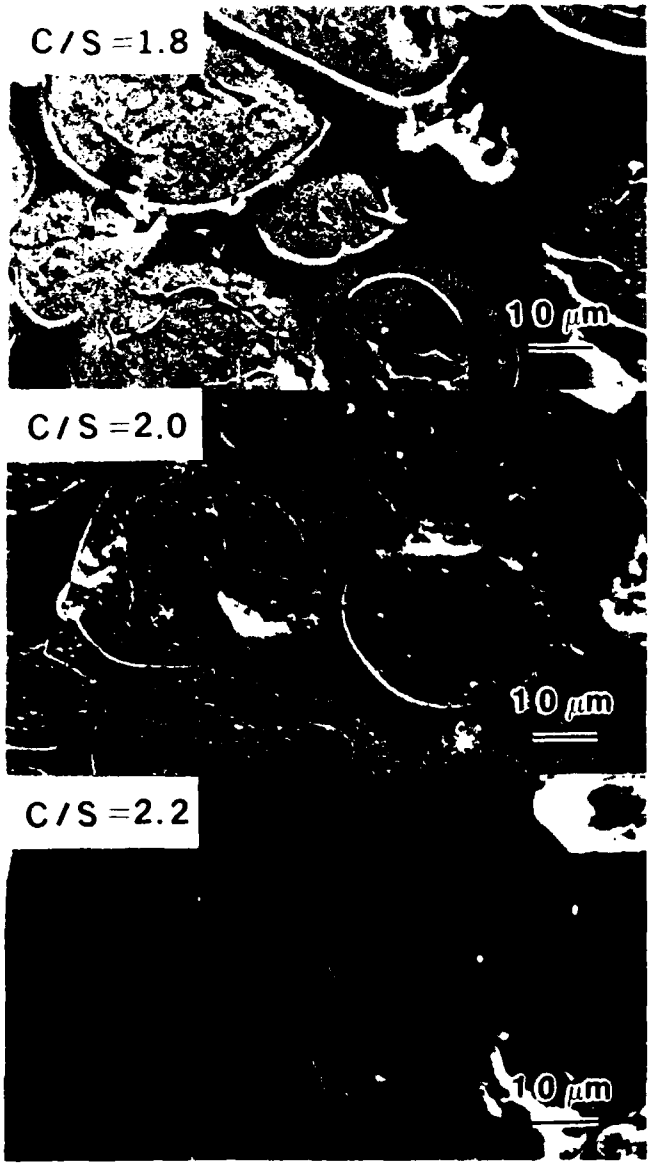

Fig. 1. SEM micrographs of dicalcium silicates doped with 2.3 wt% Al_2O_3 (C/S is CaO/SiO_2).

Transmission electron microscopy (TEM)[*] was undertaken to study the microstructure on a fine scale and to identify phases crystallographically. Quantitative analyses using energy dispersive spectroscopy (TEM/EDS) were based on the thin-film approximation (TFA) using program THIN, version 2.3, as a comparison with the EPMA results. Experimental proportionality constants (K ratios) for TEM/EDS analyses were obtained from natural or synthetic standards, a synthetic mullite ($2Al_2O_3 \cdot SiO_2$) single crystal** for Si and Al, and synthetic wollastonite ($CaO \cdot SiO_2$) for Ca and Si. The thickness was kept below the TFA limit by monitoring the beam current and overall count rate.

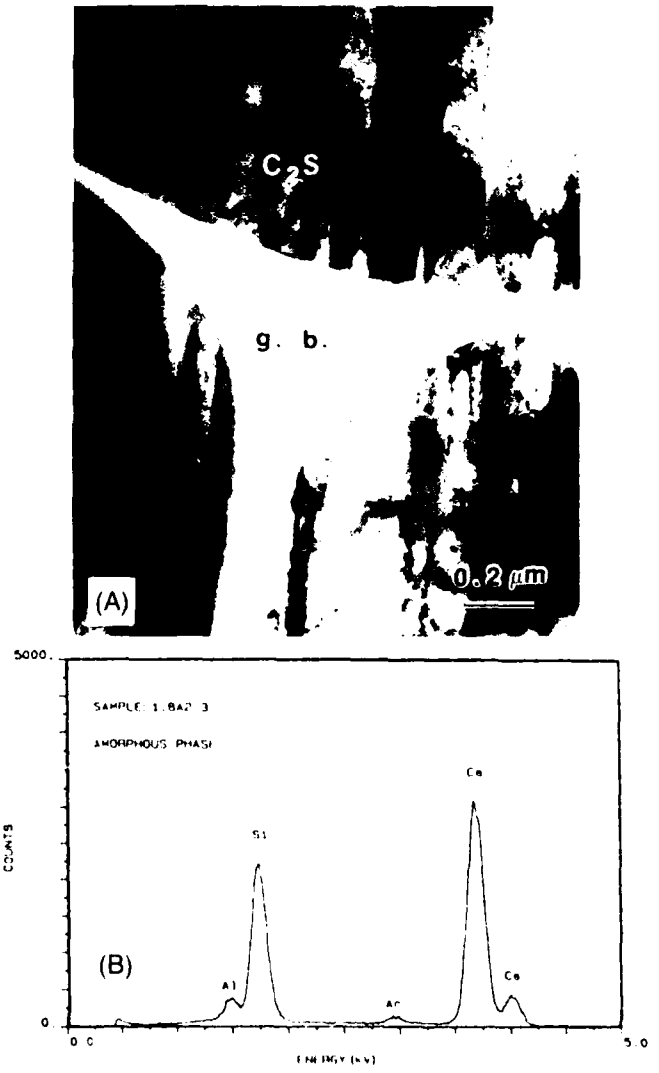

Fig. 2. Amorphous grain-boundary phase (gb) in a silica-rich specimen (CaO/SiO_2 = 1.8) doped with 2.3 wt% Al_2O_3. (A) TEM micrograph (C_2S is Ca_2SiO_4) and (B) EDS spectrum.

Fig. 3. TEM micrographs of narrow-banded structures (arrows) across (100) twins in doped lime-rich specimens ($CaO/SiO_2 = 2.2$): (*A*) bands filled with second phase in a 1.5-wt%-K_2O-doped specimen and (*B*) empty bands (cracks) in a 3.0-wt%-Al_2O_3-doped specimen.

Low signal-to-noise ratios for minor elements were the major difficulty and source of error during each analysis. The effect of beam heating on specimen composition was also checked before each set of analyses. Specimens for TEM were prepared by vacuum impregnation followed by standard mechanical thinning, dimpling, and ion-milling techniques. The ion-thinned specimens were then coated with carbon.

III. Results

(1) X-ray Diffraction

Table I presents X-ray diffraction data as a function of dopant content and shows that, in the absence of dopant, the β form could not be stabilized under the cooling conditions used. β-Ca_2SiO_4 became the major phase when 1.0 wt% K_2O or 0.5 wt% Al_2O_3 was added, but there was no clear indication that departure from stoichiometry influenced the polymorphic composition in a systematic way. It is interesting to note that some Al_2O_3-doped samples showed delayed transformation. When the CaO/SiO_2 ratio was 1.8, the presence of low-lime crystalline phases was detected, confirming their formation as predicted from phase diagrams. Upon annealing at various temperatures below the firing temperature for 1 h, increasing quantities of such phases were observed, as shown in Table II.

(2) Electron Microscopy Observations

(A) General Microstructure: Stabilized β-Ca_2SiO_4 preparations which contained either K_2O or Al_2O_3 as dopant showed microstructures typical of those shown in Fig. 1. A grain-boundary phase was prominent in all silica-rich preparations ($CaO/SiO_2 = 1.8$) and was also present in lime-rich samples ($CaO/SiO_2 = 2.2$), although very much reduced in volume. Individual Ca_2SiO_4 grains were, for the most part, separated by this phase except in lime-rich specimens. Selected area electron diffraction of intergranular areas, such as Fig. 2, showed that the grain-boundary phase was amorphous.

The β-Ca_2SiO_4 grains all showed the characteristic twinned lamellar structure which corresponded to Insley's type II classification in optical microscopy of dicalcium silicate.[15] In the lime-rich specimens, parallel "narrow-band" lamellae crossing twins were frequently observed (Figs. 3(*A*) and (*B*)). These were similar to Insley's type I classification.[15] There was, however, a marked difference in the narrow-banded structure between K_2O-doped and Al_2O_3-doped specimens. In the former, the bands contained the amorphous boundary phase (Fig. 3(*A*)), whereas this was absent in the latter where the bands appeared to be parallel cracks (Fig. 3(*B*)).

(B) Formation of Additional Crystalline Phases: Other crystalline phases were observed to form when the CaO/SiO_2 ratio deviated from stoichiometry. Under silica-rich conditions ($CaO/SiO_2 = 1.8$), rankinite ($Ca_3Si_2O_7$) was detected by XRD (Table I) and TEM (Fig. 4) in the K_2O-doped system when the doping level was 1.5 wt%. In the Al_2O_3-doped system, gehlenite ($Ca_2Al_2SiO_7$) crystals were observed by both XRD and TEM when the doping level was equal to or higher than 3 wt% Al_2O_3 (Fig. 5). Both rankinite and gehlenite crystals were identified by electron diffraction and microanalyses (Table III), and both appeared to be crystallizing from the amorphous grain-boundary phase (Figs. 4 and 5). Although their formation was consistent with phase diagrams, the chemical composition of the amorphous phase before crystallization occurred was quite close to that of wollastonite ($CaSiO_3$). Upon annealing at temperatures below the sintering temperature, wollastonite crystallized, presumably also from the amorphous phase (see Table II). For lime-rich samples ($CaO/SiO_2 = 2.2$) with high levels of Al_2O_3 (>3.0 wt%), tricalcium aluminate ($Ca_3Al_2O_6$) and tricalcium silicate (Ca_3SiO_5) were detected and confirmed by XRD, electron diffraction, and microanalyses. Tricalcium aluminate crystals formed around the β-Ca_2SiO_4 grains (Fig. 6). This may have been due to the low eutectic temperature (~1335°C from the CaO-Al_2O_3-SiO_2 phase diagram) for the composition range studied. The formation of $Ca_3Al_2O_6$ and that of Ca_3SiO_5 were both consistent with the phase diagram, although the amounts are too small to be detected unequivocally by XRD.

(3) Quantitative Microanalysis

The results of TEM EDS quantitative analyses of β-Ca_2SiO_4 grains from K_2O-doped and Al_2O_3-doped specimens are shown in Figs. 7 and 8, respectively, and those of the amorphous phases and other additional crystalline phases in Table III. In TEM, individual grains, grain boundaries, and other crystalline phases could be analyzed with higher accuracy because of the smaller probe size and reduced electron-beam spreading in thin sections.

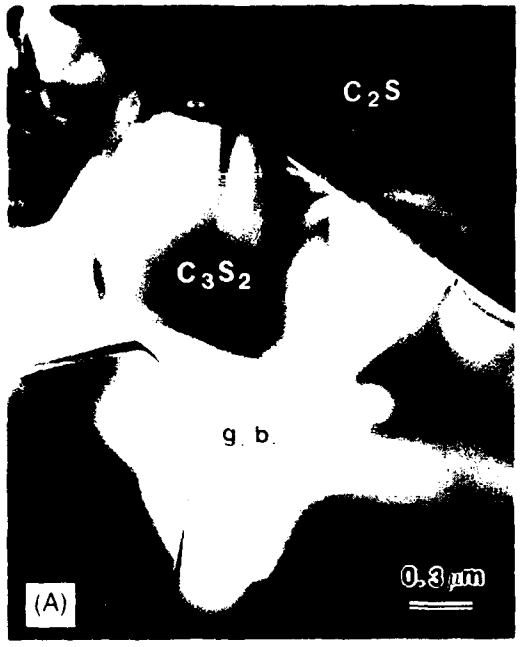

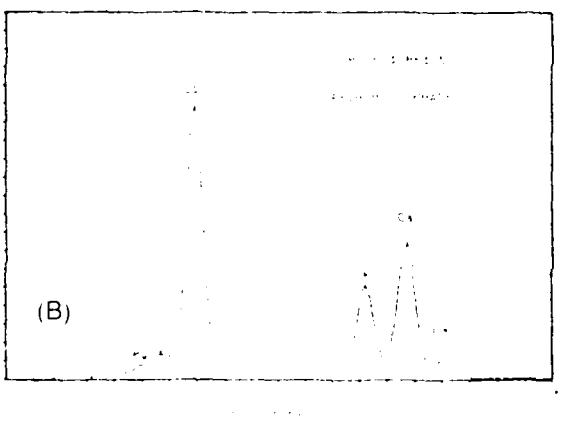

Fig. 4. Specimen with CaO/SiO$_2$ = 1.8 and doped with 1.5 wt% K$_2$O. (*A*) TEM micrograph showing rankinite (C_3S_2 is $Ca_3Si_2O_7$) crystal growing from the amorphous grain-boundary phase (gb). (*B*) EDS spectrum of the adjacent grain-boundary phase.

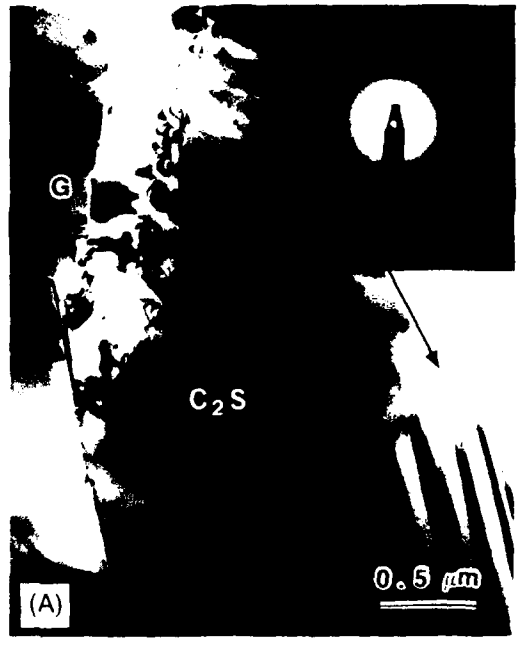

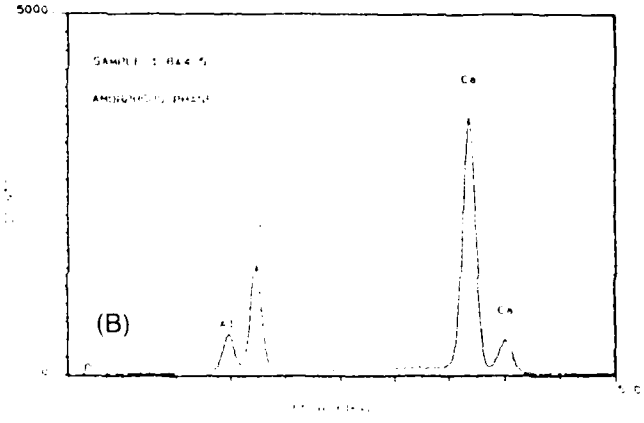

Fig. 5. Specimen with CaO/SiO$_2$ = 1.8 and doped with 4.5 wt% Al$_2$O$_3$. (C_2S is Ca_2SiO_4.) (*A*) TEM micrograph showing a gehlenite (G is $Ca_2Al_2SiO_7$) crystal filling the grain boundary region with a small amount of residual amorphous grain boundary phase (inset is selected area diffraction pattern). (*B*) EDS spectrum of the residual amorphous grain boundary phase.

The results are summarized as follows.

(1) The amount of K_2O in β-Ca_2SiO_4 grains was very low and close to the detection limit. No more than half of the dopant additions were observed in grains, but a small amount of substitution apparently occurred.

(2) K_2O was concentrated in the amorphous grain boundary phase and in inclusions that were occasionally observed with grains.

In Al_2O_3-doped specimens, the dopant was concentrated in amorphous phases under silica-rich conditions (CaO/SiO$_2$ = 1.8). However, high levels of Al_2O_3 were found in β-Ca_2SiO_4 grains under lime-rich conditions, reaching a saturation limit of about 5.0 wt%. The stoichiometric compositions tended to show a mixed effect between CaO/SiO$_2$ = 1.8 and 2.2.

(3) The average CaO/SiO$_2$ ratio of β-Ca_2SiO_4 grains was about 2.9 ± 0.1, regardless of the nominal CaO/SiO$_2$ ratio of the original compositions or the dopant used. The formation of β-$Ca_3Si_2O_7$ apparently did not occur. Instead Ca_2SiO_4 and $CaAl_2O_4$ were observed.

(5) The major change in going from silica-rich to lime-rich compositions (CaO/SiO$_2$ = 1.8 to 2.2) was the change in the CaO/SiO$_2$ ratio of grain boundary phases and the formation of *additional crystalline phases*. However, it was not possible to do an accurate elemental balance because of the difficulty in determining the relative amount of each phase.

As shown in Fig. 1, in samples with CaO/SiO$_2$ = 1.8, the microstructure appeared to consist of large "grains" (10 to 50 μm across) separated by an extensive second phase. Closer examination by SEM revealed that the large grains were really agglomerates of smaller grains separated by thin grain boundaries (0.1 to 0.5 μm), as shown in Fig. 9. The orientations of the fine, but distinct, striations in each grain, caused by twinning, helped to identify separate grains. Therefore, because of the spatial resolution limitation of the EPMA technique, the analyses may have contained significant contributions from the grain boundary phase within an agglomerate. Note in Table IV that the results of EPMA tended to overestimate the amount of dopant intake into the β-Ca_2SiO_4 grains or to underestimate the dopant present at the grain boundary. TEM-EDS quantitative analysis, even though relatively tedious, gave more accurate results with no contribution from the boundary phases. However, since dopant levels were low, the EPMA was still a valid technique in evaluating the CaO/SiO$_2$ ratio of β-Ca_2SiO_4 grains. The CaO/SiO$_2$ ratios obtained from EPMA analyses were essentially very close to those obtained from TEM-EDS quantitative studies.

Table III. TEM/EDS Quantitative Microanalyses on Amorphous Grain Boundaries and Additional Crystalline Phases

Dopant	Initial composition: Dopant content (wt%)	Initial composition: [CaO] + [K_2O] * / [SiO_2] + 2[Al_2O_3]]	Features analyzed†	Average composition (wt%)‡: CaO	SiO_2	K_2O	Al_2O_3	[CaO] + [K_2O] * / [SiO_2] + 2[Al_2O_3]]
K_2O	1.0	1.8	gb	46.0	50.9	3.1		1.01
		2.0	gb	39.2	54.4	6.4		0.85
		2.2	NB or gb	63.5	33.4	3.1		2.10
	1.5	1.8	C_3S_2 crystals	58.6	40.8	0.6		1.56
			gb	21.5	70.0	7.6		0.41
		2.0	gb	31.1	50.4	17.0		0.89
		2.2	NB or gb	59.1	34.5	4.9		2.01
Al_2O_3	0.5	2.0	gb	50.6	36.7		12.8	1.05
	1.5	1.8	gb	47.2	43.4		9.4	0.92
	2.3	1.8	gb	47.3	45.3		7.5	0.94
		2.0	gb	46.3	37.9		15.8	0.88
		2.2	C_3A crystals	64.1	6.3		29.7	3.33§
			C_3S crystals	72.2	26.7		1.1	2.76
	3.0	1.8	C_2AS crystals	43.8	32.9		23.3	1.01¶
			gb	43.3	41.4		15.3	0.79
		2.0	gb	47.7	3.9		48.4	0.84
		2.2	C_3S crystals	73.0	25.7		1.3	2.87
			C_3A (?) crystals	63.5	19.6		16.9	3.37§
	4.5	1.8	C_2AS crystals	43.3	26.5		30.1	1.05¶
			gb	38.8	45.1		16.1	0.66
		2.2	C_3A crystals	62.4	4.7		32.9	3.08§
			C_3A crystals	74.3	24.5		1.2	3.08

*Equivalence of atomic ratio (Ca + 0.5K)/(Si + Al), where Ca, K, Si, and Al are concentrations of each atomic species. †C_3S_2 is $Ca_3Si_2O_7$; C_2AS is $Ca_2Al_2SiO_7$; C_3A is Ca_3SiO_5. NB is phases present in narrow-banded structure; gb is grain boundary. ‡Values based on repeated analyses, typically 10 for each specimen. Standard deviations for CaO and SiO_2 (major elements) are approximately ±2% (for Ca_2SiO_4 grains); for K_2O and Al_2O_3 (minor elements), the deviations are very much higher because of poor signal-to-noise ratios. Error bars are shown in Figs. 7 and 8. §Value of [CaO]/([Al_2O_3] + 0.5[SiO_2]) molar ratio is equal to (Ca)/(0.5(Si + Al)) atomic ratio. ¶Value of [CaO] + [Al_2O_3] + [SiO_2]) molar ratio is equal to (Ca) (0.5Al + Si) atomic ratio.

IV. Discussion

(1) Effect of Excess Silica (CaO/SiO_2 = 1.8) and Dopant Additions

As shown in Table I, changing from the stoichiometry (CaO/SiO_2 = 2.0) to silica-rich (CaO/SiO_2 = 1.8) did not stabilize the high-temperature phase at room temperature. β-Ca_2SiO_4 was stabilized only when appreciable amounts of dopants, higher than or equal to 1 wt% K_2O or 0.5 wt% Al_2O_3, were present in the system. Electron microscopy studies showed that extensive amounts of amorphous phase were associated with some additional crystalline phases in the grain-boundary region. TEM EDS quantitative analyses further indicated that the majority of the dopant was located in the amorphous grain-boundary phase. The dopant levels in the β-Ca_2SiO_4 grains were much lower than those reported previously[3,5] and were close to the limits of detection for the EDS technique. These discrepancies were believed to originate from the natural limitation of the experimental techniques (EPMA) applied by previous researchers, as shown in Table IV. The formation of amorphous and crystalline phases was in accordance with the relevant phase diagrams. The apparent deviations arise from metastability.

(2) Effect of Excess Calcia (CaO/SiO_2 = 2.2) and Dopant Additions

Earlier reports concerning the formation of β-$Ca_3Si_2O_7$ could not be substantiated. The formation of Ca_3SiO_5 and $Ca_3Al_2O_6$ was observed as predicted from the phase diagram. The results of TEM EDS analyses showed that only a small amount of K_2O was found in the β-Ca_2SiO_4 grains. Hence, chemical stabilization was less likely. The frequently observed narrow bands crossing the twins are believed to be characteristic of fast quenching through the $\alpha \rightarrow \alpha'_H$ transformation[17,18] and may be responsible for the stabilization effect. Similar microstructures have also been observed in other systems.[19,20] It has been shown that the high-temperature β phase can be retained by fast quenching through the $\alpha \rightarrow \alpha'_H$ transformation[21,22] in pure Ca_2SiO_4 preparation. A correlation between the narrow-banded structure and stabilization by quenching through the $\alpha \rightarrow \alpha'_H$ transformation had also been suggested.[23]

As mentioned previously, a difference between the narrow-banded structure of K_2O-doped and Al_2O_3-doped systems was observed. A second phase was present in the narrow-banded structure of K_2O-doped specimens (Fig. 3(*A*)), but was absent in specimens doped with Al_2O_3 (Fig. 3(*B*)). Similar bands, partially filled with a second phase, have also been observed in BaO-doped β-Ca_2SiO_4.[17] It is hypothesized that the narrow bands are cracks caused by volume changes accompanying the $\alpha \rightarrow \alpha'_H$ transition, which can be subsequently filled by a liquid phase

Fig. 6. Specimen with CaO/SiO_2 = 2.2 with 4.5 wt% Al_2O_3, showing TEM micrograph of a tricalcium aluminate (C_3A is $Ca_3Al_2O_6$) at the boundary region with insert of the corresponding tricalcium aluminate selected area diffraction pattern, [100] beam direction.

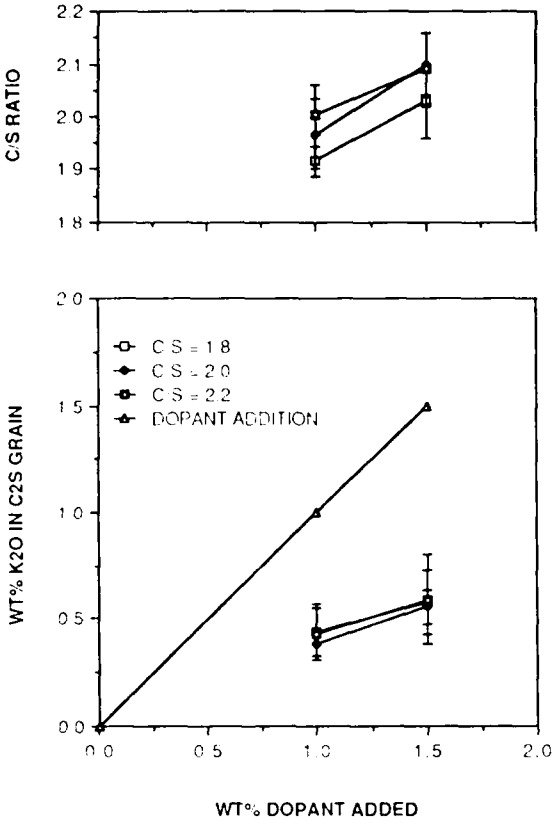

Fig. 7. TEM/EDS quantitative microanalyses of β-Ca_2SiO_4 grains in K_2O-doped specimens.

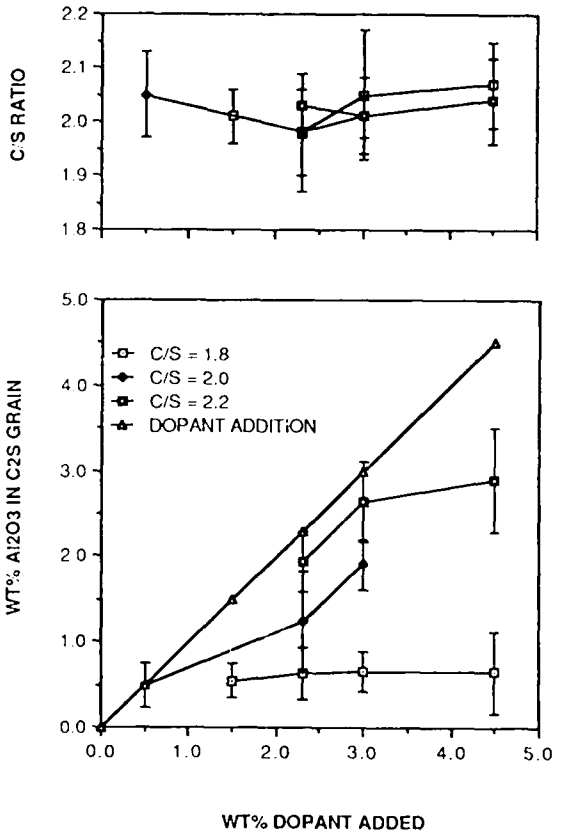

Fig. 8. TEM/EDS quantitative microanalyses of β-Ca_2SiO_4 grains in Al_2O_3-doped specimens.

prior to solidification. This effect could influence the stabilization of β-Ca_2SiO_4. At the transformation temperature, this volume change is estimated to be -4.8%,[23] to which should be added thermal contraction as the system is cooled into the β-phase field.

(3) Stabilization of β-Ca_2SiO_4

The present results show that studies using XRD alone can lead to erroneous conclusions concerning the level of dopant substitution in β-Ca_2SiO_4; XRD does not detect the presence of dopant-rich amorphous phases. The low-level dopant substitutions found in individual β-Ca_2SiO_4 grains suggest that chemical substitution might not be the major factor for stabilization of the β-Ca_2SiO_4. Physical parameters, such as critical particle size effect[6,14] or additional matrix constraint from a continuous glassy phase,[24,25] might be more important mechanisms. Partial crystallization of the amorphous phase by annealing has been found to promote formation of γ-Ca_2SiO_4.[26] However, in calcia-rich systems, appreciable aluminum substitution was observed; therefore, chemical stabilization cannot be completely ruled out. A more detailed study needs to be conducted in order to elucidate the operating stabilization mechanisms.

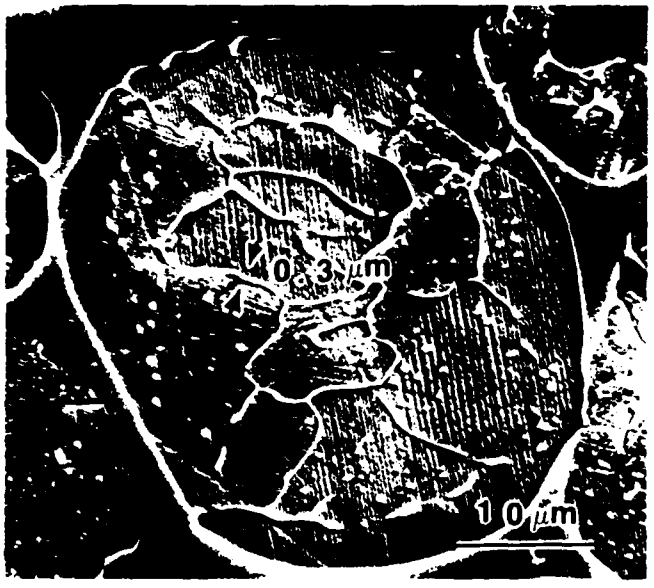

Fig. 9. SEM micrograph of a specimen with $CaO/SiO_2 = 1.8$ doped with 1.0 wt% K_2O showing a large "agglomerate" of β-Ca_2SiO_4 grain (10 to 50 μm) consisting of several smaller grains separated by thin grain boundaries (0.1 to 0.5 μm).

V. Conclusion

Stabilization of β-Ca_2SiO_4 by excess lime in the absence of dopants could not be attained under the processing conditions used. The existence of $Ca_{1.5}SiO_{3.5}$ and $Ca_{2.2}SiO_{4.2}$ could not be confirmed. Changes in bulk stoichiometry were accommodated by the formation of an amorphous grain-boundary phase and other crystalline phases.

The β-Ca_2SiO_4 grains had the well-known twinned lamellar structure and their stoichiometry was essentially $CaO/SiO_2 = 2.0 \pm 0.1$. Little dopant was observed in the β-Ca_2SiO_4 grains except for the Al_2O_3-doped specimens under lime-rich conditions, where levels of Al_2O_3 up to 3.0 wt% were detected. The microstructures developed were quite complex. Under silica-rich conditions ($CaO/SiO_2 = 1.8$), large agglomerates of Ca_2SiO_4 grains were surrounded by extensive amorphous boundary phases which also separated the grains. Amorphous inclusions were observed within some grains. Under lime-rich conditions ($CaO/SiO_2 = 2.2$), less amorphous phases were present. A narrow-banded structure was frequently observed within β-

Table IV. Comparison between EPMA and TEM/EDS Quantitative Microanalysis*

Initial composition					Average composition (wt%)†			
Dopant	Dopant content (wt%)	Mole ratio CaO/SiO_2	Technique applied	Features analyzed‡	CaO	SiO_2	K_2O	Al_2O_3
K_2O	1.0	1.8	EPMA	Grain	63.3	35.3	0.7	
			TEM/EDS	Grain	63.8	35.8	0.4	
K_2O	1.5	2.2	EPMA	Grain	64.4	35.0	1.2	
			TEM/EDS	Grain	65.2	33.7	0.6	
K_2O	1.5	1.8	EPMA	gb	46.2	49.4	3.4	
			TEM/EDS	gb	21.5	70.0	7.6	
				Rankinite	58.6	40.8	0.6	
Al_2O_3	4.5	1.8	EPMA	gb	42.2	40.0		15.4
			TEM/EDS	gb	38.8	45.1		16.1
				Gehlenite	43.3	26.5		30.1

*Selected data. gb is amorphous grain boundary; rankinite is crystals of $Ca_3Si_2O_7$; and gehlenite is crystals of $Ca_2Al_2O_7$. †Values based on repeated analyses, typically 10 for each specimen. Standard deviations for CaO and SiO_2 (major elements) are approximately ±2% (for Ca_2SiO_4 grains); for K_2O and Al_2O_3 (minor elements), the deviations are very much higher because of poor signal-to-noise ratios. Error bars are shown in Figs. 7 and 8.

Ca_2SiO_4 grains, but there was a marked difference between K_2O-doped and Al_2O_3-doped specimens. In the former, the bands contained a second phase, whereas this was absent in the latter where the bands appeared to be parallel cracks.

Other crystalline phases were observed to crystallize under silica-rich conditions from the amorphous phase when the dopant levels were 1.5 wt% K_2O or ≥3.0 wt% Al_2O_3. They were identified as rankinite ($Ca_3Si_2O_7$) in K_2O-doped systems and gehlenite ($Ca_2Al_2SiO_7$) in Al_2O_3-doped systems. In lime-rich systems, $Ca_3Al_2O_6$ and Ca_3SiO_5 also formed to compensate for the stoichiometric change in Al_2O_3-doped systems. Recrystallization was consistent with the relevant phase diagrams.

The study suggests that the role of solid-state substitution in stabilizing Ca_2SiO_4 needs to be reexamined and that physical factors may be playing a more influential role.

Acknowledgments: The authors thank Dr. K. C. Hsieh for valuable discussions. The electron microscopy was conducted in the Center for Microanalysis of the Materials Research Laboratory and the Center for Electron Microscopy, both at the University of Illinois at Urbana-Champaign.

References

[1] H. E. Schwiete, W. Kronert, and K. Deckert, "Existence Range and Stabilization of High-Temperature Modification of Dicalcium Silicate," *Zem.-Kalk-Gips*, **9**, 359–66 (1968).

[2] H. Midgley, "The Polymorphism of Calcium Orthosilicate," *Proc. Int. Congr. Chem. Cem., 6th*, Suppl. Paper 1, 1–16 (1974).

[3] S. N. Ghosh, P. B. Rao, A. K. Paul, and K. Raina, "The Chemistry of Dicalcium Silicate Minerals," *J. Mater. Sci.*, **14**, 1554–66 (1979).

[4] W. M. Kriven, "Displacive Transformation Mechanisms in Zirconia Ceramics and Other Nonmetals", pp. 223–37 in Tailoring Multiphase and Composite Ceramics. Edited by R. E. Tressler, G. L. Messing, C. G. Pantano, and R. E. Newnham. Plenum Press, New York, 1986.

[5] J. S. Moya, P. Pena, and S. de Aza, "Transformation Toughening in Composites Containing Dicalcium Silicate," *J. Am. Ceram. Soc.*, **68** [9] C-259–C-262 (1985).

[6] W. M. Kriven, C. J. Chan, and E. A. Barinek, "The Particle Size Effect of Dicalcium Silicate in a Calcium Zirconate Matrix", to be published in Advances in Ceramics, Vol. 24, Science and Technology of Zirconia III. Edited by S. Somiya, N. Yamamoto, and H. Yanagida. American Ceramic Society, Westerville, OH, 1988.

[7] A. Guinier and M. Regourd, "Structure of Portland Cement Minerals," *Proc. Int. Symp. Chem. Cem., 5th*, **1**, 1–32 (1968).

[8] A. Ghose and P. Barnes, "Electron Microprobe Analysis of Portland Cement Clinkers," *Cem. Concr. Res.*, **9**, 747–56 (1979).

[9] V. I. Korneev and E. B. Bygalina, "Thermal Stabilization of β-$2CaO \cdot SiO_2$," *Proc. Int. Symp. Chem. Cem., 5th*, **1**, 285–88 (1968).

[10] J. Forest; written discussion of Ref. 7, pp. 32–37.

[11] G. Tromel, W. Fix, and R. Heinke, "High-Temperature Investigation to 1900°C on Calcium Orthosilicate and Tricalcium Silicate," *Tonind. Ztg. Keram. Rundsch.*, **93**, 1–8 (1969).

[12] V. I. Korneev, "Composition Zones of Silicate Phases in Portland Cement Clinker," *Proc. Int. Congr. Chem. Cem., 6th*, Suppl. Paper, Sect. 1–1, 1–10 (1974).

[13] A. Wolter, "Formation and Stability of Tricalcium Silicate and Alite," *Forschungsber. Landes Nordrhein-Westfalen*, **3092**, 91 (1982).

[14] N. Yannaquis and A. Guinier, "Polymorphic $\beta \rightarrow \gamma$ Transition of Calcium Orthosilicate," *Bull. Soc. Fr. Mineral. Cristallogr.*, **82**, 126–36 (1959).

[15] B. Matković, V. Carin, T. Mechanisms in Zirconia Clenić, and J. F. Young, "Influence of $BaSO_4$ on the Formation and Hydration Properties of Calcium Silicates: 1, Doped Dicalcium Silicates," *Am. Ceram. Soc. Bull.*, **68** [8] 825–29 (1981).

[16] S. Chopra, A. Ghose, and J. F. Young, "Electron-Optical Studies of Stabilized α′- and β Dicalcium Silicate," *Proc. Int. Conf. Cem. Microsc., 5th*, 11–22 (1983).

[17] A. Ghose, S. Chopra, and J. F. Young, "Microstructural Characterization of Doped Dicalcium Silicate Polymorphs," *J. Mater. Sci.*, **18**, 2905–14 (1983).

[18] C. J. Chan, A. Ghose, W. M. Kriven, and J. F. Young, "Microstructure of Nonstoichiometric Dicalcium Silicate Doped with Potassium Oxide"; pp. 11–23 in Proceedings of Beijing International Symposium on Cement and Concrete, Vol. 1, Beijing, China, 1985, China Building Industry Press, Beijing, China, 1986.

[19] C. J. Chan, W. M. Kriven, and J. F. Young, "Microstructure Characterization of Nonstoichiometric Dicalcium Silicate Doped with Aluminum Oxide"; pp. 452–53 in Proceedings of the 44th Annual Meeting of Electron Microscopy Society of America (EMSA), Albuquerque, NM, 1986, San Francisco Press, San Francisco, CA, 1986.

[20] H. Insley, "Structural Characteristics of Some Constituents of Portland Cement Clinker," *J. Res. Natl. Bur. Stand. (US)*, **17**, 353–61 (1936).

[21] G. Yamaguchi and S. Takagi, "The Analysis of Portland Cement Clinker," *Proc. Int. Symp. Chem. Cem., 5th*, **1**, 181–218 (1968).

[22] M. Gawlicki, "The Role of Thermal Treatment on Dicalcium Silicate Polymorphic Transitions", pp. 67–73 in Proceedings of the 14th Conference on Silicate Industry and Silicate Science, Vol. 3, Budapest, Hungary, 1985, Omikk Tekniform, Budapest, Hungary, 1985.

[23] C. J. Chan and W. M. Kriven, "Effect of Kinetics on Ca_2SiO_4 Microstructural Development," published abstract 112-B-87, *Am. Ceram. Soc. Bull.*, **66** [3] 519 (1987).

[24] D. M. Roy, "Studies in the System CaO-Al_2O_3-SiO_2-H_2O—III. New Data on the Polymorphism of Ca_2SiO_4 and Its Stability in the CaO-SiO_2-H_2O," *J. Am. Ceram. Soc.*, **41** [8] 293–99 (1958).

[25] A. Derdacka-Grzymek, "Stabilization Mechanism of Polymorphic Transformation of the Beta-Gamma Ca_2SiO_4" (in Pol.), *Pol. Akad. Nauk. Krakowie. Kom. Ceram.*, **29**, 1–40 (1978).

[26] C. J. Chan, W. M. Kriven, and J. F. Young, unpublished results.

END

FILMED

6-89

DTIC